

Report No. 18

ULTRASONIC RAILROAD WHEEL INSPECTION USING EMATS

Raymond E. Schramm
A. Van Clark, Jr.

National Institute of Standards and Technology
(formerly National Bureau of Standards)
U.S. Department of Commerce
Boulder, Colorado 80303-3328

December 1988



Stimulating America's Progress
1913-1988

Report No. 18

ULTRASONIC RAILROAD WHEEL INSPECTION USING EMATS

Raymond E. Schramm
A. Van Clark, Jr.

Fracture and Deformation Division
Institute for Materials Science and Engineering
National Institute of Standards and Technology
Boulder, Colorado 80303-3328

December 1988

Prepared for
U.S. Department of Transportation
Federal Railroad Administration
Washington, DC 20590



U.S. DEPARTMENT OF COMMERCE, C. William Verity, Secretary

Ernest Ambler, Acting Under Secretary for Technology

NATIONAL INSTITUTE OF STANDARDS AND TECHNOLOGY, Raymond G. Kammer, Acting Director

CONTENTS

	Page
ABSTRACT	1
INTRODUCTION	1
EMAT Program	1
Residual Stress in Railroad Wheel Rims	2
Cracks in Railroad Wheel Treads	3
Publications	5
Publication Reprints and Preprints:	
1. "Ultrasonic Characterization of Residual Stress and Texture in Cast Steel Railroad Wheels," A. V. Clark, H. Fukuoka, D. V. Mitrakovic, and J. C. Moulder in <u>Review of Progress in Quantitative Nondestructive Evaluation</u> , Vol. 6B, D. O. Thompson and D. E. Chimenti, eds., Plenum Press, New York (1987), 1567-1575.	7
2. "Characterization of Residual Stress and Texture in Cast Steel Railroad Wheels," A. V. Clark, Jr., H. Fukuoka, D. V. Mitrakovic, and J. C. Moulder, <u>Ultrasonics</u> 24, 281-288 (1986).	17
3. "Flaw Detection in Railroad Wheels Using Rayleigh-Wave EMATs," R. E. Schramm, A. V. Clark, Jr., D. V. Mitrakovic, and P. J. Shull in <u>Review of Progress in Quantitative Nondestructive Evaluation</u> , Vol. 7B, D. O. Thompson and D. E. Chimenti, eds., Plenum Press, New York (1988), 1661-1668.	25
4. "Ultrasonic Characterization of Residual Stress and Flaws in Cast Steel Railroad Wheels," A. V. Clark, R. E. Schramm, H. Fukuoka, D. V. Mitrakovic in <u>Proceedings: IEEE 1987 Ultrasonics Symposium</u> , B. R. McAvoy, ed., Institute of Electrical and Electronic Engineers, New York (1988), 1079-1082.	33
5. "EMAT Examination for Cracks in Railroad Wheel Treads," R. E. Schramm, P. J. Shull, A. V. Clark, Jr., and D. V. Mitrakovic, submitted to <u>Proceedings: Nondestructive Testing and Evaluation for Manufacturing and Construction</u> , Urbana, Illinois, Aug. 9-12, 1988.	37
6. "EMATs for Roll-By Crack Inspection of Railroad Wheels," R. E. Schramm, P. J. Shull, A. V. Clark, Jr., and D. V. Mitrakovic, submitted to <u>Review of Progress in Quantitative Nondestructive Evaluation</u> , Vol. 8, La Jolla, California, Aug. 1988.	45
7. "Ultrasonic Characterization of Residual Stress and Texture in a Heat-Treated Steel Railroad Wheel," A. V. Clark, H. Fukuoka, D. V. Mitrakovic, and J. C. Moulder, submitted to <u>Materials Evaluation</u> .	53

ULTRASONIC RAILROAD WHEEL INSPECTION USING EMATS

Raymond E. Schramm and A. Van Clark, Jr.
Fracture and Deformation Division
National Institute of Standards and Technology
Boulder, Colorado 80303

This is report number 18 in a series covering the research performed by the National Institute of Standards and Technology (formerly National Bureau of Standards) for the Federal Railroad Administration. This issue collects seven reprints and preprints of papers written by the Fracture and Deformation Division over the last two years on the ultrasonic nondestructive evaluation of railroad wheels for the presence of residual stresses and cracks. All this work concentrated on the use of electromagnetic-acoustic transducers (EMATs).

Tensile residual stresses and tread cracks are major factors in wheel failure. Catastrophic breakdowns may lead to injuries, repair costs, and lost time. Current inspection methods are largely visual, and thus inefficient. Two ultrasonic techniques are applicable to these wear defects:

1. Birefringence. A stress field effects the velocity of a shear horizontal wave depending on its polarization. Precise velocity measurements in a wheel rim may allow calculation of the amount and direction of stresses.

2. Pulse-echo. A Rayleigh (surface) wave transducer mounted inside the rail can introduce a signal to interrogate the circumference of a wheel as it rolls by. An echo indicates a flaw's presence and size.

For both systems, we hope to produce instruments for testing at a field site.

Key words: EMAT; nondestructive evaluation; railroad wheel; residual stress; roll-by inspection; ultrasonic.

INTRODUCTION

EMAT Program

Railroad safety is the focus of two current programs in the Fracture and Deformation Division of the U.S. National Institute of Standards and Technology (NIST, formerly National Bureau of Standards) in Boulder, Colorado. These areas of research are:

1. Detection and quantification of residual stresses present in the rim of railroad wheels.
2. Detection and depth sizing of cracks in the tread of railroad wheels.

The results of these nondestructive evaluation (NDE) problems come together since a tread crack in a wheel with a tensile hoop stress in the rim can lead to slow or explosive wheel failure. The consequences to personal safety, schedule delays, track, and rolling stock can be both catastrophic and expensive. For each problem, we apply a special type of ultrasonic transducer to the cast wheels. The Federal Railroad Administration is sponsoring these projects.

NIST researchers have been active in applying the unique properties of electromagnetic-acoustic transducers (EMATs) to ultrasonic nondestructive evaluation since 1980. During this time we have developed considerable experience in transducer design and have built state-of-the-art electronics. Our prior work has involved quantitative measurement of such parameters as weld flaw size, residual stress, and sheet metal texture.

An EMAT contains two basic elements: a coil which is excited by high-current radio-frequency power to produce an eddy current in the specimen, and a magnet to generate a static field. The operational principle is that the Lorentz force generates a mechanical wave inside the wheel itself. The Lorentz force \underline{F} is an electromotive force caused by the interaction of moving charge (eddy current \underline{J}) with the external magnetic field (\underline{B}); i.e., $\underline{F} = \underline{J} \times \underline{B}$ where \times is the vector cross-product. Industrial devices, especially motors, use this force extensively. Application to the generation of sound is relatively recent. Since the ultrasonic signal is generated directly inside the specimen, a major EMAT advantage over the standard piezoelectric transducers is elimination of any couplant - the sound does not originate inside the probe and then traverse several coupling media before encountering the wheel. With a bit of cleverness in orienting the electric and magnetic fields, it is possible to generate any mode and polarization of ultrasound.

Residual Stress in Railroad Wheel Rims

Tensile residual stress in a wheel rim from causes such as heating during heavy drag braking can contribute to catastrophic failure. Current procedures call for an inspector to measure the extent of a certain color rust between the rim and the hub to determine whether to pull a wheel from service. Destructive tests at the Transportation Test Center (TTC) in Pueblo, Colorado, have indicated that about half the wheels removed were still safe to use (Britto Rajkumar, TTC, personal communication). To quantify these measurements, we are examining the possibility of using acoustic birefringence. The speed of shear-wave sound varies slightly depending on its polarization and propagation direction with respect to the stress field. Measuring the traverse time of an echo through the wheel rim to within a few nanoseconds for two transducer orientations (radial and hoop directions) should determine whether there is any stress present, its direction, and magnitude. The goal is to develop a simple EMAT probe and meter system usable in a railroad wheel shop.

We have examined the feasibility of developing such a field instrument. Some progress made to date includes:

1. Development in theory and experimental procedures.
2. Design and construction of a digital delay gate to permit timing measurements with the required accuracy.
3. Comparison between birefringence measurements made with piezoelectric transducers and EMATs.
4. Qualitative comparison between ultrasonic and destructive measurements.
5. Preliminary tests on a series of drag-braked wheels.

Besides stress, another contributor to the acoustic birefringence, and often the major one, is the texture or preferred orientation in the specimen. For cast steel wheels, preferred orientation occurs as the grains orient along thermal gradients during cooling. The ability to separate the effects of these two elements remains the major question in this part of the program. Since the texture is largely a function of the metal alloy and the heat treatment it has received, it is our hope that it will be possible to determine a base birefringence for each type or class of wheel and then subtract this from the value measured on a wheel under test. To make an initial determination of the feasibility of such a procedure, we plan to make measurements on a series of rim blocks cut from the drag-braked wheels tested in item 5, above. When these blocks are removed during destructive tests at TTC, the residual stress will be relieved so that our subsequent EMAT examinations will show only the effects of texture. With this information, we can quantify our initial measurements, and determine the consistency of the baseline on at least this small sample. While awaiting the preparation of the rim blocks, we have shifted our emphasis to a second, and separate, program to detect cracks in the tread.

Cracks in Railroad Wheel Treads

Currently, cracks in the treads of railroad wheels are found mainly by visual inspection during maintenance. Since each major rail line suffers about 25-30 derailments every year as a result of cracked wheels, this approach does not appear to be satisfactory.

In the early 1970's, a company introduced an automatic ultrasonic method to examine each wheel as it rolled by a checkpoint in a railyard. The ultrasonic probe, situated inside the rail, is a pair of piezoelectric transducers within a liquid-filled rubber boot. To aid the transmission of the probing signal into and back out of the wheel, there are two nozzles spraying fluid onto the tread as it passes. The basic idea, as in many ultrasonic approaches, is to inject high frequency sound and then electronically analyze echoes generated by any flaws present. The concept and engineering of this system are very good, but the device has achieved only very limited acceptance (there are only two currently active installations in this country). Two problems seem to have prevented large scale implementation: (1) a very high rate of false positive indications, and (2) fragility, since the boot is very susceptible to small cuts which release the pressurized liquid couplant and disrupt operation. Unfortunately, as wheel treads abrade, wear does develop occasional slivers which are short-lived but very sharp and hazardous.

For more than ten years, the Fraunhofer Institute for Nondestructive Testing (IzfP, Saarbrucken, Federal Republic of Germany) has been working on an ultrasonic inspection system based on the same concept and physics, but taking a different approach to the transducers. The German approach employs noncontacting electromagnetic-acoustic transducers (EMATs) that do not require an acoustic couplant to the wheel as do the conventional transducers. EMATs simplify the mechanics of the rail mounting (since they are generally smaller and more compact), cut the number of false positives (since they have a purer mode of operation and eliminate many extraneous interfaces in the signal path), and should be more durable (since there is no pressurized rubber boot). About two years ago IzfP installed a prototype system in Wuerzburg for use on the high-speed German Experimental Intercity Train (ICE).

This new system inspects the forged wheels of passenger cars and locomotives of German design, all of which have tightly controlled wear profiles. In our current project, we seek to use EMATs to inspect cast wheels on freight cars of U.S. designs, generally with a variety of tread wear patterns and damage states. Thus there are major differences between German and U.S. applications of roll-by inspection systems.

While EMATs cannot operate efficiently at large liftoffs (distance to the workpiece), they can generally tolerate a separation on the order of millimeters, and this is sufficient for roll-by inspection. Another EMAT advantage is its high degree of selectivity, an ability to reject most signals with an undesired polarization. This means a simpler echo pattern and less confusion in data interpretation. In all the work of interest here, the signal is a Rayleigh (surface) wave which travels around the outer tread of the wheel and does not penetrate into the surface very far (<10-15 mm, in this case).

Over the past two years, we have worked to develop an EMAT system tailored to the environment of the U.S. rail system. Some of the progress made to date includes:

1. Design of Rayleigh wave EMATs using the new NdFeB permanent magnets and a meanderline coil on a flexible substrate.
2. Development of a MOSFET power amplifier for the transmitter that is capable delivering as much as 140 A.
3. Construction of a very low noise preamplifier for the receiver.
4. Assembling a short (4 m) length of railroad track to allow us to conduct low-speed rolling tests on actual wheel sets.
5. Packaging of the analog electronics (items 2 and 3) into a single, rugged unit suitable for use in field tests.
6. A simple trigger system to indicate wheel presence.
7. Start on the construction of digital electronics that will process the analog signals automatically and generate any desired alarms to indicate flawed wheels.
8. Contact with railroads and other research facilities to obtain materials and information.

Tests made with the system described above indicate:

1. Good signal-to-noise ratio which should simplify the signal processing that will be necessary.
2. Some tolerance to transducer liftoff so a protective cover for the meanderline should be possible.
3. Differences in echo amplitudes based on flaw depths, indicating an ability to distinguish artificial flaws (sawcuts) with a depth Δ the critical 6 mm.
4. Good operation with the transducer mounted inside the rail.
5. An ability to trigger the electronics with the presence of the wheel and the capture of a digitized signal from a moving wheel.

Publications

Over the past two years, we presented the results of the work done under this sponsorship at six meetings:

1. Review of Progress in Quantitative Nondestructive Evaluation, La Jolla, California, August 1986.
2. Review of Progress in Quantitative Nondestructive Evaluation, Williamsburg, Virginia, June 1987.
3. 1987 IEEE Ultrasonics Symposium, Denver, Colorado, October 1987.
4. Review of Progress in Quantitative Nondestructive Evaluation, La Jolla, California, August 1988.
5. Nondestructive Testing and Evaluation for Manufacturing and Construction, Urbana, Illinois, August 1988.
6. Third International Symposium on Nondestructive Characterization of Materials, Saarbrucken, Federal Republic of Germany, October 1988.

Papers were written for the proceedings of each of these meetings. In addition, a paper was published in the international journal Ultrasonics, and another has been accepted for publication in Materials Evaluation, the journal of the American Society for Nondestructive Testing. This NISTIR is a collection of the reprints and preprints of these papers (the papers for meetings 4 and 6 were prepared at the same time and are virtually identical so paper 6 is not included here).

ULTRASONIC CHARACTERIZATION OF RESIDUAL STRESS AND TEXTURE IN CAST STEEL RAILROAD WHEELS

A. V. Clark, H. Fukuoka*, D. V. Mitraković** and
J. C. Moulder

Fracture and Deformation Division
National Bureau of Standards
Boulder, Colorado 80303

ABSTRACT

An ultrasonic technique has been used to characterize the state of residual stress and texture in the rims of cast steel railroad wheels. Orthogonally polarized shear-horizontal (SH) waves are propagated through the thickness of the rim in pulse-echo mode. The (normalized) difference of arrival times of these waves (acoustic birefringence) depends upon both texture and stress. The birefringence, B , was measured with two transducers: an electromagnetic-acoustic transducer (EMAT) and a piezoelectric transducer made of PZT.

Two wheels were tested. The first wheel had a sawcut, which locally relieved the residual (hoop) stress. Measurement of the birefringence at the sawcut allowed us to estimate the contribution of texture, which we subtracted from values of B at stressed locations. Values of hoop stress obtained with the EMAT and PZT transducer agreed to within 10 MPa, for transducers placed on the center of the back face of the rim.

The second (uncut) wheel had been heat treated and air quenched, giving a different microstructure. Measurements of B were made with both transducers at different radial and circumferential locations. We estimate that the values of hoop stress obtained with the two transducers will differ by less than 25 MPa for this wheel. Furthermore, the EMAT required less surface preparation of the rim than the PZT transducer, indicating the potential for use of EMATs for residual stress measurements in the field.

INTRODUCTION

Residual stresses can be a significant factor in railroad wheel failure. These residual stresses have two origins: (1) stress due to fabrication of the wheel and (2) in-service stress induced by drag braking.

* NBS Guest Worker; on leave from Osaka University, Osaka, Japan.

** NBS Guest Worker; on leave from University of Belgrade, Belgrade, Yugoslavia.

Contribution of the National Bureau of Standards: not subject to copyright in the United States.

For cast steel wheels, fabrication stresses occur during cooling due to differential shrinkage. If these stresses are above the yield stress, inhomogeneous plastic deformation results and residual stresses are then necessary so that compatibility is satisfied.

The same process that creates residual stresses during cooling occurs (in reverse) during drag braking. The heat input into the tread of the wheel during braking causes expansion of this region of the wheel. Each volume element of the rim tries to expand but is constrained by its neighbors. If the resulting compressive stresses exceed yield stress, inhomogeneous plastic deformation results; as the wheel cools after braking, a tensile hoop stress will result to make all the regions of the rim fit together.

Residual stresses due to fabrication are compressive, while those due to drag braking are (usually) tensile. When the latter stresses exceed the former, the rim will be in a state of net tensile stress. If a crack occurs in the rim, those tensile stresses will act as crack-driving forces and that can lead to wheel failure. Therefore it is highly desirable to have a non-destructive testing method for measuring such residual stresses.

In this paper, we present results of a study on the feasibility of using ultrasonic methods to characterize residual stress state in cast steel railroad wheels.

THEORY

It can be shown, both analytically and experimentally, that the presence of stress in metals induces a small sound velocity change. For isotropic materials, the normalized difference in velocity of orthogonally polarized shear-horizontal (SH) waves is proportional to the difference of principal stresses. This normalized difference in velocities is called the acoustic birefringence, in analogy to the birefringence effect in photoelasticity, so

$$B = \frac{V_\theta - V_r}{1/2(V_\theta + V_r)}, \quad (1)$$

where V_θ and V_r are velocities of SH-waves polarized in the hoop and radial directions respectively.

For anisotropic (textured) materials, birefringence depends on texture and principal stresses [1,2]:

$$B = B_0 + C_A(\sigma_\theta - \sigma_r), \quad (2)$$

where B_0 is unstressed birefringence due to texture, C_A is stress-acoustic constant and σ_θ and σ_r are principal stresses in hoop and radial directions.

Combining equations (1) and (2) we have

$$\frac{V_\theta - V_r}{1/2(V_\theta + V_r)} = B_0 + C_A(\sigma_\theta - \sigma_r). \quad (3)$$

From equation (3) it is possible to calculate the difference in principal stresses if the unstressed birefringence and velocities of orthogonally polarized shear waves are known.

Instead of measuring velocities V_θ and V_r we actually measure arrival times T_θ and T_r of shear waves polarized in hoop and radial directions. Since the SH-waves propagate through the same thickness,

$$\frac{V_\theta - V_r}{1/2(V_\theta + V_r)} = \frac{T_r - T_\theta}{1/2(T_r + T_\theta)}, \quad (4)$$

so that the equation for calculating the difference in principal stresses is given by

$$\frac{T_r - T_\theta}{1/2(T_r + T_\theta)} = B_o + C_A(\sigma_\theta - \sigma_r). \quad (5)$$

Problems arising in using equations (5) for obtaining the difference in principal stresses are: (1) the influence of texture and (2) the small value of stress-acoustic constant ($C_A \sim 10^{-5}$ MPa). The value of B_o can be obtained by measurements on unstressed reference samples (provided that the wheels are sufficiently homogeneous). Because of the small value of the stress-acoustic constant, we use electronics capable of measuring arrival times within ± 1 ns.

EXPERIMENTS

Fukuoka et al. used conventional piezoelectric SH-wave transducer to measure the residual stress state in rolled steel wheels [3,4]. They measured birefringence in the as-received state (residual stress due to rolling), after drag braking, and after cutting into blocks (stress relieved). The total residual stress measured ultrasonically was compared with destructive measurements and agreed within 40 MPa [3,4].

In our work, we investigated the feasibility of using electromagnetic-acoustic transducers for measurements in the field. The EMAT has the advantage that it requires no acoustic couplant to generate sound in a metal. Consequently, an EMAT can be scanned and rotated over the rim of the wheel with ease. Being noncontacting, an EMAT may require less preparation of the surface (where the sound is generated) than a piezoelectric device.

To determine whether these potential advantages could be realized in practice, we performed a series of experiments on two cast steel wheels (one sawcut and one uncut) which had been removed from service. We measured the birefringence with an SH-wave EMAT in pulse-echo setup using a simple velocity measurement system (described elsewhere [5]). We also measured the birefringence using the same piezoelectric transducer used in Refs. 3 and 4. The birefringence method using this piezoelectric transducer has been successful in determining residual stresses in rolled wheels [3,4]. Consequently, we used results obtained with this transducer as a benchmark against which our EMAT measurements were compared.

The first set of measurements was made on a sawcut wheel. The measurements were made from the back face of the rim, 19 mm from the inner edge of the rim. This corresponds to the centerline of the front face (see Fig. 1).

Six different regions of the back face of the rim were milled in preparation for using both PZT and EMAT transducers (see Fig. 2). We measured the birefringence near the center of each milled region at least three times with both transducers. The values of birefringence thus obtained are plotted in Fig. 3. The error bars represent the standard deviation of the measurements of birefringence at each of the milled regions.

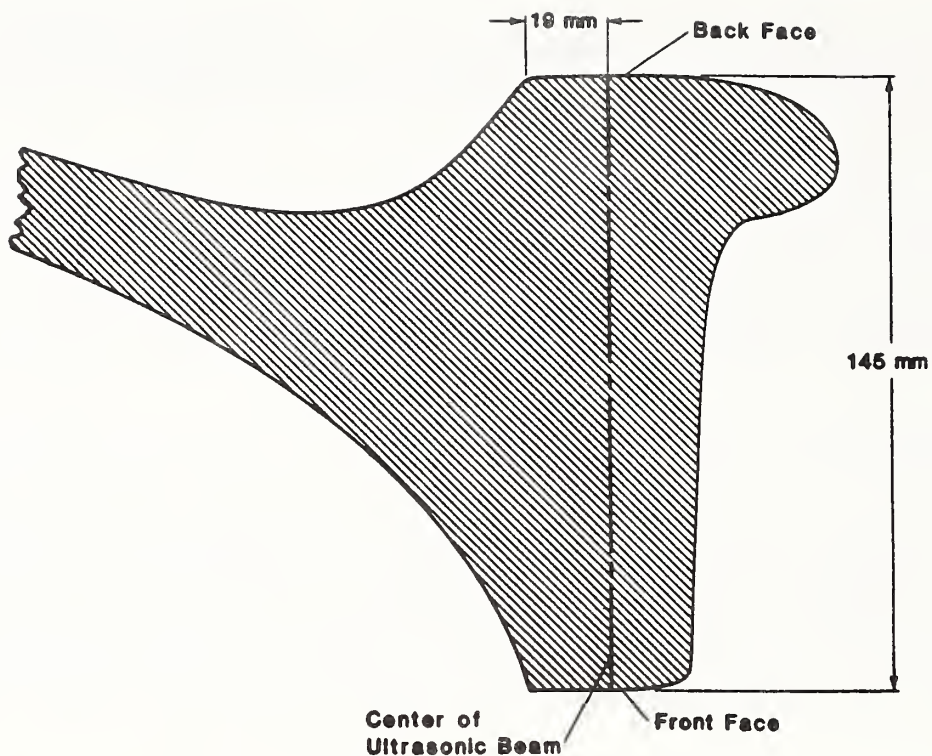


Fig. 1. Cross-section of rim, of cast steel railroad wheel. Transducers placed on back face; center of ultrasonic beam shown as broken line.

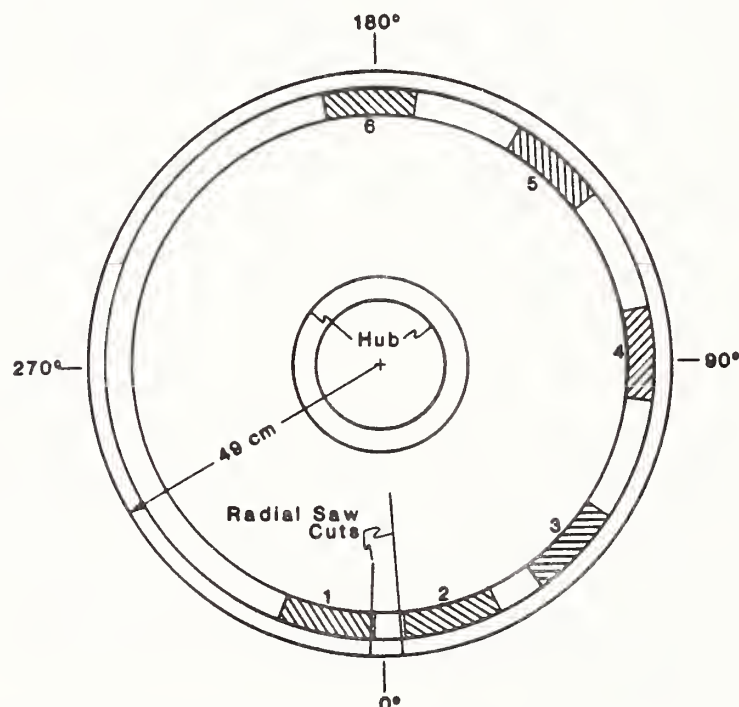


Fig. 2. Top view of sawcut wheel. Shaded regions correspond to areas where back face of rim was milled.

We were able to measure B_0 for the wheel as the mean value of the birefringence measured on both sides of the sawcut. Knowing B_0 we could convert the birefringence measurements to stress. We used the same value for the stress-acoustic constant C_A (-7.6×10^{-6} /MPa) that was used in Refs. 3,4 and subtracted B_0 from B to obtain $\sigma_\theta - \sigma_r$ (see equation 2). Results obtained are shown in Fig. 4 for both transducers.

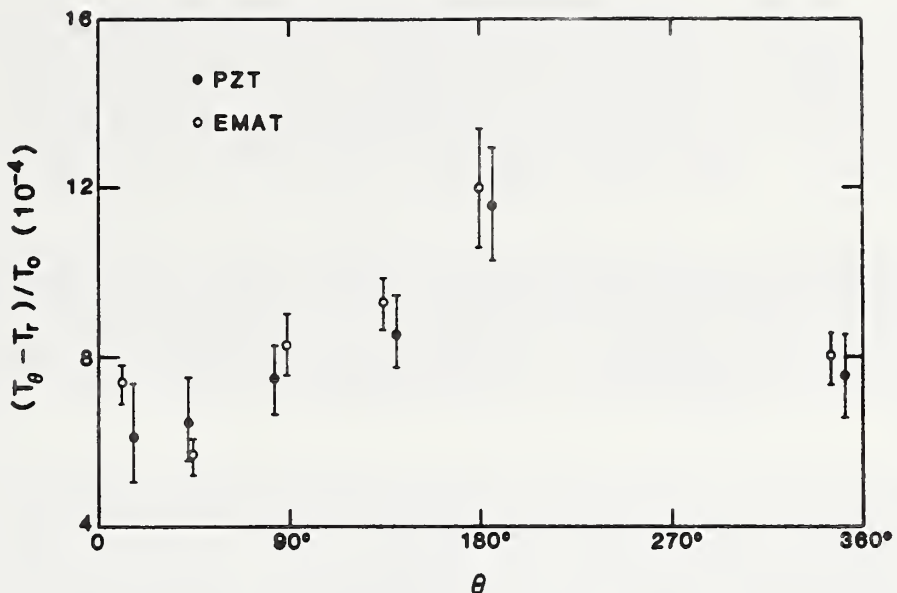


Fig. 3. Birefringence as function of circumferential position.

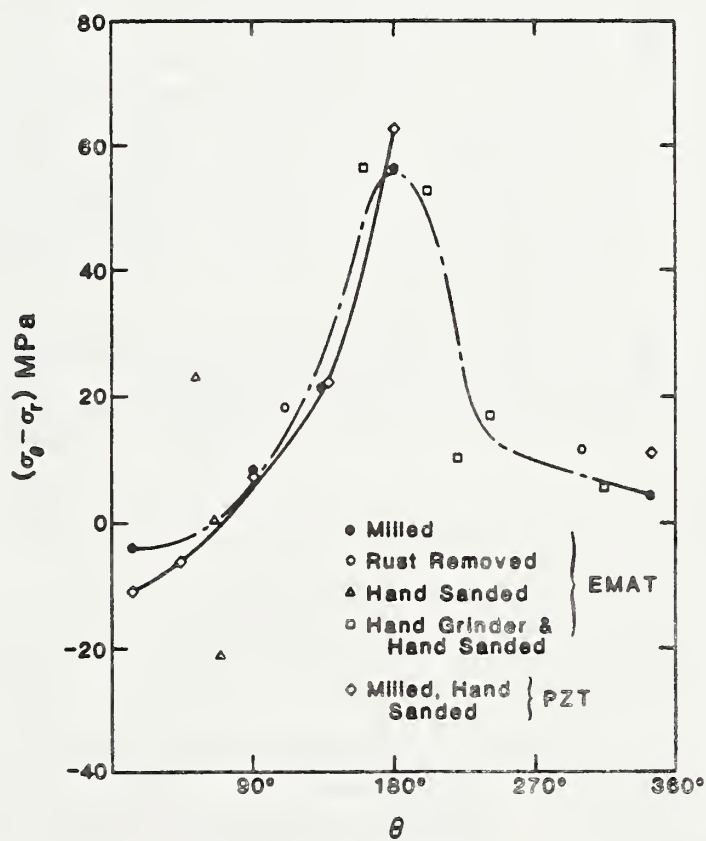


Fig. 4. Principal stress difference as function of circumferential position.

There are several interesting features in this figure. First, there is good agreement between EMAT and PZT results. In fact, the difference of peak stress measured with the different transducers is less than 10 MPa.

Second, the peak stress occurs at 180° circumferentially around the wheel from the sawcut. This is in qualitative agreement with results obtained by researchers at Transportation Test Center [6]. They found that sawcutting relieved the stress near the cut but left the stress 180° from the cut almost unchanged.

Third, the EMAT results are almost symmetric about 180° (the line opposite the sawcuts). In fact, if the residual stresses and the degree of texture were homogeneous, one would expect $\sigma_\theta - \sigma_r$ to display this symmetry after sawcutting. The symmetry of the EMAT results is encouraging, since it does indicate that the residual stresses and the texture were axisymmetric prior to sawcut. This reduces the number of required measurements around the rim of the wheel.

With the EMAT we made measurements not only on the milled regions, but also at other locations where we used various surface preparation treatments. The results obtained using the EMAT on these variously prepared surfaces are indicated by different symbols in Fig. 4. Qualitatively, it appears that the degree of surface preparation is not particularly significant for EMAT measurements.

A second set of birefringence measurements was made with both an EMAT and PZT transducer on an uncut cast steel wheel which had been heat treated and air quenched. This process results in a grain structure which is finer than in cast steel wheels and consequently shows a better signal-to-noise ratio in ultrasonic measurements. Measurements were performed on the front face of the wheel, which is the side accessible in the field.

To characterize the effect of surface preparation we made measurements at the center of the front face of the rim and for varying degrees of surface preparation. Results of these measurements at different circumferential locations are shown in Fig. 5. For comparison we also have shown results obtained by the PZT transducer on a milled surface at the same locations. There is a good agreement between results obtained by EMAT and the PZT transducer. The difference in EMAT birefringence measurements for different surface preparations is usually less than 2×10^{-4} . This is equivalent to a stress uncertainty of about 25 MPa, assuming a value of -7.6×10^{-6} /MPa for the stress-acoustic constant, C_A .

The good agreement between EMAT measurements on surfaces with varying degrees of surface preparation is quite encouraging. From a practical point of view, it minimizes the amount of time or labor necessary to prepare the surface.

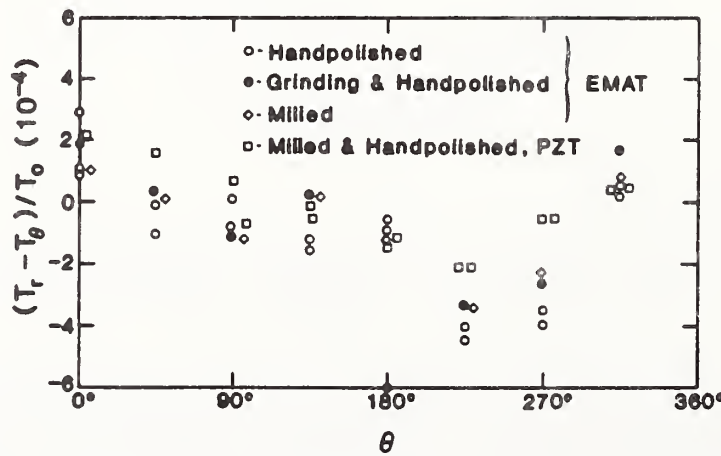


Fig. 5. Effect of surface preparation on birefringence measurements.

We were also interested in determining whether there is a radial variation of birefringence. (In fact, a radial dependence of birefringence was found by Fukuoka, et al. [3,4] on rolled steel wheels, using the PZT transducer). We measured the birefringence at 5 different radii, at 4 different circumferential positions (marked as 0° , 90° , 180° and 270°). Both EMAT and PZT measurements were made after the wheel was milled.

The results of the birefringence measurement at different radii are shown in Fig. 6. The data points are the mean value of measurements at 4 circumferential positions, and the error bars represent the standard deviation. The birefringence has a gradient, becoming increasingly negative as the outer edge of the rim is approached. The gradient as measured by the EMAT is almost linear and, assuming a constant texture, it has value of about 6 MPa/mm.

In the ideal case, both the texture and residual stress would be axisymmetric. If this is the case, then the standard deviations of B shown in Fig. 6 would vanish. The presence of the standard deviations (which are larger than experimental errors) implies that there is some asymmetry in the birefringence. To show this asymmetry better, we have plotted the birefringence as a function of circumferential position in Fig. 7, with the radial distance (from center of the rim) as a parameter.

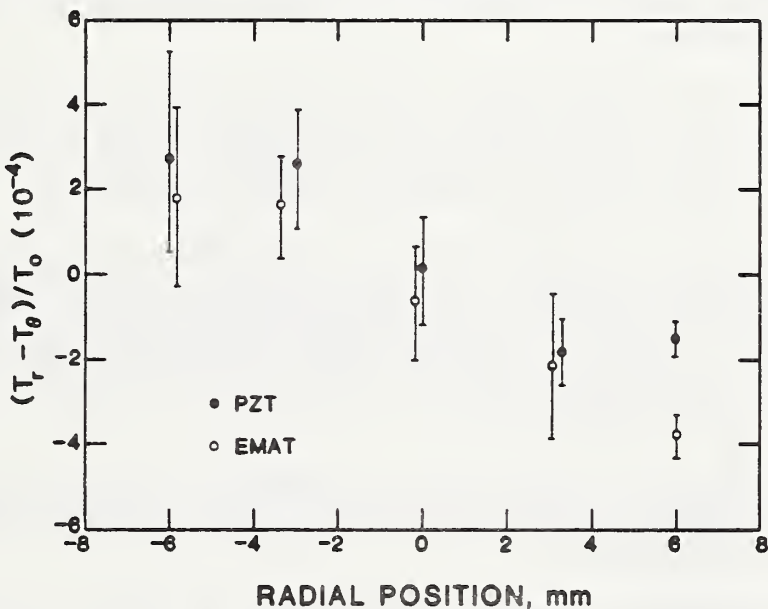


Fig. 6. Radial variation of birefringence.

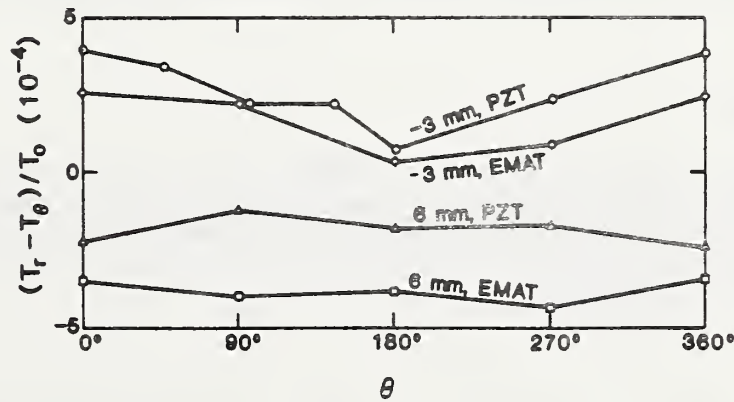


Fig. 7. Birefringence as function of circumferential position, for radii of +6 mm, -3 mm. Radial position measured outward from center of front face of rim.

For axial symmetry, the birefringence would be a straight line with zero slope (constant as function of circumferential position). The data in Fig. 7 for the radius -3 mm from center of the rim show a departure from axial symmetry with a minimum algebraic value of B in the region about 180° (with good agreement between an EMAT and a PZT measurements). On the other hand, the values of B for +6 mm from the center of the rim show not only good agreement for both transducers measurements but also a behavior which is very close to axial symmetry.

CONCLUSIONS

We have performed proof-of-concept experiments which show that EMATs can be used to characterize residual stress in cast steel railroad wheels. We have developed a system which measures arrival times with an electronic precision of ± 1 ns, for pulse-echo operation.

The birefringence was measured on two railroad wheels with different microstructure. The cast steel wheel had a sawcut, which enabled us to measure B_0 and hence convert our birefringence measurements to stress. We found good agreement between piezoelectric and EMAT results (stresses agreed to within 10 MPa). We also found that the EMAT was somewhat insensitive to surface preparation.

On the heat-treated wheel, we characterized this sensitivity and found that the scatter in EMAT results due to surface preparation was equivalent to about 25 MPa. This indicates that for practical use (e.g. in a railroad yard) only minimum surface preparation may be necessary.

We measured the birefringence on this wheel as a function of both radial and circumferential position. A steep gradient of birefringence in the radial direction was found; if the texture is homogeneous, the gradient was about 6 MPa/mm. Values of birefringence measured with EMAT and piezoelectric transducers were in good agreement, showing that the EMAT could be used to resolve this steep gradient.

The birefringence in the rim was found to be nearly axisymmetric close to the tread (where the wheel sits on the rail) but more erratic as the inner edge is approached.

To determine the accuracy of the method, we plan to perform destructive tests to measure the residual stress. Blocks cut from the rim will be used to measure B_0 . An average value will then be used in equation (5) for ultrasonic predictions of residual stress and comparison made with destructive results.

ACKNOWLEDGMENTS

The work was supported by the Federal Railroad Administration, Department of Transportation, under the supervision of Claire Orth, Research Manager. We were greatly assisted by the generous cooperation and encouragement of Mr. Britto Rajkumar of the American Association of Railroads, Pueblo, CO who provided the wheels.

REFERENCES

1. Y. Iwashimizu, Y., and K. Kubomura, Int. J. Solids Structures 9, 99-114 (1973).

2. K. Okada, J. Acoust. Soc. Japan (E) 1, 193-200 (1980).
3. H. Fukuoka, H. Toda, K. Hirakawa, H. Sakamoto, and Y. Toya, "Nondestructive Assessments of Residual Stresses in Railroad Wheel Rim by Acoustoelasticity," to be published in J. of Eng. for Industry, ASME, New York City.
4. H. Fukuoka, H. Toda, K. Hirakawa, H. Sakamoto, and Y. Toya, Acoustoelastic Measurements of Residual Stresses in the Rim of Railroad Wheels, in: "Wave Propagation in Inhomogenous Media and Ultrasonic Nondestructive Evaluation," AMD-Vol. 6, G. C. Johnson, ed., ASME, New York City (1984).
5. A. V. Clark, H. Fukuoka, D. V. Mitrakovic, and J. C. Moulder, "Characterization of Residual Stress and Texture in Cast Steel Railroad Wheels," to be published in Ultrasonics.
6. B. Rajkumar, Transportation Test Center, American Assoc. of Railroads, Pueblo, CO, private communication.

Characterization of residual stress and texture in cast steel railroad wheels

A.V. Clark, Jr, H. Fukuoka*, D.V. Mitraković† and J.C. Moulder

Fracture and Deformation Division, National Bureau of Standards, Boulder, CO 80303, USA

Received 20 May 1986

Residual stress and texture were characterized in the rim of a cast steel railroad wheel, using both an electromagnetic acoustic transducer (EMAT) and a piezoelectric transducer. Orthogonally polarized shear horizontal waves were propagated through the thickness of the rim, and arrival times measured (by the pulse-echo method) with a precision of $\approx 10^{-5}$. The difference in arrival times (birefringence) is related to the difference in principal stresses and also to texture. The wheel had been sawcut in a previous experiment and the residual stress had been relieved at the sawcut. The birefringence was measured at the sawcut and subtracted from the birefringence measured at stressed regions. This allowed us to map variations in stress around the circumference of the wheel. Stresses measured with the EMAT and piezoelectric transducer agreed to within 10 MPa.

Keywords: stress; texture; steel; EMATs; transducers

The presence of residual stress in railroad wheels can be a significant factor in wheel failure. These residual stresses have two origins: 1, stresses due to fabrication of the wheel and 2, in-service stresses induced by drag braking. For cast steel wheels (the most common type in the US) fabrication stresses occur as the wheel cools in the mould; differential shrinkage gives rise to thermal strains (and stresses). If these stresses are above yield stress (for the corresponding temperature), then inhomogeneous plastic deformation results. Residual stresses are then necessary so that compatibility is satisfied; e.g. so all regions of the wheel fit together without voids.

The same process that creates residual stresses on cooling also occurs (in reverse) during braking. The heat input into the tread of the wheel (region in contact with the rail) causes expansion of this region of the wheel, especially the rim. Each volume element of the rim tries to expand but is constrained by its neighbours. Consequently, thermal expansion during braking causes a compression; if these compressive stresses exceed yield stress, inhomogeneous plastic deformation results. As the wheel cools after braking, a tensile hoop stress may result to make all the regions of the rim 'fit together'.

Residual stresses due to casting will probably be compressive, whereas those due to excess braking will probably be tensile. If the latter stresses exceed the former, then the rim will be in a state of net tensile stress. Consequently, if a crack occurs in the rim, these tensile stresses can act as crack-driving forces and lead to wheel failure.

*NBS guest worker, on leave from Osaka University, Osaka, Japan

†NBS guest worker, on leave from University of Belgrade, Belgrade, Yugoslavia

It is highly desirable to have a non-destructive testing method for measuring such residual stresses. One promising technique which has been investigated is the acoustic birefringence technique. It can be shown both analytically and experimentally that the presence of stress in metals induces a small velocity change (acoustoelastic effect). Subject to certain restrictions, the difference in velocity of orthogonally polarized shear horizontal (SH) waves will be proportional to the difference of principal stresses. This normalized difference in velocities is called the acoustic birefringence, in analogy to the birefringence effect in photoelasticity.

Piezoelectric SH wave transducers have been used to measure the residual stress state in Japanese rolled steel wheels^{1,2}. The birefringence was measured in the as-received state (residual stresses due to rolling), after drag braking (additional stresses due to thermal expansion), and after cutting into blocks (stress relieved). The total residual stress (measured ultrasonically) was compared with destructive measurements; the two agreed to within 40 MPa^{1,2}.

In this Paper, we present results of a study on the feasibility of using ultrasonics to characterize residual stress states in cast steel wheels of US manufacture. We were interested in using electromagnetic acoustic transducers (EMATs) for these measurements.

The EMAT has the advantage that it requires no acoustic couplant to generate sound in a metal (or other conductor). Consequently, an EMAT can be scanned, rotated, etc. over the rim of the wheel with ease. Being non-contacting, it may require less preparation of the surface (where sound is generated) than piezoelectric devices. To determine whether these potential advantages could be realized in practice, we performed a series of experiments

on a cast steel wheel which had been removed from service. We measured the birefringence with an SH wave EMAT using a simple velocity measurement system (described later). Since the birefringence method using piezoelectric transducers had been successful in determining residual stresses^{1,2}, we measured the birefringence using both an EMAT and a piezoelectric transducer. (In fact we used the same transducer as was used in References 1 and 2.) The residual stress, as measured by both devices, was found to be in excellent agreement.

Theory

Stress causes a small change in phase velocity in metals. Consider the case of a homogeneous, isotropic metallic plate in a state of plane stress. Let a pure mode shear horizontal (SH) wave be propagated through the thickness of the plate; the wave is polarized first along the σ_1 (principal stress) axis, and then along the σ_2 axis, with corresponding transit times T_1 and T_2 . The acoustic birefringence, B , is defined as the normalized difference in arrival times and is proportional to the difference in principal stresses

$$B \equiv \frac{T_2 - T_1}{(1/2)(T_2 + T_1)} = C_A(\sigma_1 - \sigma_2) \quad (1a)$$

Since both SH waves travel through the same material thickness

$$B = \frac{V_1 - V_2}{(1/2)(V_1 + V_2)} \quad (1b)$$

where V_1 is the phase velocity of an SH wave polarized along σ_1 and V_2 is the phase velocity of an SH wave polarized along σ_2 .

The magnitude of the stress-acoustic constant, C_A , is rather small, $\approx -7.6 \times 10^{-6}$ MPa for railroad wheels^{1,2}. Consequently, the stress-induced birefringence is also small. In fact, for many common structural elements, there will be unstressed birefringence, B_0 , due to fabrication processes (rolling, casting, etc.) which is the same magnitude as the stress-induced birefringence.

The theoretical problem of an SH wave propagating through a slightly anisotropic body in a state of plane stress has been solved by Iwashimizu and Kubomura³ and also by Okada⁴. For brevity, we repeat only the results of their calculations here. It was found that pure mode SH waves could be propagated only when the waves were polarized along certain directions (also called acoustic axes). These axes were oriented at angle ϕ relative to the axes of material symmetry (to be defined later). ϕ is given by³

$$\tan 2\phi = \frac{2C_A \sigma_{12}}{B_0 + C_A(\sigma_{11} - \sigma_{22})} \quad (2)$$

Here the normal stresses, σ_{11} , σ_{22} , and the shear stress, σ_{12} , are referenced to the material symmetry axes. In the absence of shear stress, the acoustic axes coincide with the material symmetry axes. Plane stresses are assumed in the above.

The birefringence (difference in velocity of SH waves polarized along the acoustic axes) is given by³

$$B^2 = [B_0 + C_A(\sigma_{11} - \sigma_{22})]^2 + (2C_A \sigma_{12})^2 \quad (3)$$

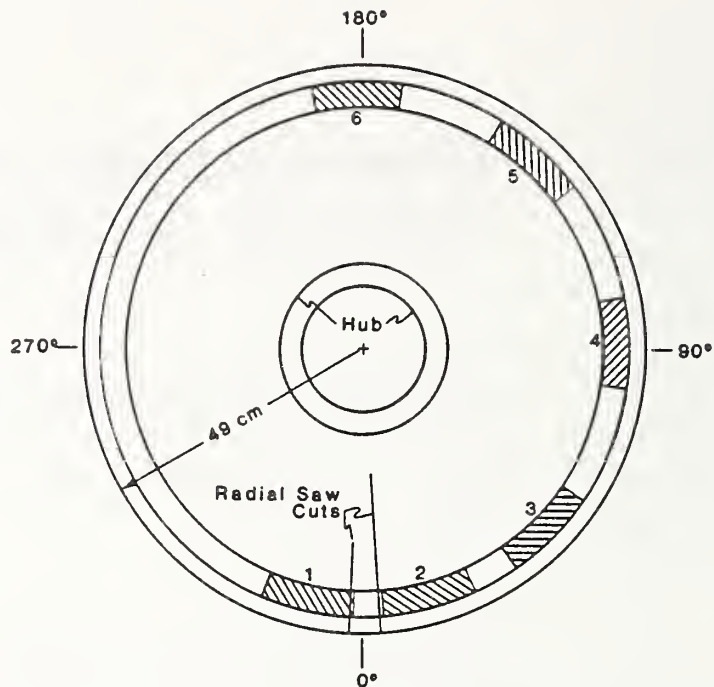


Figure 1 Top view of the sawcut wheel used in the experiments. Shading indicates milled regions 1–6. Angle θ is measured circumferentially around the rim from the midpoint of the sawcuts, in an anticlockwise direction

Note that Equation (3) reduces to Equation (1) when there is no shear stress and no unstressed birefringence.

A discussion of material symmetry axes is in order here. Normally one treats common alloys such as steel and aluminium as isotropic. However, as stated previously, processes such as rolling and casting induce a preferential orientation of the crystallographic axes of the grains (single crystals) which make up the structural elements. It is this anisotropy that gives rise to the unstressed birefringence, B_0 . The directions of the preferential orientation are the material symmetry axes.

The theory which leads to Equations (2) and (3) assumes orthotropic symmetry, i.e. any small volume element of the material has three axes of two-fold symmetry. This assumption works quite well for rolled plates of aluminium and steel alloys. One of the purposes of our experiments was to test its validity for cast steel wheels.

Experimental procedure

Railroad wheel

A cast steel wheel, shown in Figure 1, was obtained from the Department of Transportation (DOT) Test Center in Pueblo, Colorado, USA. This wheel has been removed from service because of the 'four inch rule'⁵ to prevent possible failure due to build-up of residual stresses induced by braking*. (If such stresses are tensile, they become crack-driving forces for any cracks existing in the wheels.) The wheel had been sawcut as part of a test programme being conducted by the American Association of Railroads for the DOT. Consequently, the circumferential (hoop) stress had been relieved at the sawcut. The wheel was milled at several locations on the front and back faces of the rim. The milled locations are

*Simply put, the four inch rule prescribes that if a band of discolouration > 4 in wide forms near the rim, the wheel has to be removed

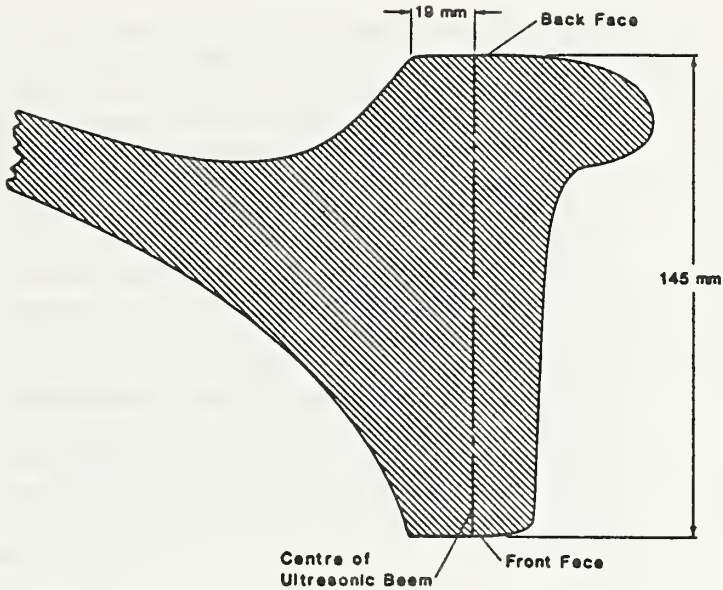


Figure 2 Cross-section of the wheel in the vicinity of the rim. Transducers were placed on the back face of the rim, 19 mm radially outward from the (inner) edge of the rim

indicated in *Figure 1*, and a cross-section of the rim is shown in *Figure 2*. The milling was done to give a smooth surface for coupling acoustic energy from a piezoelectric transducer into the wheel (as described later). No particular effort was made to make the milled surfaces plane parallel.

In addition, other locations around the circumference of the wheel were cleaned by a variety of techniques. Some locations were merely hand-sanded to remove surface rust, leaving large pitted areas on the surface. Others were ground with a hand grinder, and then sanded. This was done to characterize the effect of surface preparation on the velocity measurements made with electromagnetic acoustic transducers (EMATs). All measurements were made with the centre of the transducer aperture 19 mm from the inner edge of the rim, as shown in *Figure 2*.

Velocity measurement system

A simple time-interval averaging system was used for birefringence measurements. The set-up used with the EMAT is shown in *Figure 3*. The essentials of the operation are as follows. When the pulser excites the transducer, it also excites a time-interval probe which generates a TTL pulse which sends a start signal to a counter. The counter runs at 100 MHz clock rate until it receives a stop signal. To suppress the effect of noise (a significant problem with EMAT operation), the counter can be set to average many such time intervals. We typically used an average of 10^3 such intervals.

We wished to avoid dependence of arrival time measurements on signal amplitude. This was accomplished as follows. The received signal was amplified by a broadband receiver, followed by a high-pass filter to remove any variations in d.c. level with amplifier gain. The signal was then input to the stop probe, which generates a TTL pulse when the signal reaches a selected threshold. In order to make arrival time measurements insensitive to amplitude variations, the threshold level was set to 0 V. The output of the probe was input to a specially constructed digital delayed gate (DDG), described in more detail in the Appendix. In essence the DDG accomplishes the same purpose as a distortion-free analog gate, but does so by using logic circuit electronics.

The stop probe will, of course, generate a signal each time the voltage level reaches zero. Since the EMAT system has a low signal-to-noise ratio, it is necessary to eliminate the stop probe output pulses which correspond to those zero crossings generated by noise (rather than the echo received by the transducer). Typically, we set the delay on the DDG so that its output corresponded to a selected zero crossing in the RF echo waveform.

Velocity measurements with EMATs

The wheel was placed in a horizontal position. Since the EMAT contained a permanent magnet, no fixture was necessary to keep it in place. Measurements were made in the pulse-echo mode, with the transducers (both EMAT and piezoelectric) placed on the back face of the rim. The EMAT has an aperture 1×1 cm and was excited with a quasimonochromatic tone burst having a frequency of 2.8 MHz. Arrival times were measured with the EMAT polarized in the radial (r) and circumferential (θ) directions. For the cast steel wheel used here, only the first echo was useable for these measurements; the signal-to-noise ratio was too small for the second echo and further echoes could not be distinguished from noise on the scope trace.

Our measurements were conducted in close proximity to a welding laboratory and a laboratory equipped with mechanical testing machines (a noisy RF environment). Nevertheless, the precision in arrival time measurements made with our time-interval averaging system was ± 1 ns (or better). Since the arrival time of the first echo was ≈ 90 μ s, our (electronic) precision is of the order of 10 ppm. This was achieved with a signal whose amplitude (after amplification) ranged from ≈ 200 to ≈ 800 mV (zero to peak).

We observed that the signal amplitude varied with orientation. In fact, the peak amplitude was about twice as large for an SH wave polarized in the radial direction as in the circumferential direction. Consequently, it is essential that the stop signal to the counter be triggered by a TTL pulse (from the stop probe) which corresponds to a zero

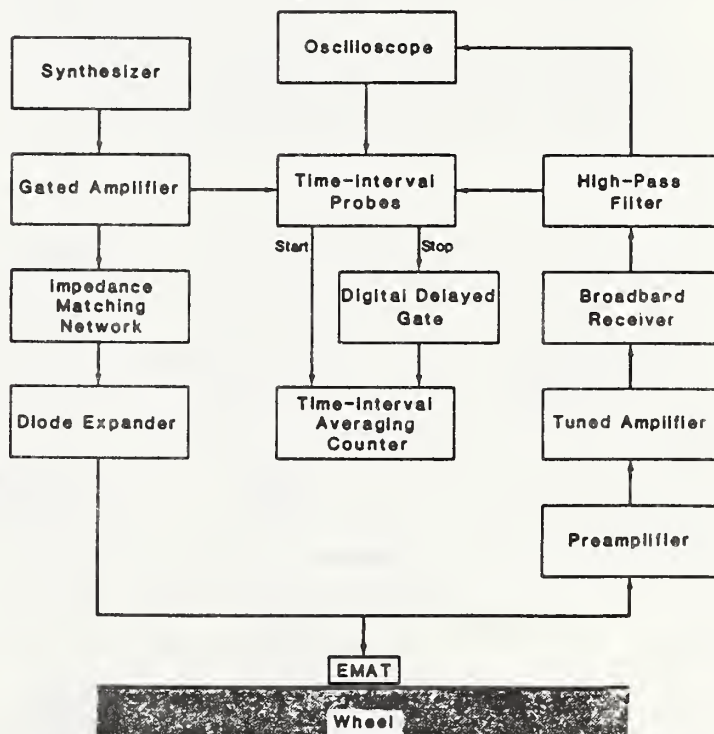


Figure 3 Time-interval averaging system used for EMAT measurements

crossing (phase = $2n\pi$) in the received RF waveform (first echo).

The permanent magnet in our EMAT has a rotationally symmetric magnetic field. This is important, since it avoids the possibility that magnetic hysteresis effects could cause variations in the efficiency of converting electromagnetic energy into acoustic energy as the EMAT is rotated. We also observed an increase in signal strength when the EMAT was left in a given location for several hours. This is probably due to an increase in magnetic induction caused by the permanent magnet. (The amplitude of the acoustic signal is proportional to the magnitude of the applied magnetic induction in the skin depth of an electromagnetic wave incident on the wheel.)

Relative velocity (birefringence) measurements were made with the EMAT polarized first in one principal stress direction (e.g. radial direction) and then in the orthogonal direction. This operation was repeated at least three times, since it was observed that arrival time measurements at the same location with the same orientation exhibited a scatter typically of the order of ≈ 5 ns. The arrival times in each orientation were averaged, and the differences (of the two averages) were taken to give the birefringence

$$B \equiv \frac{\langle T_r \rangle - \langle T_\theta \rangle}{1/2(\langle T_r \rangle + \langle T_\theta \rangle)} \quad (4)$$

where $\langle T_\theta \rangle$ is the average arrival time of the SH wave polarized in the circumferential direction and $\langle T_r \rangle$ is the average arrival time of the SH wave in the radial direction.

We attribute the scatter in arrival times to variations in the coupling between the EMAT and wheel surface. Even though EMATs are non-contacting devices, there are effects of lift-off (distance between EMAT and surface). One effect is, of course, a decrease in the amplitude of the acoustic signal generated by the EMAT. A second (usually smaller) effect is a phase shift (in frequency space) or an equivalent delay in the time domain. One explanation for this phenomenon is as follows. Consider the equivalent circuit for the EMAT. This consists of the inductance of the EMAT coil plus a complex impedance due to the electromagnetic field set up by the EMAT in the skin depth of the conductor beneath it⁶. This impedance consists of a resistance (eddy current resistance) plus an inductance. The impedance (in frequency space) has been

shown to be a function of lift-off⁶, so variations in lift-off will give variations in arrival times.

Variations in lift-off come from two sources in our experiments. At locations which have not been milled, there are pits remaining on the surface. Since the EMAT is not precisely registered each time it is placed on the surface, the effective lift-off varies from one placement to another.

The other source of lift-off is caused by the construction of the EMAT itself. A copper shield is placed over the front of the EMAT. The shield has an aperture 1×1 cm cut in it. (This is done to obtain a linearly polarized SH wave.) The copper shield is not flat but has small bulges which must be flattened out by a (small) force applied to the case which houses the EMAT. To apply a constant force, we usually placed a weight on top of the EMAT case. This partially succeeded in reducing lift-off variations, but still left the previously mentioned spread of ≈ 5 ns in arrival times.

Velocity measurements with piezoelectric transducers

We wished to compare our EMAT measurements with those performed using conventional piezoelectric transducers. We used a specially constructed device (fabricated at Osaka University, Japan) which consisted of two transducers of PZT. The transducers were orientated so that they generated orthogonally polarized SH waves, and then one transducer was bonded on top of the other. Leads were arranged so that either the top or bottom transducer could be separately excited by means of a switch.

A powder backing made of copper and epoxy was bonded to the upper transducer to act as an acoustic absorber and increase the bandwidth of the device. A small piece of rubber was bonded to the backing material. Even if the axis of the device is not normal to the wheel surface, the transducers will have enough freedom to rotate so that they are at a tangent to the surface.

The piezoelectric transducer was spring loaded to ensure a constant pressure on the viscous couplant which was used to couple a shear wave into the wheel. The device which housed the transducer and the spring was mounted on the wheel with a stand which had a magnetic base.

The electronics used to drive this stacked transducer device were different from those used to drive the EMATs; compare Figures 3 (EMAT) and 4 (PZT). The reason for using two different arrangements is as follows. With the PZT device, the waveforms generated by the upper and lower transducer are different. The upper transducer is 'loaded' on its front face by the lower transducer, whereas the lower transducer is 'loaded' on its front face by the wheel. When using the gated amplifier (shown in Figure 3), we could not identify corresponding zero crossings in the waveforms generated by the lower and upper transducer. Consequently, we used a single pulser which shock excited the PZT transducers. By properly tuning an impedance matching device connected between pulser and transducers it was possible to obtain clearly identifiable features in the waveforms generated by each transducer and identify the corresponding zero crossings.

We found that (for the same receiver gain) the signal received by the upper transducer was always smaller than that of the lower transducer. Furthermore, the waveforms generated by the transducers were not purely sinusoidal. We attempted to compensate for this by changing the receiver gain so that the peak signal amplitude was the same in both waveforms.

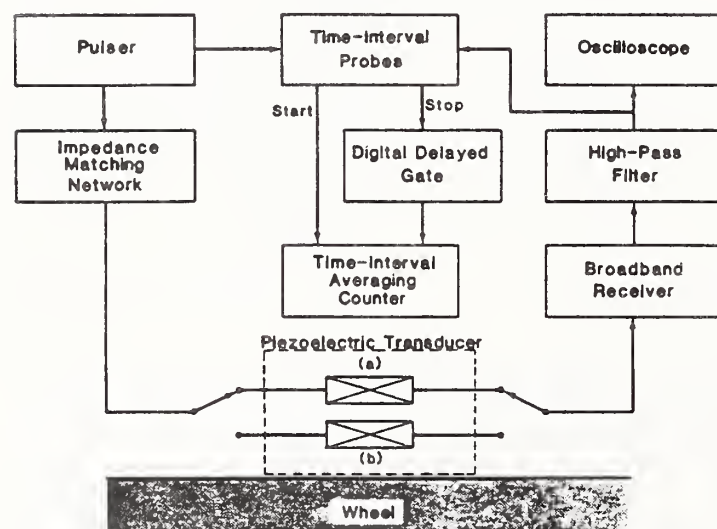


Figure 4 Time-interval averaging system used for PZT transducer measurements. (a) Upper transducer; (b) lower transducer

We used the following procedure. The signal received by the lower transducer usually had a peak amplitude of ≈ 400 mV with the (variable) receiver gain set to zero[†]. Consequently, the vertical amplifier on the oscilloscope was first set on 200 mV per division and then taken out of calibration and adjusted until the peak of the waveform was two (large) units above the ground level (with the scope operating in the d.c. mode, rather than a.c.). The switch (shown in Figure 4) was then operated so that the signal from the upper transducer was received and displayed on the scope with the (uncalibrated) gain on the vertical scope amplifier unchanged, and the variable gain on the receiver was changed until the peak waveform for the upper transducer reached the same level on the oscilloscope (two large units) as that of the lower transducer. We found that this procedure seemed to result in the minimum shift in apparent arrival time with gain (≈ 20 ns).

Using this procedure is a somewhat arbitrary choice, since we noted a change in apparent arrival time with receiver gain. In fact, we would expect some differences in birefringence as measured with the EMAT and the PZT transducer. With the EMATs excited by a toneburst, zero crossings correspond to zero phase in the echo. For shock excitation of the PZT transducers, which do not have a purely sinusoidal response, zero crossings do not necessarily correspond to zero phase, since a change in gain caused a change in time of zero crossing. In fact, we expect some systematic errors, δt_θ and δt_r , in PZT arrival time measurements. However, if we use a consistent arrival time measurement procedure, we expect that the difference between birefringence measured by EMAT and PZT will be constant. The results of our measurements seemed to bear this out, as will be shown subsequently.

One advantage of the design of this stacked transducer is that couplant thickness variations are eliminated. Both transducers generate SH waves which propagate through the same couplant thickness. The arrival time of an SH wave in the upper transducer will, of course, be increased by twice the time an SH wave requires to propagate through the lower transducer. To compensate for this, the arrival times for both transducers were first measured with the lower transducer polarized in the radial direction, then the (stacked) transducer was rotated 90° and the new arrival times measured. The birefringence was calculated from

$$B \equiv 1/2[(T_r^l + T_r^u) - (T_\theta^l + T_\theta^u)]/T_0 \quad (5)$$

where superscripts *l* and *u* refer to the lower and upper transducers, respectively, e.g. T_r^l is the arrival time measured with the lower transducer polarized in the radial direction. T_0 is the average of all arrival times.

Results

Texture study

The theory of acoustoelasticity, which led to the relations of Equations (2) and (3), was based on the assumption of orthotropic symmetry^{3,4}, which usually occurs in rolled plates of aluminium and steel alloys. Since we are dealing with a cast steel wheel, it was necessary to characterize the texture (preferred orientation) to see whether the theories of References 3 and 4 could be applied to our wheel. It has been observed that for a slightly orthotropic rolled plate,

[†]The receiver has a fixed gain of ≈ 30 dB, plus a variable gain

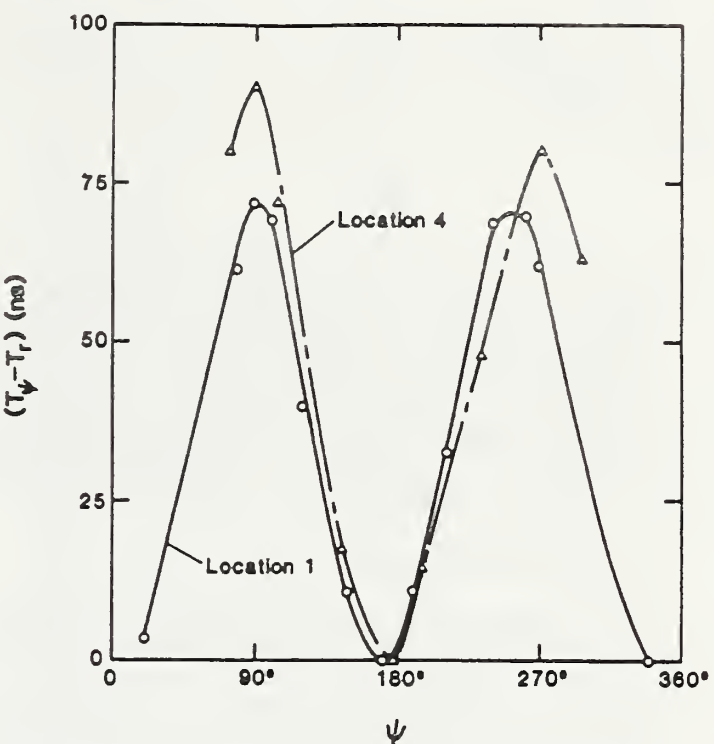


Figure 5 Angular variation of arrival times for unstressed region (—) and stressed region (— —) of sawcut wheel. Angle ψ is measured anticlockwise; $\psi = 0^\circ, 180^\circ$ when measuring T_r ; $\psi = 90^\circ, 270^\circ$ when measuring T_θ

the measured arrival time of an SH wave (propagating through the plate at normal incidence) varies in a sinusoidal manner⁷. The maximum and minimum arrival times are obtained when the transducer is polarized along the acoustic axes. (For a treatment of the theory behind this effect, see Reference 7).

We measured the angular variations of arrival times in the sawcut wheel. Locations 1 and 2 on the wheel (adjacent to the sawcuts) experienced a relief of hoop stress. We used our EMAT to measure the arrival time variation at location 1 as the transducer was rotated. The result is shown by the solid line in Figure 5. The velocity is fastest for a wave polarized in the radial (*r*) direction and slowest for the wave polarized in the circumferential (*θ*) direction.

To be sure that the acoustic axes are oriented along radial and circumferential directions at stressed locations in the sawcut wheel, we also measured the angular variation of arrival times at location 4 (see Figure 1). This location was 90° around the wheel circumference from the sawcuts: hence, the residual stress there should not be completely relieved by the sawcuts. The angular variation of arrival times at location 4 is shown as the broken line in Figure 5. The data show that the radial and circumferential directions are still acoustic axes for stressed locations. Consequently, a necessary condition for the application of the theory of References 2 and 3 has been satisfied.

Furthermore, we see that the radial and circumferential directions still appear to correspond to the fast and slow acoustic axes, respectively. The material symmetry axes still coincide with the principal stress axes, and from Equation (2) the shear stress, $\sigma_{\theta\theta}$, vanishes. The birefringence Equation (3) becomes

$$B - B_0 = C_A(\sigma_\theta - \sigma_r) \quad (6)$$

for the cast wheel.

The unstressed birefringence, B_0 , was measured at locations 1 and 2 (on either side of sawcuts). The values were slightly different at each of the two locations, and

Table 1 Values of unstressed birefringence

Location	Transducer	$B_o \times 10^{-4}$
1	PZT	7.6
2	PZT	6.2
1	EMAT	8.1
2	EMAT	7.4

were different for EMATs and the PZT transducer (see Table 1). We took the average of the unstressed birefringence measured at locations 1 and 2 as the value of B_o to be used in Equation (6). For the PZT measurements, we have $B_o = 6.9 \times 10^{-4}$, for the EMAT, $B_o = 7.8 \times 10^{-4}$. The difference between these values may be due to the way arrival times are measured with the EMAT and PZT transducers, as described previously.

Birefringence measurements

The birefringence was measured at the milled regions 1–6, using the PZT transducer. The milled surface was ≈ 18 cm long (arc length) at each region (see Figure 1). We measured B at least three times at each milled region. The birefringence was measured near the centre of each milled region. The values of birefringence thus obtained are plotted in Figure 6. The vertical axis actually equals $-B$ since we defined B by $B = (T_r - T_\theta)/T_o$. The error bars represent the standard deviation of the (three or more) measurements of B at each of the six milled regions.

Also shown in Figure 6 are the results of EMAT measurements on the milled surfaces. With the EMATs, we measured B at three separate locations on each milled region and at locations ± 25 mm from the centre. Consequently, B was measured at a total of 18 locations. At each location, we measured B at least three times. We took the average of all measurements at a given milled region (nine or more) as the value of B ; we measured at the centre of the milled region. This tends to minimize any (local) variation in B_o , remembering that $B = B_o + C_A(\sigma_\theta - \sigma_r)$.

Values of B thus obtained are in good agreement with PZT values. Note that the PZT values are usually lower than EMAT values; this 'd.c. shift' is due to the difference in the way arrival times are measured with the two different transducers. Furthermore, the shift is about the same as the difference in B_o as measured with the EMAT and the PZT transducer.

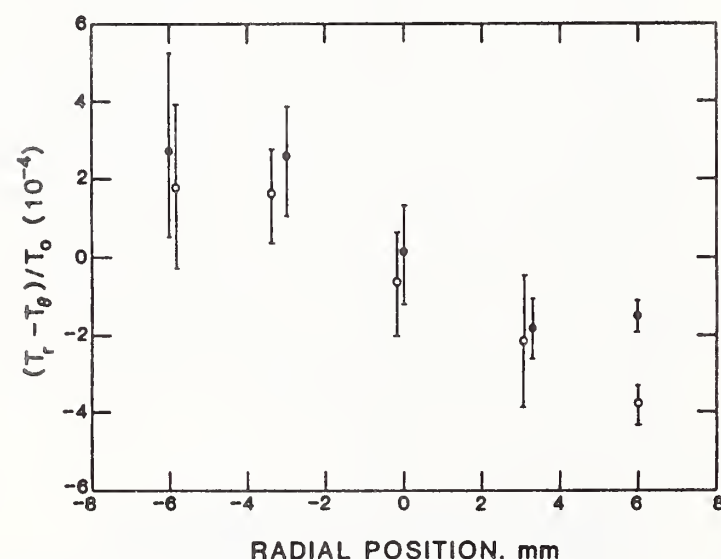


Figure 6 Birefringence measurements made on rim of sawcut wheel, using both the EMAT (○) and PZT (●) transducer

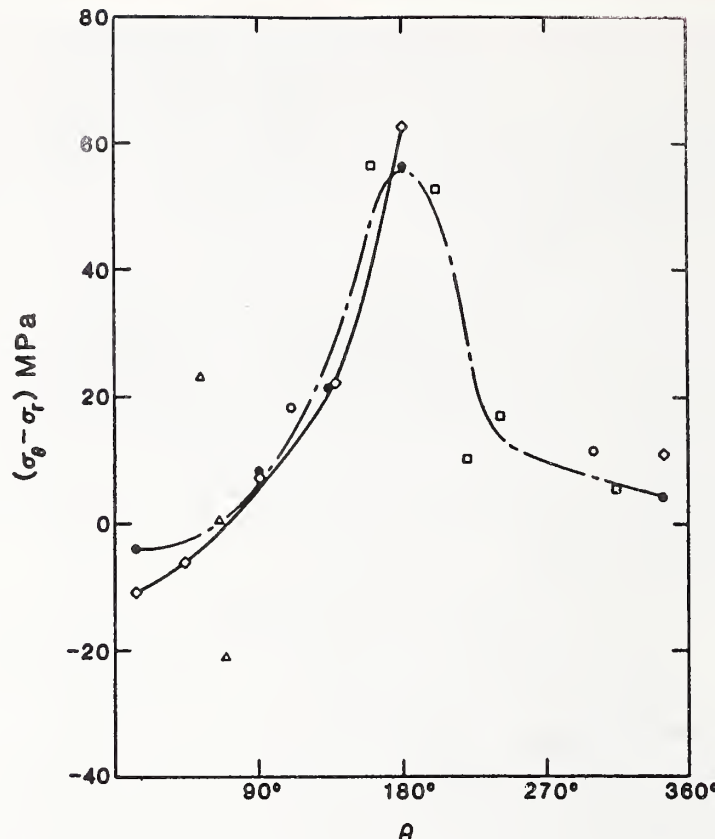


Figure 7 Differences in principal stresses measured on the rim of the sawcut wheel, using both the EMAT and PZT transducer. The EMAT measurements were made using a variety of surface preparations: ●, milled; ○, rust removed; △, hand sanded; □, hand ground and hand sanded. ◇, PZT, milled and hand sanded

Stress measurement

Since we were able to measure B_o for the wheel (due to the sawcut), we can convert the birefringence measurements to stress. We used the same value of the stress-acoustic constant, $C_A = -7.6 \times 10^{-6}$ MPa, that was used in References 1 and 2 and subtracted B_o from B to obtain $\sigma_\theta - \sigma_r$ [see Equation (6)]. The results obtained are shown in Figure 7 for the EMAT and PZT.

There are several interesting features about this figure. First, notice that the peak stress occurs at 180° circumferentially around the wheel from the sawcuts. This is in qualitative agreement with results obtained by researchers at the Transportation Test Centre, USA⁸. There, they found that sawcutting relieved the stress near the cut, but left the stress 180° from the cut almost unchanged. The second interesting feature about Figure 7 is the good agreement between the EMAT and PZT results. In fact, the difference of peak stress as measured with the different transducers is < 10 MPa. This agreement shows that there was indeed a constant difference in birefringence measurements between the PZT and EMAT; since we subtract $B - B_o$ to obtain $\sigma_\theta - \sigma_r$, the differences cancel out.

A third feature of note is that the EMAT results are almost symmetric about 180° (the line opposite sawcuts). In fact, if the residual stresses (due to casting and braking), and the degree of texture were homogeneous, then one would expect $\sigma_\theta - \sigma_r$ to display this symmetry (about 180°) after sawcutting. The symmetry of the EMAT results is pleasing, since it does indicate that the residual stresses and the texture were axisymmetric prior to sawcutting. We hope to check this hypothesis of axial symmetry by measurements on an uncut wheel.

For the EMAT, we made measurements not only on the milled regions but also at other locations where we used various surface preparation treatments. At some locations, we merely removed a layer of rust with abrasive paper leaving a surface consisting of both bright metal and pits. At other locations, we used a hand grinder followed by hand sanding with abrasive paper. The resulting surface was smoother, but still contained pits. At other locations, we used only abrasive paper, but sanded for a longer time than when merely removing rust. The surface finish was intermediate between the rust-removed surfaces and surfaces cleaned with a hand grinder.

The results obtained using the EMAT on these various surfaces are indicated by different symbols in *Figure 7*. Qualitatively, it appears that the degree of surface preparations is not particularly significant as far as EMAT measurements are concerned. For instance, the EMAT data from 0 to 90° agrees quite well with PZT data, except for two points which are off the PZT curve. However, even these points are only out by 25 MPa. For 180–360°, the EMAT data is, as mentioned above, approximately the mirror image of the data from 0 to 180° (symmetry about the 180° line).

We expected systematic errors, δt_θ , δt_r , in PZT measurements of arrival times. The effect of these errors appears to have cancelled out in taking the difference $B - B_o$ to obtain stresses, since the EMAT and PZT measurements of $\sigma_\theta - \sigma_r$ are in good agreement.

Conclusions

We have developed a simple time-interval averaging system which allows us to measure arrival times with a precision of ± 1 ns or better, using SH waves propagating through the rim of a cast steel railroad wheel. This precision was obtained with a PZT transducer and also with an EMAT, both operated in the pulse-echo mode.

We used our EMAT to measure the variation in arrival times on regions next to the sawcut in our wheel. For these cases, the hoop stress (assumed much larger than the radial stress) vanished, so differences in arrival times are due to texture induced by casting the wheel. We found that when the SH wave was polarized in the radial direction, it had the fastest arrival time: the slowest arrival time occurred for polarization in the circumferential direction. Furthermore, the arrival time displayed an approximately sinusoidal variation with polarization angle. This satisfies a necessary condition for the wheel texture (averaged through the rim thickness) to be orthotropic. The material symmetry axes for the rim appear to be oriented in the thickness, radial and circumferential direction.

This allows us to use the current theories of acousto-elasticity, which assume orthotropic symmetry^{3,4}. The birefringence is related to stress through Equation (3). The angle ϕ between pure mode polarization directions (acoustic axes) and the material symmetry axes is related to stress through Equation (2).

We measured the angular variation of arrival time at a stressed location and again found that the fastest and slowest arrival times occurred for SH waves polarized along the radial and circumferential directions, respectively. Since the acoustic axes still correspond to the material symmetry directions ($\phi = 0$), Equation (2) shows that there is no shear stress ($\sigma_{\theta r} = 0$). The relation between birefringence and stress can be simplified to

$$B - B_o = C_A(\sigma_\theta - \sigma_r) \quad (6)$$

To obtain the hoop stress, σ_θ , (assuming negligible σ_r) we

must first obtain the unstressed birefringence (which is due to casting induced texture). We were able to do this for the sawcut wheel by measuring the birefringence on either side of the sawcuts (locations 1 and 2). We did this with both the EMAT and PZT transducer and found a small difference ($\approx 1.0 \times 10^{-4}$) in B_o as measured by the two transducers.

We measured the birefringence at different locations around the circumference of the wheel. To avoid damage to the PZT transducer, we had certain regions of the rim milled and then hand polished. We measured B at these regions (1–6) with both types of transducers and found that the EMAT values were usually slightly larger than the PZT values ($\approx 1.0 \times 10^{-4}$). We also measured B at other locations with just the EMAT. The rim was subjected to various kinds of surface preparation at these locations. We did this so that we might characterize the relation between quality of EMAT measurements and degree of surface preparation.

Finally, we converted our values of $B - B_o$ to hoop stress, and compared the EMAT and PZT results. We found that the peak stress occurred at the 180° position (opposite the sawcuts), as expected. The peak stress as obtained by the EMAT was within 10 MPa of the stress obtained by the PZT transducer. We also obtained good agreement at the other milled locations as well. The stress displayed a high degree of symmetry about the 180° position, indicating that the texture is axisymmetric, and that the hoop stress was axisymmetric before sawcutting. The EMAT results also indicated that reliable measurements of B could be obtained with minimal amounts of surface preparation, e.g. using a hand grinder.

The good agreement between the EMAT and PZT results indicates that in field applications, the former can be used instead of the latter. This is important, since the EMAT requires less surface preparation, operates with a simpler mounting fixture, needs no couplant, and can be easily scanned and rotated. Some of the disadvantages of the EMAT (such as poor signal-to-noise ratio) have been overcome with our system, which uses carefully matched electronics to minimize noise. Furthermore, the time-interval averaging feature of our velocity measurement system allows us to operate in an RF environment which approximates conditions in the field.

Clearly, much remains to be done in the future. We hope to make additional measurements on uncut wheels to determine, for example, whether the stress and texture are axisymmetric. We also will measure the birefringence as a function of radial position. We hope to develop a method of determining B_o on uncut wheels and, finally, to determine σ_θ by ultrasonic results.

Acknowledgements

The work was supported by the Federal Railroad Administration, Department of Transportation, under the supervision of C. Orth, Research Manager. We were greatly assisted by the generous co-operation of Mr Britto Rajkumar of the American Association of Railroads, Pueblo, CO, who provided both the wheel and encouragement. This Paper is a contribution of the National Bureau of Standards and is not subject to copyright.

References

- 1 Fukuoka, H., Toda, H., Hirakawa, K., Sakamoto, H. and Toya, Y. Non-destructive assessments of residual stresses in railroad wheel rim by acoustoelasticity *J Eng Industry (ASME)* submitted for publication
- 2 Fukuoka, H., Toda, H., Hirakawa, K., Sakamoto, H. and Toya, Y.

Acoustoelastic measurements of residual stresses in the rim of railroad wheels, in: *Wave Propagation in Inhomogeneous Media and Ultrasonic Nondestructive Evaluation* Vol 6 (Ed. Johnson, G.C.) ASME (1984)

- 3 Iwashimizu, Y. and Kubomura, K. Stress-induced rotation of polarization directions in slightly anisotropic materials *Int J Solids Structures* (1973) 9 99-114
- 4 Okada, K. Stress-acoustic relations for stress measurements by ultrasonic techniques *J Acoust Soc Jpn (E)* (1980) 1 (3) 193-200
- 5 Association of American Railroad Specification, Interchange Rule 41
- 6 Frost, H.M. Electromagnetic-ultrasound transducer: principles, practice and applications' in: *Physical Acoustics* Vol XIV (Eds Mason, W.P. and Thurston, R.N.), Academic Press, New York, USA (1979)
- 7 Jackson, C.W. Characterization of stressed metals using acoustic shear waves *PhD Dissertation* Stanford University, USA (1984)
- 8 Rajkumar, B. American Association of Railroads, Pueblo, CO, USA, personal communication (1985)
- 9 Clark, A.V. and Moulder, J.C. Residual stress determination in aluminium using electromagnetic acoustic transducers *Ultrasonics* (1985) 23 253-259

Appendix

EMATs have a relatively low signal-to-noise ratio. Consequently, our time-interval probes will often trigger (generate a square wave pulse) on noise as well as on the zero crossings in the echo. It is necessary to reject these spurious pulses when measuring arrival times. On thin aluminium plates, we had found that using an analog gate was a satisfactory solution⁹. However, this solution was found to be unsatisfactory for thick steel sections such as the rim. We therefore adopted the following approach. Rather than gate out the echo and send the gated signal to the probe, we simply gated out the desired probe pulses from the undesired pulses. (The former pulses, of course, correspond to zero crossings in the echo, and the latter to noise.) The gating was accomplished using digital logic circuits rather than analog circuits. This resulted in less

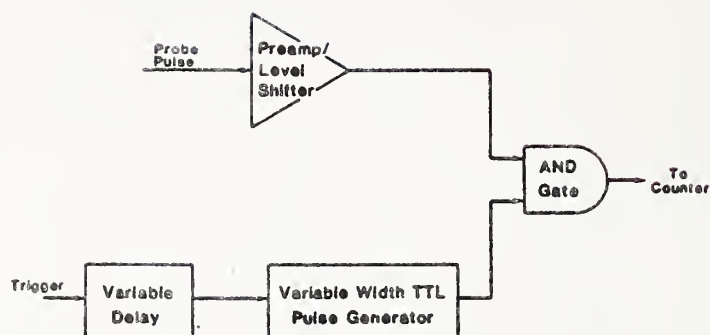


Figure 8 Block diagram of digital delay gate

signal distortion (to avoid changing the apparent arrival time).

The circuits (shown in Figure 8) work as follows. Voltages from the probes were converted from the range -0.5 to +0.5 V to digital logic circuit levels (TTL) by using a fast preamplifier level shifter. The preamplifier had a typical rise time of ≈ 6 ns so that it could follow the rapid rise times of the probe pulses. After a time delay (which we can vary), a 'one-shot' device is triggered. This causes the voltage on one terminal of a logic gate (AND gate) to be at logical level '1' (+5 V). The signal from the preamplifier is input to the other gate terminal. When the probe generates the leading edge of a square wave pulse (and the preamplifier correspondingly generates the leading edge of a TTL pulse), both terminals of the AND gate will be at logical level '1' and the gate output will also be at logical level '1' (5 V). When the probe generates the falling edge of the square wave pulse, the gate output returns to logical level '0' (0 V). Consequently, the AND gate output essentially replicates the probe pulses. The gate output goes to the STOP channel of the counter. The trigger level of the counter can be set to stop the counter when it receives a voltage anywhere in the level -5 to +5 V. We adjusted the trigger level to obtain the optimum precision (better than ± 1 ns) in arrival times.

Review of Progress in Quantitative NDE,
eds. D. O. Thompson and D. E. Chimenti
(Plenum Press, NY, 1988), Vol. 7B,
1661-1668.

FLAW DETECTION IN RAILROAD WHEELS USING RAYLEIGH-WAVE EMATS

R. E. Schramm, A. V. Clark, Jr., D. V. Mitrakovic, **
and P. J. Shull

Fracture and Deformation Division
National Bureau of Standards
325 Broadway
Boulder, Colorado 80303

INTRODUCTION

Early work at the University of Houston [1] showed the efficacy of Rayleigh waves for detecting cracks in the tread of railroad wheels. Development work has been going on at the Fraunhofer Institute in Saarbrucken (IzfP) on an automated system using EMATs that could be installed in a railyard and used in a roll-by mode [2]. A prototype of their system is now operational in Luxembourg.

European railroad wheels are generally forged while U.S. wheels are cast. Also, the IzfP system characterizes flaws in locomotive wheels; our system inspects rolling stock (freight cars). Because the tread and track shapes differ between U.S. and European equipment, the U.S. Department of Transportation Federal Railroad Administration started a program to develop an on-line system for use on American equipment. Our previous work with EMATs has demonstrated their usefulness in generating long-wavelength SH waves to detect and size planar flaws [3,4].

EXPERIMENTAL

Our EMAT transducer was actually a separate transmitter and receiver for pitch-catch operation. As noted in Fig. 1, the transmitter meanderline was a printed circuit on polymer film. The conductor was 1-mm wide and the 6-mm period corresponds to the desired wavelength at 500 kHz. The choice of a five cycle length was based on the curvature of the wheel and the space required to mount the EMAT in the track. The geometry of the receiver coil was identical. This meanderline, however, was laid-up with wire on acetate-based adhesive tape. The enamel coated wire was 0.14 mm in diameter and series-wound through the pattern six times. This multiplicity added to the receiver sensitivity. Both coils were flexible to conform to the wheel shape and achieve the best electromagnetic coupling. We laid these two units atop one another and then shifted them along their length by a quarter period to keep the elements of one from shielding the other.

** NBS guest worker, on leave from the University of Belgrade, Belgrade, Yugoslavia.

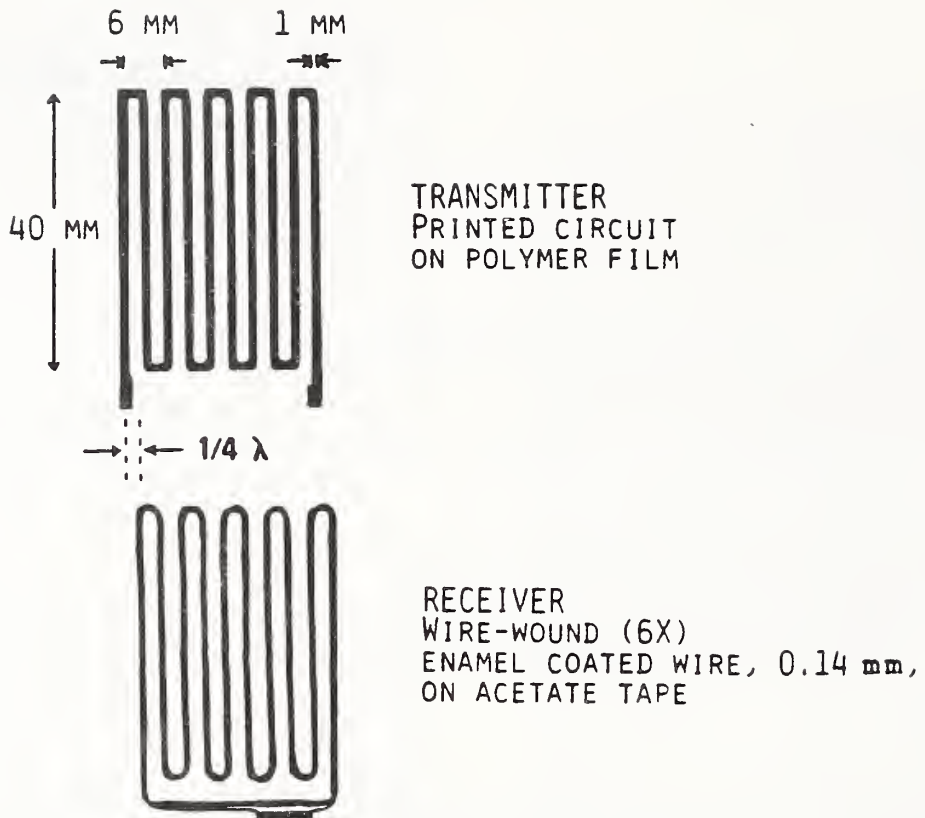


Fig. 1. Configuration of transmitter and receiver meanderlines on flexible substrates. They were placed on top of each other with a $1/4$ wavelength lateral shift to prevent mutual shielding.

Figure 2 is an exploded sideview of the entire EMAT package. The two meanderlines were closest to the wheel (generally with a thin plastic sheet between for mechanical protection of the coils). Next was a thin (about 4 mm uncompressed) flexible polymer foam to allow good contact pressure against the curved tread. The compliance of this foam should also help with the problem of wheel profile changing with wear. The 1-mm thick aluminum sheet had several purposes. It was the pressure plate acting on the coils through the foam layer. The aluminum served as an eddy current shield to prevent any ultrasound generation in the magnet. This sheet was also part of a box which served as mechanical support for the overall system as well as container and handle for the magnet. The single Nd-Fe-B magnet was 52-mm long, 26-mm wide, and 31-mm high. Since the wheel is ferromagnetic, the magnet is strongly attracted and provides considerable pressure to hold the coils tightly against the tread. The field was normal to both the coils and the wheel rim. This transducer is bidirectional, generating or receiving Rayleigh waves traveling in both directions around the tread circumference.

The block diagram in Fig. 3 shows the relatively simple system used for these preliminary measurements. A function generator provides the rf signal for the gated MOSFET power amplifier which drove the transmitter. For these measurements, the input current to the transducer was ten cycles at 500 kHz and limited to 120 A peak-to-peak. (Present system maximum is 140 A.) Careful impedance matching of both coils on the wheel was necessary to ensure maximum efficiency. The preamplifier and amplifier were tuned devices with very low noise capable of maintaining a good signal-to-noise ratio. In the present system, only the function generator and the oscilloscope are commercial devices.

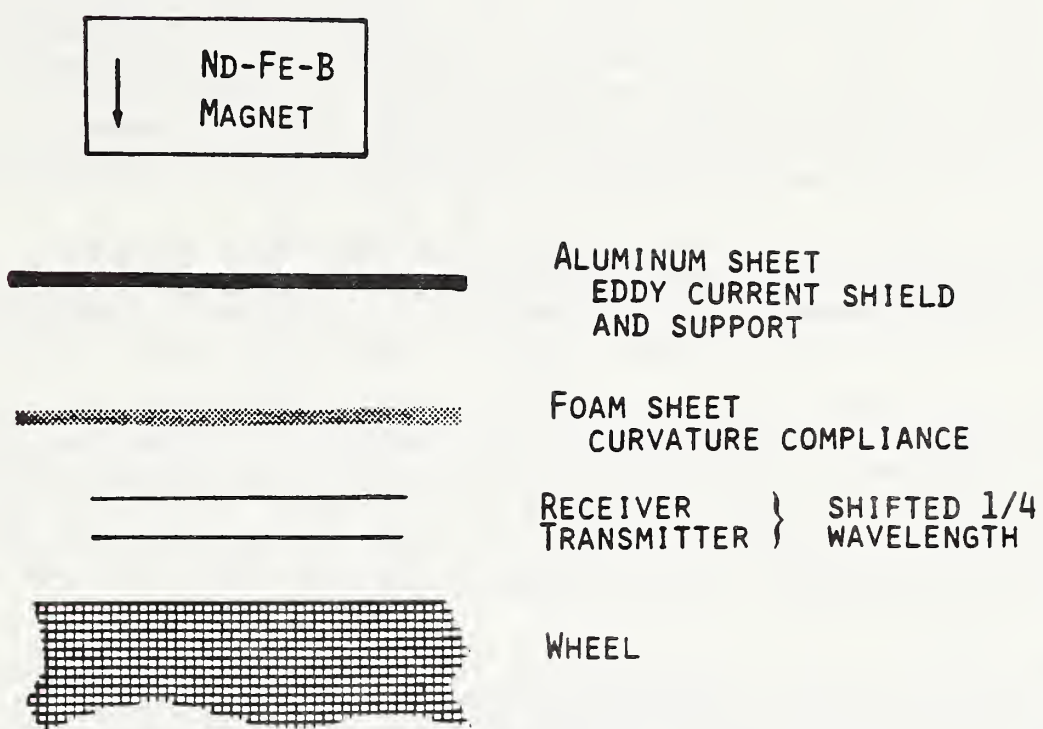


Fig. 2. Exploded sideview showing sequence of transducer parts.

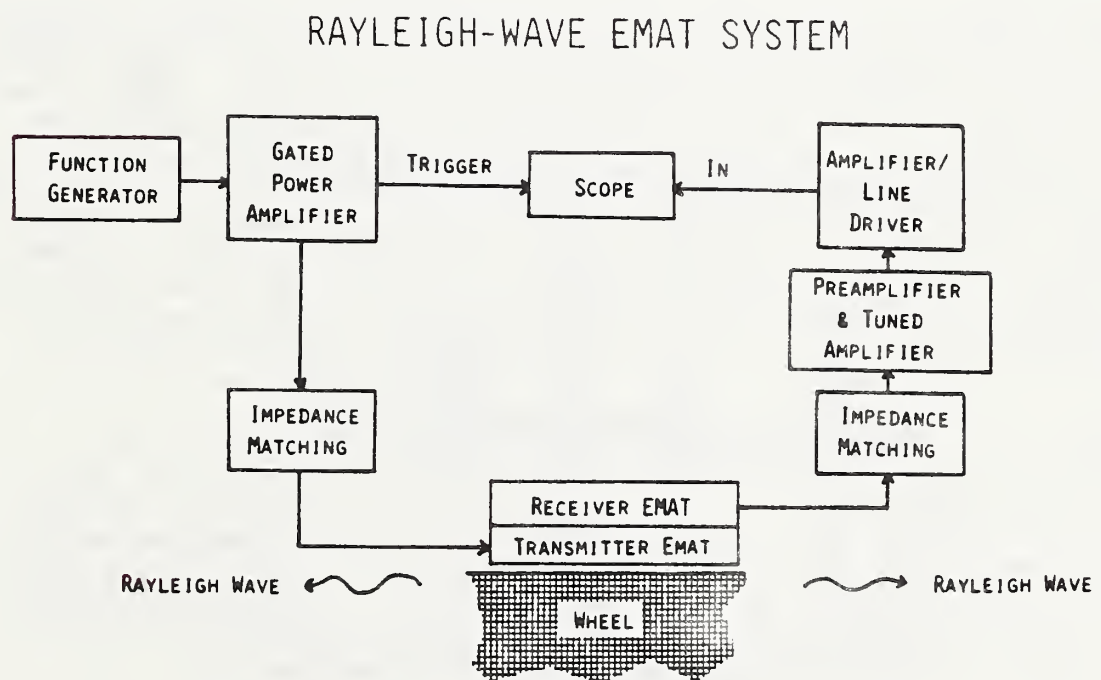


Fig. 3. Block diagram of laboratory system.

RESULTS

To characterize the ultrasonic beam from our EMAT, we cut a shallow circular slot into a flat carbon-steel plate and made several measurements of the signal reflected from this flaw. These involved both translating the EMAT parallel to the slot at 16- and 32-cm separations and also rotating it at the 32-cm location. The results indicated that the beam is about 9 degrees wide (6-dB down points). On repeating the rotational sequence with the transducer turned end-for-end, the results were virtually identical and showed the truly bidirectional nature of this device.

With the EMAT on an unflawed railroad wheel, the signal traveled unimpeded around the rim. It was possible to observe at least 14 round trips before the signal decayed into the noise level. With a wheel circumference of about 2.6 m, this meant we could watch the signal travel more than 36 m.

With a small slot in the rim only 1-mm deep, it was possible to see a distinct reflection. However, the critical cracks for U.S. wheels are about 6-mm deep. Therefore, we are interested in distinguishing between cracks of greater depth (no longer safe) and those of lesser depth (satisfactory for continued use). Accordingly, we sawcut an initial circular flaw into the center of the tread along a wheel radius with a maximum depth of 5.6 mm and a surface length of 38 mm.

While EMATs are non-contact devices, the signal strength does decrease rapidly with any increase in separation from the specimen. Since an inspection system in a railyard would have to cope with a wide range of conditions during actual use, we examined the decrease in the signal-to-noise ratio (S/N) with increasing liftoff (Fig. 4). The signal reflected from the 5.6-mm deep slot does drop dramatically but is still useful even at the 1.5-mm liftoff; probably, 1 mm or less should be possible in practice.

A typical oscilloscope trace taken from the sawcut wheel is in Fig. 5. The first signal, A, is a reflection of the Rayleigh wave which has traveled about 30% of the circumference to the slot and back. Signals B and D have traveled once and twice, respectively, around the entire rim. Signal C is a reflection of the beam which has traveled 70% of the circumference to the slot and back. Since the tread was fairly rusty from exposure while in storage, the transducer coupling varied slightly with location. (Note: after sanding to clean the rust from a small section of tread there was virtually no change in the data.) In railyard usage the tread will likely be bright metal from rolling wear, but other factors such as dirt may cause variations in liftoff. As a consequence, the round-trip signal, B, was used as a normalizing factor, i.e., the measurement parameter was the ratio of the amplitude of flaw signals and first round-trip signal (A/B and C/B).

With a slot depth of 5.6 mm and length of 38 mm, we measured the amplitudes of signals A, B, and C as a function of position on the wheel, moving the transducer in 5-cm steps from one side of the flaw all the way around to the other. The arrival time of signals B and D remained constant; as the distance from the slot increased, signals A and C moved closer to B until they coincided with it at the half-way point. On advancing the EMAT, the signals crossed in arrival time and then receded from B. Obviously, the signal timing indicates the flaw position relative to the probe.

The plot of normalized signal versus EMAT position in Fig. 6a has three very distinct regions. The first section shows a very large negative slope up to about 70 cm. With the beam divergence of 9 degrees noted above, the ultrasonic energy has not spread out to the full tread width of 10 cm until it has traveled 70-80 cm. Therefore, inside this distance the flaw intercepts a very large fraction of this concentrated energy and generates a

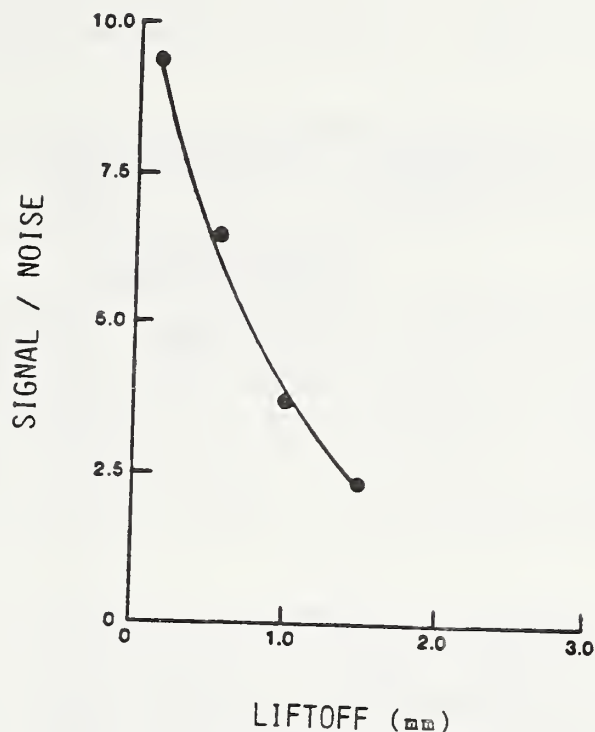


Fig. 4. Signal-to-noise ratio as a function of separation between EMAT and wheel.

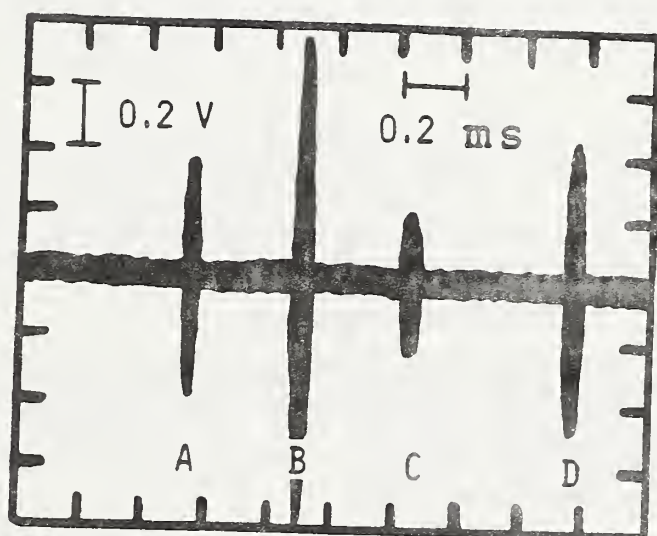


Fig. 5. Typical oscilloscope pattern on wheel. A and C are slot echos. B and D are round trip signals.

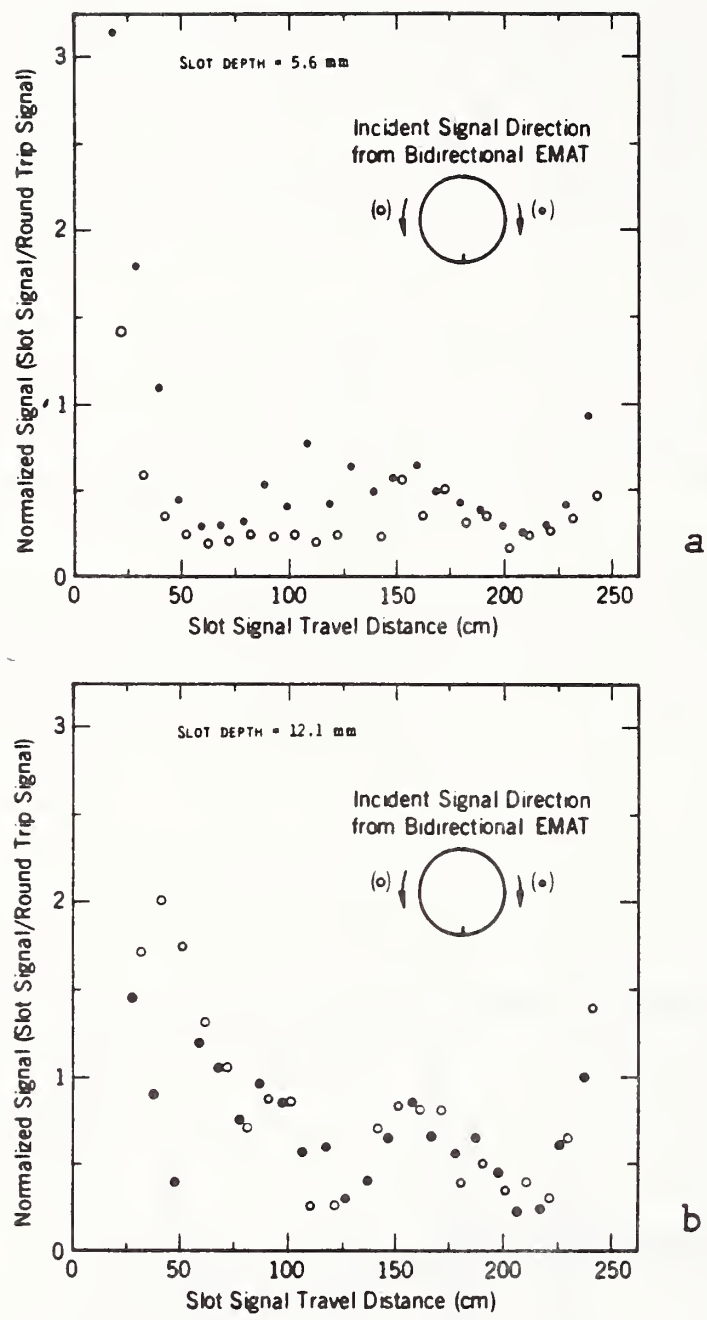


Fig. 6. Signal amplitude as a function of transducer position around the wheel circumference. The slot was located at 0 cm (262 cm).
 a) Slot depth = 5.6 mm.
 b) Slot depth = 12.1 mm.

very large reflection. Once the beam has spread out to full width, the flaw and round-trip signals remain fairly constant until about 225 cm. At this point the flaw again intercepts a large fraction of the ultrasonic beam. The flaw consequently decreases the size of the round-trip signal and causes an increase in the signal ratio.

The signals traveling in the opposite directions should generate the same data. While this trend appears, there does seem to be a slight systematic shift. Possibly there is a slight difference in the smoothness of the two sides of the sawcut slot.

As a next step, we used the same saw blade to enlarge the slot to a depth of 12.1 mm and a surface length of 53 mm. The repeat measurements are plotted in Fig. 6b and the data follow the same basic pattern as in Fig 6a. For the deeper flaw, the initial high-slope section extends to approximately 100 cm. While there seems to be some increase in scatter, the signal level is somewhat higher than for the shallower flaw; i.e., size discrimination does seem possible. In both Figs. 6a and b, there seems to be a local maximum occurring at about 150 cm; we are currently seeking an explanation for it.

To explore the feasibility of mounting a transducer of this general design in a rail, the magnet was placed in a brass box and inserted into a machined recess in a short section of track. With the foam and coils taped onto the box, the track assembly was placed in a position relative to the wheel approximating that expected in service. Even with this crude form of the transducer, the ultrasonic signals approached those seen with the aluminum box mount and without the surrounding ferritic iron. The steel rail does not seem to cause any deterioration in performance due to distortion of the magnetic field. Furthermore, the liftoff between the tread and the track-mounted EMAT does not seem to degrade the signal appreciably.

DISCUSSION

While these results are preliminary, they have been achieved in only a few months. They do indicate that the electronics and this transducer design will generate a strong Rayleigh wave in a cast iron railroad wheel. On the basis of two artificial flaws it appears likely that depth discrimination is possible with a rather simple approach.

Two locations on the circumference, each about 10-cm long, cannot be inspected with the current design. One location is centered right at the transducer and is the result of dead time due to the recovery of the receiver amplifier following the transmitter pulse. Another is exactly half way around the circumference where any flaw signal will coincide with the round-trip signal.

In addition to the signal amplitude, it will be necessary to determine the signal time in order to locate the fault (if desired) and determine which portion of the sizing curve to use. Another possible flaw sizing parameter is the decay rate of the round-trip signals: the deeper the flaw the more rapid the decay.

Some steps remaining to produce a useful system are:

1. Measure additional artificial flaw sizes at various locations across the tread.
2. Inspect real cracks.
3. Determine size discrimination capability.
4. Develop a sizing algorithm for automatic operation.

5. Develop a reliable in-rail transducer mounting system.
6. Determine variability due to wheel position and liftoff.
7. Perform a field test.

ACKNOWLEDGEMENTS

This work was sponsored by the U.S. Department of Transportation Federal Railroad Administration, Washington, D.C. Conversations with H. J. Salzburger of IzfP were an invaluable guide in this work. We also wish to thank the Transportation Test Center, American Association of Railroads, Pueblo, Colo., and, in particular Britto Rajkumar, for advice and also providing test wheels.

REFERENCES

1. D. E. Bray, N. G. Dalvi, and R. D. Finch, *Ultrasonics* 11, 66 (1973).
2. H. J. Salzburger and W. Repplinger, in Ultrasonics International 83, conference organizers Z. Novak and S. L. Bailey (Butterworth & Co. Ltd., Kent, Great Britain, 1983), pp. 8-12.
3. R. E. Schramm and T. A. Siewert, in Review of Progress in Quantitative NDE, edited by D. O. Thompson and D. E. Chimenti (Plenum Press, New York, 1986), Vol. 5B, pp. 1705-1712.
4. R. E. Schramm and T. A. Siewert, *Mat. Eval.* 44, 1136 (1986).

ULTRASONIC CHARACTERIZATION OF RESIDUAL STRESS AND FLAWS IN CAST STEEL RAILROAD WHEELS

A. V. Clark, R. E. Schramm, H. Fukuoka¹, D. V. Mitrakovic²

Fracture and Deformation Division
 National Bureau of Standards
 Boulder, Colorado 80303

ABSTRACT

Two ongoing safety problems in cast steel railroad wheels are the buildup of residual stress in the rim and the growth of cracks in the tread. Electromagnetic-acoustic transducer (EMAT) technology shows promise for the nondestructive evaluation of both. The acoustoelastic effect generates a small but measurable acoustic birefringence in the presence of stress fields, while Rayleigh waves are sensitive to surface disruptions from flaws. Experimental investigations of both problems indicate that these noncontact inspection methods lend themselves to automated use in a railyard.

Residual Stress Characterization

Tensile residual stresses are a significant factor affecting railroad wheel integrity. Should a crack occur in the rim, tensile stresses will act as crack-driving forces and that can lead to wheel failure. Therefore a non-destructive testing method for measuring residual stresses is highly desirable. We present results of a study using ultrasonic methods to characterize the stress state in cast steel railroad wheels.

Stress in metals induces a small sound velocity change. For isotropic materials, the normalized difference in velocity of orthogonally polarized shear-horizontal (SH) waves is proportional to the difference of principal stresses [1, 2]. This normalized difference in velocities is called the acoustic birefringence, B:

$$B = \frac{V_\theta - V_r}{1/2(V_\theta + V_r)} = \frac{T_r - T_\theta}{1/2(T_r + T_\theta)}, \quad (1)$$

where V_θ and V_r are velocities of SH-waves polarized in the hoop and radial directions

respectively, and T_r and T_θ are the respective signal arrival times. For anisotropic (textured) materials, birefringence depends on texture and principal stresses [1, 2]:

$$B = B_0 + C_A (\sigma_\theta - \sigma_r), \quad (2)$$

where B_0 is an unstressed birefringence due to texture, C_A is the stress-acoustic constant and σ_θ and σ_r are principal stresses in hoop and radial directions.

Problems arising in using Eq. 2 for obtaining the difference in principal stresses are: (1) the influence of texture and (2) the small value of stress-acoustic constant ($C_A \sim 10^{-5}$ /MPa). The value of B_0 can be obtained by measurements on unstressed reference samples (provided that the wheels are sufficiently homogeneous). Because of the small value of the stress-acoustic constant, we use electronics capable of measuring arrival times within ± 1 ns in a 90 μ s interval.

We investigated the feasibility of using electromagnetic-acoustic transducers (EMATs) for measurements in the field. The EMAT has the advantage that it requires no acoustic couplant to generate sound in a metal. Consequently, an EMAT can be scanned and rotated over the rim of the wheel with ease. Being noncontacting, an EMAT may require less preparation of the surface (where it generates the sound) than a piezoelectric device.

To determine whether these potential advantages could be realized, we performed a series of experiments on a cast steel wheel. We measured the birefringence with a commercial SH-wave EMAT in a pulse-echo setup using a simple velocity measurement system (described elsewhere [3]). We also measured the birefringence using a piezoelectric transducer. The birefringence method using this piezoelectric transducer has been successful in determining residual stresses in rolled wheels [4, 5]. Consequently, we used results obtained with this transducer as a benchmark against which our EMAT measurements were compared.

To characterize the effect of surface preparation we made measurements for varying degrees of surface preparation. For comparison we also have results

¹NBS Guest Scientist; on leave from Osaka University

²NBS Guest Scientist; on leave from University of Belgrade

Contribution of National Bureau of Standards;
 not subject to copyright

obtained by the PZT transducer on a milled surface at the same locations. There is a good agreement between results obtained by both EMAT and PZT transducers. Also, the change in EMAT birefringence measurements for different surface preparations is usually less than 2×10^{-4} . This is equivalent to a stress uncertainty of about 25 MPa, assuming a value of -7.6×10^{-6} /MPa for the stress-acoustic constant, C_A . The good agreement between EMAT measurements on surfaces with varying degrees of surface preparation is quite encouraging. From a practical point of view, it minimizes the amount of time and labor necessary to prepare the surface.

We were interested in determining whether there is a radial variation of birefringence. We measured the birefringence at five different radii in each quadrant. The results are shown in Fig. 1. The data points are the mean value of measurements at four circumferential positions, and the error bars represent the standard deviation. The PZT and EMAT results are in good agreement. The birefringence has a gradient, becoming increasingly negative as the outer edge of the rim is approached. The gradient is almost linear and, assuming a constant texture, it has a value of about 6 MPa/mm.

To determine the residual stress, it is necessary to know B_0 (see Eq. 2). We cut four sections out of the rim, thereby relieving the geometric constraints and any stresses; measurements were made on these unstressed specimens to obtain B_0 as a function of radial position (Fig. 2). We found that B_0 was more negative than B , at every radial location. Since C_A is negative, we find that the hoop stress (dominant stress) is compressive. This is in qualitative agreement with sawcutting measurements made on this wheel by the American Association of Railroads [6]. Comparison of the stressed and unstressed measurements indicates a high residual stress gradient test is likely due to a high thermal stress gradient which occurred during drag braking.

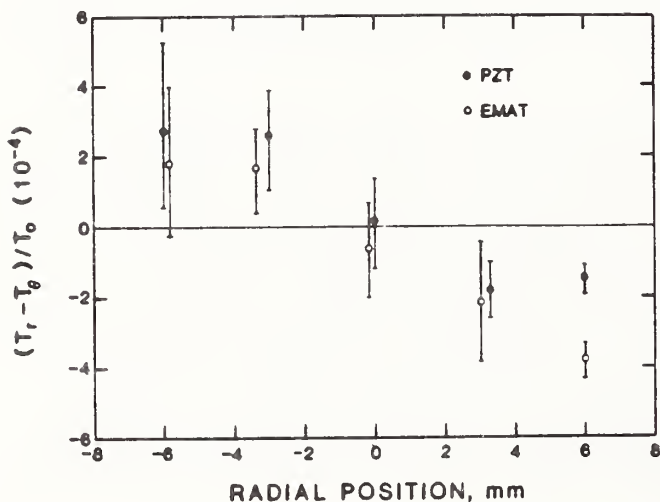


Fig. 1. Birefringence as a function of the radial position on the wheel.

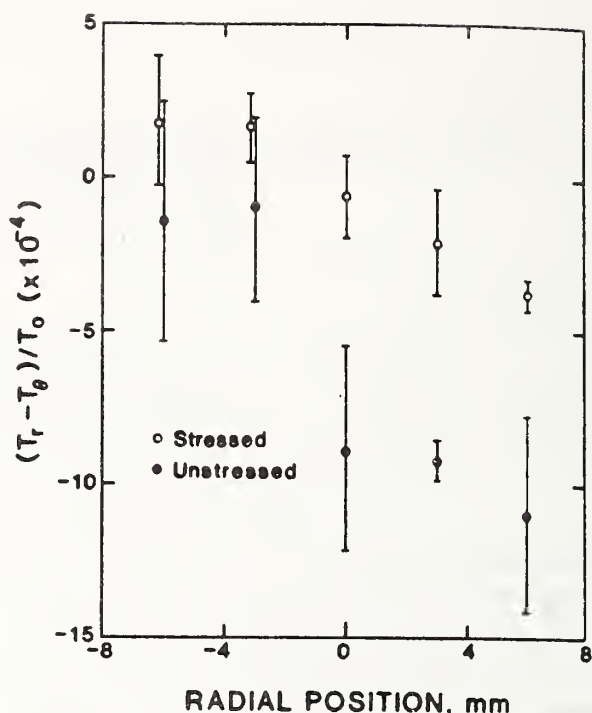


Fig. 2 Comparison of EMAT birefringence measurements on the stressed wheel and on wheel sections cut out of the rim to relieve residual stress.

Flaw Characterization

Railroad wheel flaws include cracks originating at or near the tread surface or in the flange, as well as "shelling" (peeling of the tread surface). We examined the use of Rayleigh-wave EMATs in a pitch-catch mode for possible noncontact wheel inspection.

Development work on a similar system has been going on at the Fraunhofer Institute in Saarbrucken (IzfP) to produce an automated system using EMATs that could be installed in a railyard and used in a roll-by mode [7]. European railroad wheels are generally forged while U.S. wheels are cast. Also, the IzfP system characterizes flaws in locomotive wheels; our system inspects rolling stock (freight cars). Because the tread and track shapes differ between U.S. and European equipment, the U.S. Department of Transportation Federal Railroad Administration started a program to develop an on-line system for use on American equipment.

Our EMAT transducer was a separate transmitter and receiver for pitch-catch operation. The transmitter meanderline was a printed circuit on polymer film with a 6 mm period which corresponds to the desired wavelength at 500 kHz. The receiver coil meanderline was laid-up with wire on acetate-based adhesive tape. The enamel coated wire was series-wound through the pattern six times for greater receiver sensitivity. Both coils were flexible to conform to the wheel shape and achieve the best electromagnetic coupling. We laid these two units atop one another and then shifted them along their length by a quarter period to keep the elements of one from shielding the other [8].

In the laboratory EMAT package, the two meanderlines were closest to the wheel. Next was a thin flexible polymer foam to allow good contact pressure against the curved tread. A 1 mm thick aluminum sheet was the pressure plate acting on the coils through the foam layer. The aluminum also served as an eddy current shield to prevent any ultrasound generation in the magnet. This sheet was also part of a box which served as mechanical support for the overall system as well as container for the single Nd-Fe-B magnet. The field was normal to both the coils and the wheel treads. This transducer is bidirectional, generating or receiving Rayleigh waves traveling in both directions around the tread circumference.

In the electronic system, a function generator provides the rf signal for the gated MOSFET power amplifier which drives the transmitter. The input current to the transducer was ten cycles at 500 kHz and limited to 140 A peak-to-peak. Careful impedance matching of both coils on the wheel was necessary to ensure maximum efficiency. The preamplifier and amplifier were tuned devices with very low noise and so were capable of maintaining a good signal-to-noise ratio.

With the EMAT on an unflawed railroad wheel, the signal traveled unimpeded around the rim. It was possible to observe at least 14 round trips before the signal decayed into the noise level. With a wheel circumference of about 2.6 m, this meant we could detect the Rayleigh wave after it traveled more than 36 m.

A typical oscilloscope trace taken from a saw cut wheel is in Fig. 3. The first signal, A, is a flaw reflection of the Rayleigh wave which has traveled about 30% of the circumference to the slot and back. Signals B and D have travelled once and twice, respectively, around the entire rim. Signal C is a reflection of the wave after traveling 70% of the circumference to the slot and back in the reverse direction from signal A. To account for possible variations due to liftoff (Fig. 4), the signal we used for flaw characterization was the slot reflection (A and C) divided by the round trip signal (B).

As a first test, we examined this normalized flaw signal as a function of the EMAT-flaw distance around the tread. Measurements were made as the transducer was moved circumferentially in 5 cm increments from one side of the flaw to the other (Fig. 5). Signals A and C moved closer to B as the distance increased until they coincided with it when the transducer was directly opposite the saw cut. Signal timing indicates relative flaw position.

The Rayleigh wave EMAT has a directivity pattern with the 3 dB-down points at about $\pm 4^\circ$. This factor leads to the three signal regions apparent in Fig. 5. Up to about 70 cm, the ultrasonic beam had not spread out to the full tread width of 10 cm; this means that the 4 cm long flaw intercepted a large fraction of the energy and produced a large reflection (A). Conversely, as the EMAT approached the flaw from the other side, the slot shielded

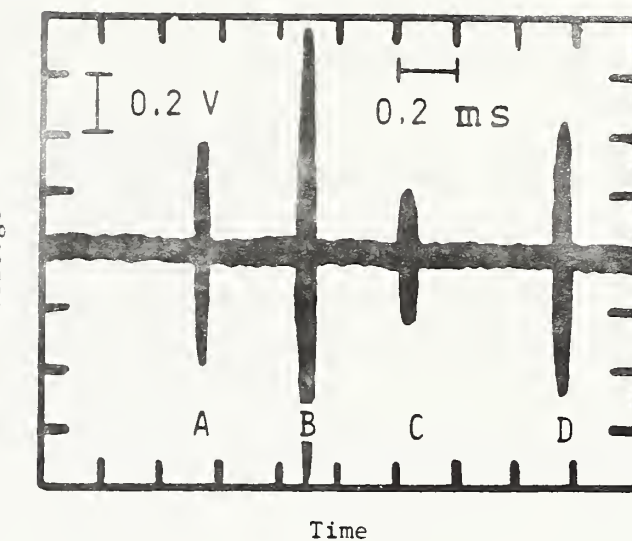


Fig. 3. Typical oscilloscope pattern on wheel. A and C are slot echos. B and D are round trip signals.

much of the round trip energy and gave a small normalizing signal (B). Consequently, on either side of our saw cut, the normalized signal was very large when the transducer was within 70 cm.

The Rayleigh waves traveling in opposite directions should generate the same data. This trend appeared in Fig. 5, but a systematic shift did emerge. Perhaps there was a slight difference in the smoothness of the two sides of the saw cut slot.

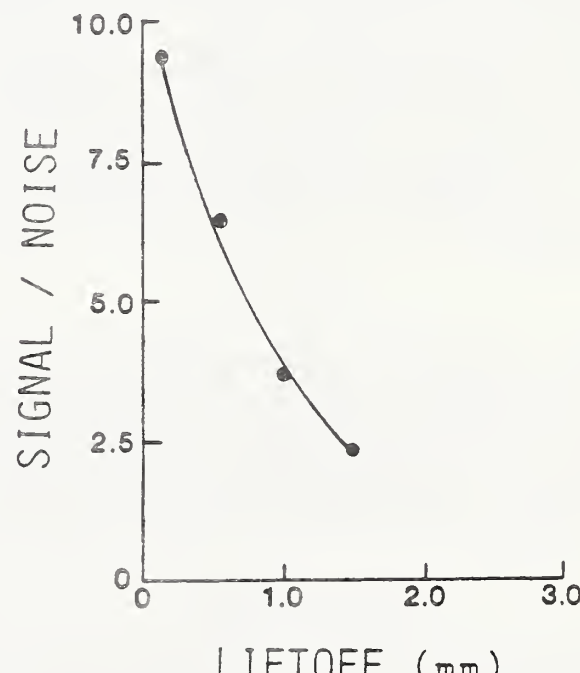


Fig. 4. While the signal/noise ratio drops rapidly as the liftoff increases, it is still useful over a considerable range of separation between the transducer and the specimen surface.

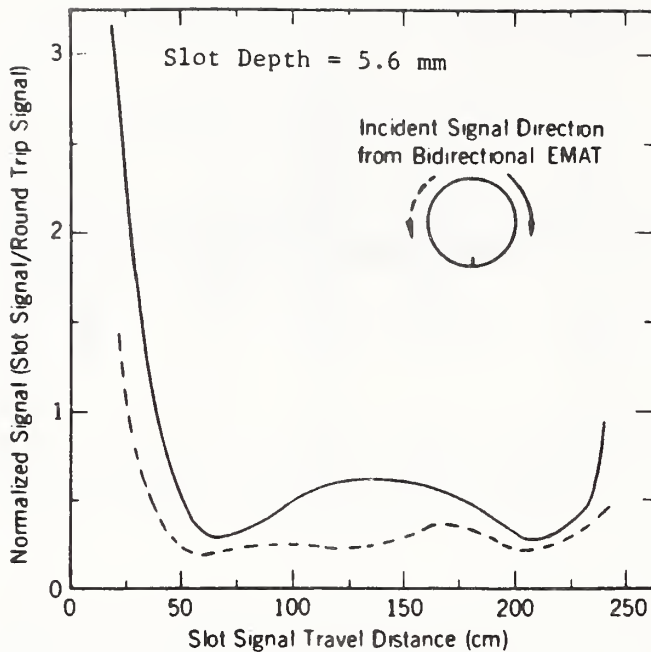


Fig. 5. Signal amplitude as a function of flaw position around the wheel circumference. The simulated flaw was a circular saw cut in the center of the tread at 0 cm (262 cm).

To explore the feasibility of mounting the transducer in a rail, the magnet was placed in a brass box and inserted into a machined recess in a short section of track. With the foam and coils taped onto the box, the track assembly was placed in a position relative to the wheel approximating that expected in service. With this form of the transducer, the ultrasonic signals approached those seen with the aluminum box mount and without the surrounding ferritic iron. The steel rail does not seem to cause any deterioration in performance due to distortion of the magnetic field. Furthermore, the liftoff between the tread and the track-mounted EMAT does not seem to degrade the signal appreciably.

Conclusions

Ultrasonic methods are viable tools for the NDE of important fracture mechanics parameters in railroad wheels. Acoustic birefringence is sufficiently sensitive to determine residual stresses while Rayleigh-wave reflections detect the presence of rim cracks. EMAT systems for field use appear practical.

Acknowledgments

We are grateful for conversations with H.J. Salzburger of IzfP. This work was sponsored by the U.S. Department of Transportation Test Center, American Association of Railroads, Pueblo, Colorado, and, in particular, Britto Rajkumar for advice and test wheels.

References

1. Y. Iwashimizu, Y., and K. Kubomura, *Int. J. Solids Structures* **9**, 99-114 (1973).
2. K. Okada, *J. Acoust. Soc. Japan (E)* **1**, 193-200 (1980).
3. A.V. Clark, H. Fukuoka, D.V. Mitrakovic, and J.C. Moulder, *Ultrasonics* **24**, 281-288 (1986).
4. H. Fukuoka, H. Toda, K. Hirakawa, H. Sakamoto, and Y. Toya, "Nondestructive Assessments of Residual Stresses in Railroad Wheel Rim by Acoustoelasticity," to be published in *J. of Eng. for Industry*, ASME, New York City.
5. H. Fukuoka, H. Toda, K. Hirakawa, H. Sakamoto, and Y. Toya, *Acoustoelastic Measurements of Residual Stresses in the Rim of Railroad Wheels*, in: "Wave Propagation in Inhomogeneous Media and Ultrasonic Nondestructive Evaluation," AMD-Vol. 6, G.C. Johnson, ed., ASME, New York City (1984).
6. B. Rajkumar, *Transportation Test Center, American Assoc. of Railroads, Pueblo, CO*, private communication.
7. H. J. Salzburger and W. Repplinger, in *Ultrasonics International 83*, conference organizers Z. Novak and S. L. Bailey (Butterworth & Co. Ltd., Kent, Great Britain, 1983), pp. 8-12.
8. R.E. Schramm, A.V. Clark, Jr., D.V. Mitrakovic and P.J. Shull, to be published in *Review of Progress in Quantitative NDE*, edited by D.O. Thompson and D.E. Chimenti (Plenum Press, New York, 1988), Vol. 7.

EMAT EXAMINATION FOR CRACKS IN RAILROAD WHEEL TREADS*

R. E. SCHRAMM, P. J. SHULL, A. V. CLARK, JR., D. V. MITRAKOVIC**

National Bureau of Standards
Fracture and Deformation Division
Boulder, Colorado 80303

Submitted to:
Proceedings, Nondestructive
Testing and Evaluation for
Manufacturing and Construction,
Urbana, Ill.
Aug. 9-12, 1988

INTRODUCTION

Cracks in railroad wheels may result from high stresses due to dynamic or static loads and residual stresses generated by such events as heating during braking. These flaws generally originate in the tread surface or flange and can lead to catastrophic wheel failure resulting in considerable equipment damage and possible derailment. This threat to personnel safety and the potential costs in time and money are inducements in the search for an effective, automated method for nondestructive examination that will identify damaged wheels needing replacement.

The current method of examination is visual observation. In the early 1970's, an ultrasonic method was introduced (1-4). This basically involves an in-rail system of piezoelectric transducers generating Rayleigh waves, electronics for signal generation and processing, and a method for tagging suspect wheels. The goal is to examine each wheel of a train as it rolls by a checkpoint in a railyard. There are currently two of these systems in operation in this country. A companion portable handheld system subsequently verifies any flaw indications. The Fraunhofer Institute (IzfP) in Saarbrücken, Federal Republic of Germany, has been developing another ultrasonic system along this line (5) but using electromagnetic-acoustic transducers (EMATs). IzfP has placed a prototype into operation.

Our current research in this area (6, 7) is the development of an ultrasonic system using EMATs designed to work on American-style wheels and rails. The objective is to check every wheel on a train, also in a roll-by mode. Like the earlier works, our system will utilize Rayleigh waves that travel around the wheel tread. We are using EMATs for two main reasons: 1. No ultrasonic path in the transducer itself and low sensitivity to phase-transformed signals mean a simplified, low-noise signal that is relatively easy to interpret with high reliability, even in an automated system; 2. Their non-contact nature eliminates the need for ultrasonic couplants, i.e., no water sprays or liquid-filled boots. Two extensive reviews of EMAT designs and applications have recently been published (8,9).

*Contribution of the National Bureau of Standards and not subject to copyright.

**NBS guest scientist on leave from the University of Belgrade, Belgrade, Yugoslavia.

EQUIPMENT

In the electronic system, a function generator provides the rf signal for the gated MOSFET power amplifier which drives the transmitter. The burst consists of 5-10 cycles at 500 kHz with a pulse repetition frequency (PRF) of 60 Hz. The receiver preamplifier is a very-low-noise design. Impedance matching is very important for both transmitter and receiver to ensure maximum efficiency.

Our EMAT device is designed for insertion into a recess cut out of the rail. Therefore, one goal in the transducer design is to keep the configuration as compact as possible to minimize both the amount of required machining in the rail and the loss of weight-bearing surface. Toward this end, we use a single permanent magnet (Nd-Fe-B for maximum field strength) 32 mm X 26 mm X 52 mm with the magnetization direction along the 32 mm direction and oriented normal to the tread. For pitch-catch operation, there are separate transmitter and receiver coils. These are meanderlines with a periodicity of 6 mm to generate a Rayleigh wave with this wavelength at 500 kHz (velocity = 3 km/s). The two coils are stacked with a slight shift to prevent their shielding each other, and then laid on top of the magnet to contact the wheel tread (Fig. 1). To prevent signal complications from ultrasound production in the magnet, we place a thin foil of copper or aluminum between the coils and the magnet to minimize eddy current generation in the Nd-Fe-B. The original coil design contained five cycles since this length was likely to correspond to the expected length of contact with the curved wheel.

The receiver coil is AWG 36 enamel-coated wire that has been wound through the pattern six times on acetate-based adhesive tape. This multiplicity adds to the sensitivity since the repetitions are series-connected. The flexible tape allows the coil to conform to the wheel's curvature.

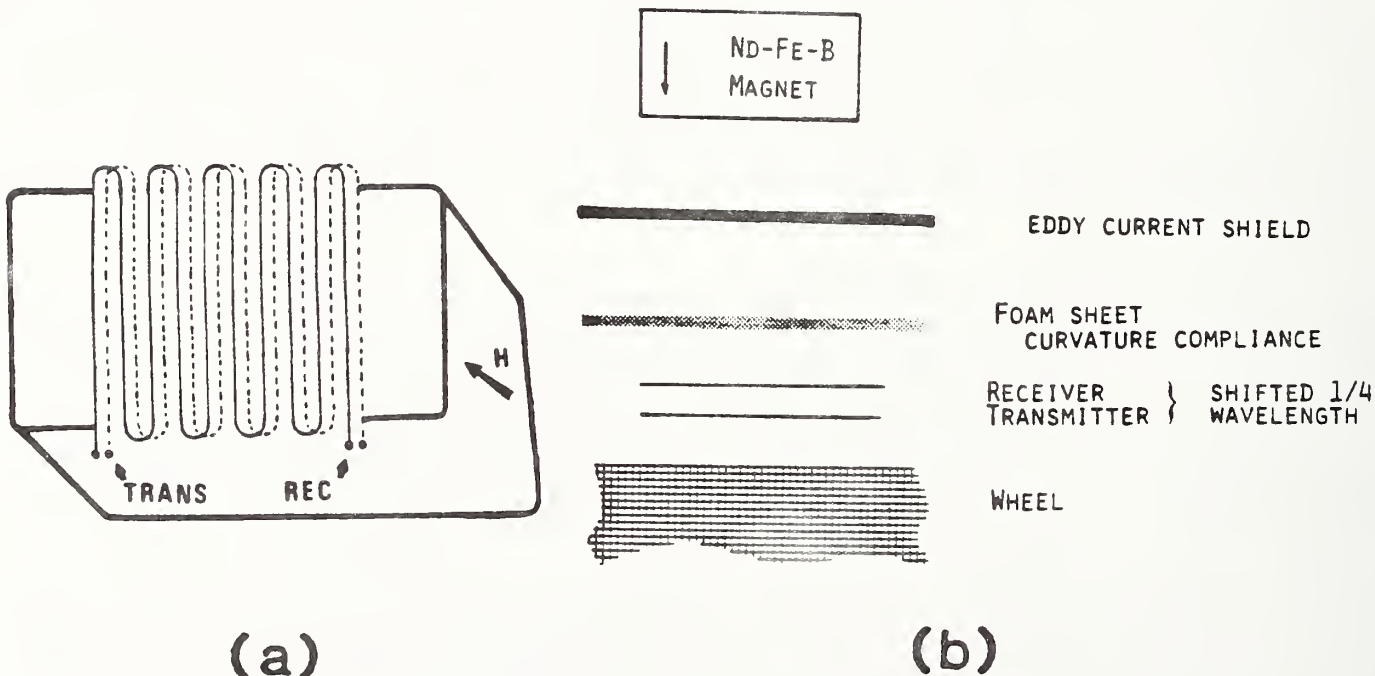


FIGURE 1. Rayleigh-wave EMAT construction.

- (a) Two meanderline coils, shifted to prevent shielding, placed atop a magnet with field H.
- (b) Exploded sideview showing sequence of transducer parts.

The transmitter coil has taken two forms. The first is a printed circuit on polymer film. The conductor is about 1 mm wide and 0.025 mm thick. In this form, the impedance is very low (about 1.3Ω , including a current limiting resistor). Our power amplifier can deliver about 140 A of rf current into this coil. The second form is identical to the wire-wound receiver, and the much higher impedance limits the drive current to only about 30 A.

The greater the current flow through the transmitter, the greater is the eddy current induced in the specimen and the greater is the ultrasound generated. While the printed circuit coil permits the maximum current, the wirewound coil passes the current through the system multiple times and the current density (A/mm^2) induced in the specimen is roughly the same, i.e., the size of our ultrasonic signal is nearly identical. Using the lower current coil will increase the longevity of the power amplifier, and will allow an increase in the pulse repetition frequency (PRF) should this prove desirable later. At present, the limit on the PRF is due to two factors in the power amplifier: ohmic heating of the MOSFET output and the time required to recharge the power supply filtering capacitors.

While EMATs are noncontact devices, their efficiency decreases rapidly with liftoff. To assure the greatest coupling with the curved wheel tread, we have been inserting a few millimeters of compliant material between the magnet and the coil pair. This material compresses under the weight of the wheel and the flexible coil backing assumes the tread shape.

By its design, this transducer should be bidirectional and generate identical sound pulses from both ends of the coil. Their travel direction is normal to the legs of the meanderline. Experimental measurements on a flat steel plate with a saw-cut notch confirmed that this was the case. Translating and rotating the transducer on this same plate indicated that the ultrasonic energy radiates in a beam spreading at about $8-9^\circ$ (using the 3-dB down points). Locating the sensor midway in the tread means that the signal must travel approximately 70 cm before it irradiates the entire width of the tread.

EXPERIMENTAL RESULTS

For the initial wheel measurements, the transducer was mounted in a small aluminum box and moved manually around a stationary wheel. On a used but unflawed wheel, this arrangement produces a signal which is still detectable after 14 round trips or more than 36 m of travel.

A small cut only about 1 mm deep generated a distinct reflection. The critical flaw depth, however, is about 6 mm so our interest is in distinguishing between cracks of greater depth (no longer safe) and those more shallow (safe for continued use). Accordingly, we sawcut an initial circular (half-penny) flaw into the center of the tread along a wheel radius. This flaw depth into the wheel was 5.6 mm at the maximum; the length was oriented along the tread width and 38 mm long at the surface.

In any field measurements, there will be many physical variables that may change the transducer-wheel coupling; among them will be variations in the tread profile due to different degrees and types of wear. Another factor is the taper of the wheel tread, i.e., the tread and the top

surface of the rail are not parallel. The use of compliant material under the coils to allow them to conform to each wheel will minimize any separation. Figure 2 gives an initial indication of what the allowable limits may be. In this case the echo amplitude from the 5.6 mm slot yielded the signal-to-noise ratio (S/N) as a function of the liftoff from the surface. An S/N of 2.5, while rather small, ought to be workable. This lower limit on S/N corresponds to a liftoff of 1.5 mm which should be quite possible to obtain in most circumstances. These preliminary data show that the test system will be useful even before future refinements.

To determine how far a wheel can move and still return a useful signal, we first built a wooden form to simulate the track surface and then examined the signal strength as the transducer moved past the wheel contact point. Again using a 3-dB down point as the outer limits, a usable signal should be available during at least 2 cm of train travel. This is the space window in which the wheel must be located to both transmit and receive our test signal. While it would be desirable to introduce multiple pulses into the wheel in order to improve statistics for a higher signal-to-noise ratio, this may not be feasible since the Rayleigh wave travels multiple times around the circumference. To avoid processing confusion, it will be necessary to delay any new pulse until the prior one has sufficiently decayed. Since each round trip takes nearly a full millisecond, this means a delay interval of at least 10 ms. To get even two test pulses into the wheel (one at the beginning and end of the 2 cm window) means the train cannot travel faster than 2 cm/10 ms or about 7 km/h. This would be unacceptably slow for a field system so we shall have to settle for a single shot. A likely scenario is to use a trigger device to start the pulse as the wheel enters the window. Recording just the data arriving before the return of second round trip signal (see below) takes nearly 2 ms so the maximum train speed could be about 2 cm/2 ms, or 36 km/h. This is much better and likely improvement in the window length could increase the allowable speed.

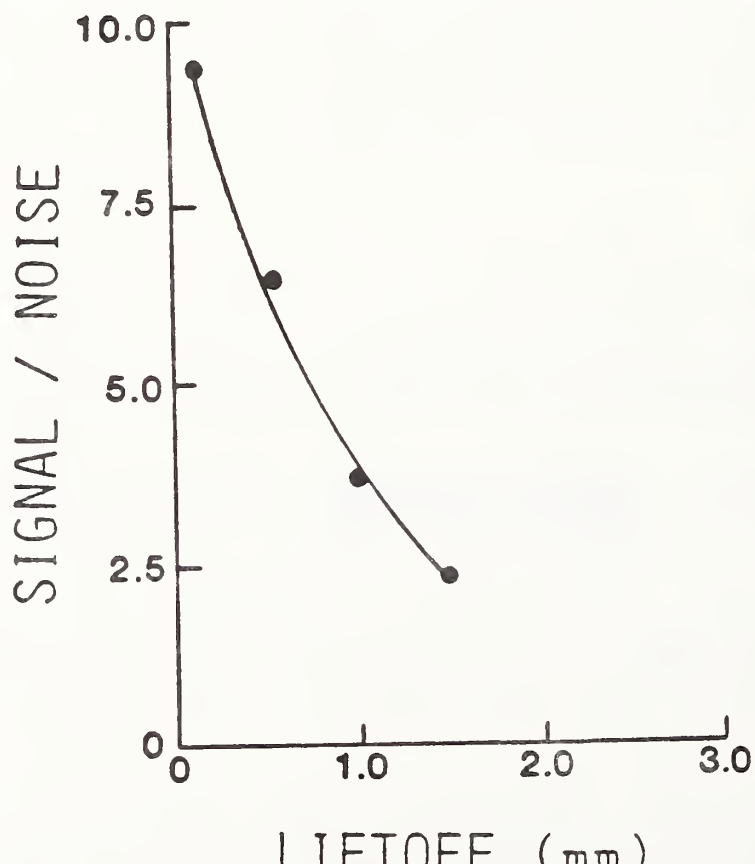


FIGURE 2. Signal-to-noise ratio as a function of separation between EMAT and wheel.

As noted above, the transducers are bidirectional. Figure 3 indicates schematically the signal paths to a flaw and the resulting scope trace. Signals A and C are echos that have traveled about 30% and 70% of the way around the wheel circumference to a flaw and then back. B and D are first and second round trip signals. Frequently some splitting occurs in these signals and this likely has at least two sources. Each round trip signal is a combination of counter-rotating signals. The path length is quite long (about 2.6 m) and some phase incoherence between these two becomes likely over this distance before they again combine on arriving back at the transducer. Also, the Rayleigh wave has some tendency to spread out to the wheel flange where it has a somewhat longer path than along the tread. The amount of ultrasonic energy in a wheel depends on the closeness of EMAT coupling and the wheel condition, e.g., grain size and residual stress state. Consequently, we are presently using the amplitude of the first round trip signal as a normalizing factor; the amplitude ratios A/B and C/B are our current flaw measurements.

To determine how the flaw position relative to the transducers affects the ultrasonic data, we measured the amplitudes of signals A, B, and C at 5 cm intervals around the entire circumference of the wheel. To obtain an idea of the sizing capability of this approach, the data were repeated for two flaw sizes, both circular sawcuts in the center of the tread; one was 5.6 mm deep and 38 mm long at the surface, and the other was the same cut enlarged to 12.1 mm deep and 53 mm long.

Data for the small flaw are in Fig. 4 and show three distinct regions. The first has a very large negative slope up to about 70 cm. With the beam divergence noted above, the ultrasonic energy needs this distance to spread out to the full tread width of 10 cm. Inside this distance, the flaw intercepts a very large fraction of this concentrated energy and generates a very large reflection. Once the beam has spread out to full width, in the second region, the flaw and round-trip signals remain fairly constant. In the third region, past about 225 cm, the flaw intercepts a large fraction of the counter-rotating ultrasonic beam; from this side, the flaw blocks a large portion of the round-trip signal and so increases the signal ratio.

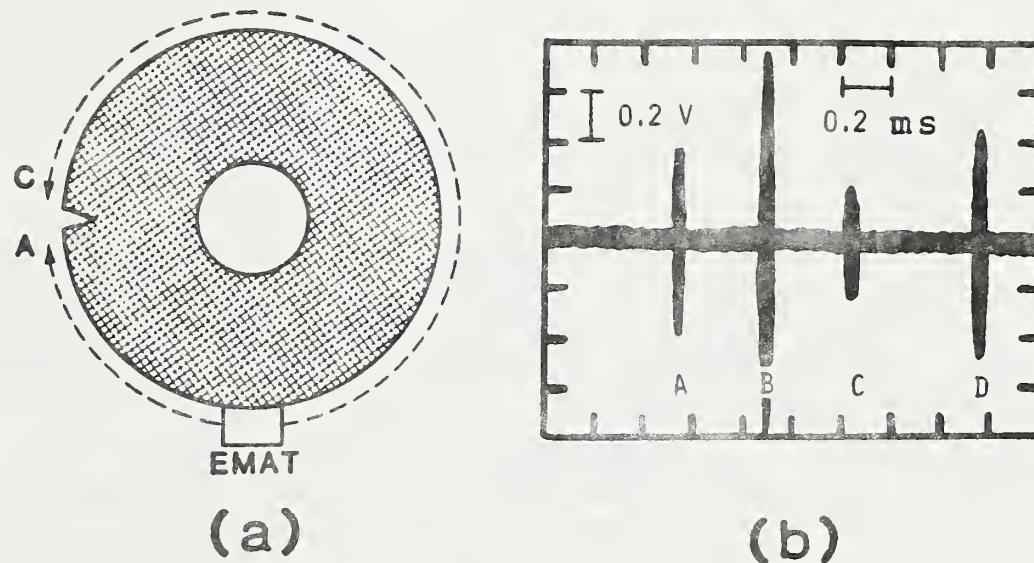


FIGURE 3. Flaw echoes.

(a) Schematic of bidirectional Rayleigh-wave travel to a flaw. A is the short path and C is the long path.

(b) Typical oscilloscope signal. A and C are short and long path flaw echoes. B and D are first and second round trip signals.

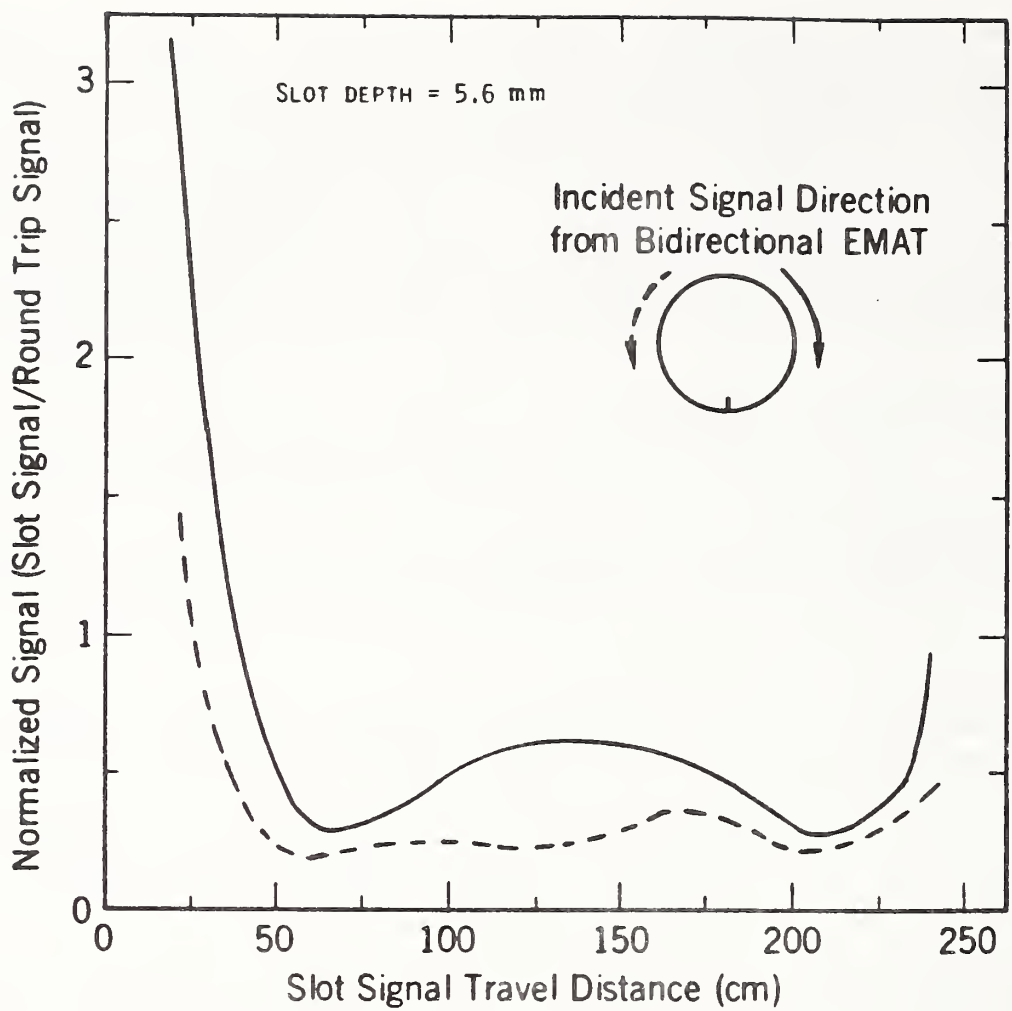


FIGURE 4. Signal amplitude as a function of flaw position around the wheel circumference. The simulated flaw was a saw cut in the center of the tread at 0 cm (262 cm). The two curves indicate data from signals traveling in opposite directions.

The data from the larger flaw show the same general trend (7) although the center region had somewhat higher values. This encourages our expectations that we will be able to achieve meaningful size discrimination.

The signals traveling in the opposite directions should generate the same data. While this appears basically true (the solid and dotted lines in Fig. 4 are close to each other), there does seem to be a slight systematic shift. Possibly there is some difference in the smoothness of the two sides of the sawcut.

Signal B's arrival time remains constant, of course, while A and C move closer to B as the EMAT-flaw distance increases until they all coincide when the flaw is exactly opposite the transducer. Thus, there are two zones on the circumference where meaningful measurements are not possible. Both of these are about 24 cm long; one is centered at the transducer and the other is exactly opposite. The first is due to recovery of the receiver amplifier following the transmitter pulse; the second is due to the merger of the round-trip and flaw signals when their acoustic path lengths become identical. As a result, approximately 80% of the tread can be inspected with each pass.

FUTURE WORK

We have recently constructed a short (4 m) section of track in which to mount the transducer (Fig. 5). Rolling an actual wheel set over the device will much more closely simulate field conditions and permit a reasonable debugging of several parts of the system: mechanical mounting, compliant coil backings, geometric variations in the size and position of magnet and coils, triggering (if necessary), and signal collection and storage. A new meanderline with 8 cycles (60% longer) will take advantage of the full length of our largest magnet. Testing will show if this will increase the space window for injecting the ultrasonic pulse and so increase the allowable train speed. With multiple wheels now available, it will be possible to generate a variety of artificial flaw sizes in the pursuit of a workable sizing algorithm. Since the wheels have a few centimeters of side-to-side play in normal operation, this rolling test will also show us the importance of the wheel position with respect to the transducer.

Automatic signal processing will be necessary before moving the system to a railyard to look for actual cracks in the field.

ACKNOWLEDGMENTS

We are grateful for discussions with H. J. Salzburger of IzfP as well as John Cowan and Richard Conway of The Fax Corporation. This work was sponsored by the U.S. Department of Transportation, Federal Railroad Administration, Washington, D.C. We also wish to thank the Transportation Test Center, American Association of Railroads, Pueblo Colorado, and, in particular, Britto Rajkumar and Dominic DiBritto for providing test wheels.

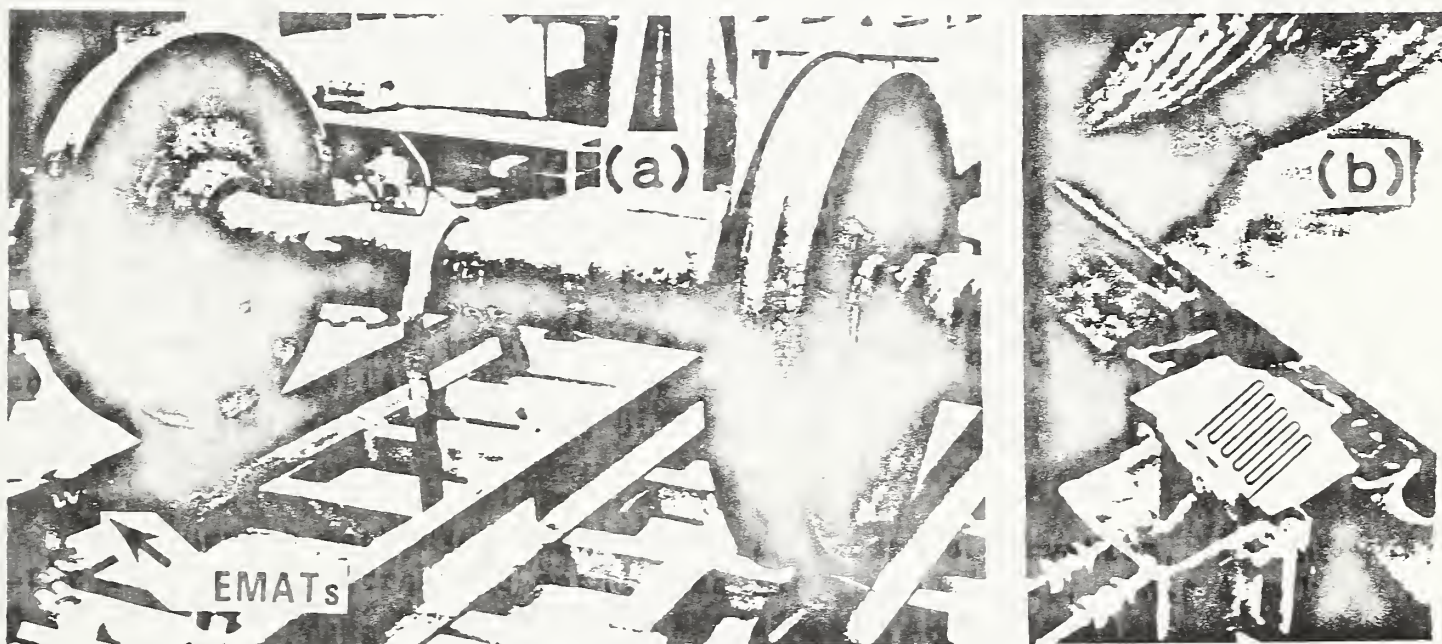


FIGURE 5. Current test configuration.

- (a) Standard wheel set rolled along a short length of track.
- (b) EMATs mounted in rail. A protective film covers the coils and they are represented schematically in this photo.

REFERENCES

1. Inspect Wheels "In Motion," Progressive Railroading, Jan., 1974.
2. Spotting the Defects in Railroad Wheels, Business Week, p. 44, Sept. 28, 1974.
3. Cracked-Wheel Detector "Could Save Millions," Railway Systems Control, May, 1975.
4. U.S. Patent 3,978,712: Sept. 7, 1976, John Vincent Cowan, Gerald De G. Cowan, and John Gerald Cowan.
5. Salzburger, H. J., and Repplinger, W., Ultrasonics International 83, conference organizers Z. Novak and S. L. Bailey (Butterworth & Co. Ltd., Kent, Great Britain), pp. 8-12, 1983.
6. Clark, A. V., Schramm, R. E., Fukuoka, H., and Mitrakovic, D.V., Ultrasonic Characterization of Residual Stress and Flaws in Cast Steel Railroad Wheels, Proceedings, IEEE 1987 Ultrasonics Symposium, Vol. 2, B. R. McAvoy, editor (Institute of Electrical and Electronic Engineers, New York), pp. 1079-1082, 1987.
7. Schramm, R. E., Clark, Jr., A. V., Mitrakovic, D. V., and Shull, P. J., Flaw Detection in Railroad Wheels Using Rayleigh-Wave EMATs, Review of Progress in Quantitative Nondestructive Evaluation, Vol. 7B, D. O. Thompson and D. E. Chimenti, editors (Plenum Press, New York), pp. 1661-1668, 1988.
8. Maxfield, B. W., Kuramoto, A., and Hulbert, J. K., Evaluating EMAT Designs for Selected Applications, Materials Evaluation, vol. 45, no. 10, pp. 1166-1183, 1987.
9. Alers, G. A., and Burns, L. R., EMAT Designs for Special Applications, Materials Evaluation, vol. 45, no. 10, pp. 1184-1194, 1987.

A nearly identical paper entitled "Crack Inspection of Railroad wheel Treads by EMATs" was submitted to Proceedings: Third International Symposium on Non-destructive Characterization of Materials, 3-6 Oct., 1988, Saarbrücken, Federal Republic of Germany.

Submitted to:
Review of Progress in Quantitative NDE,
eds. D. O. Thompson and D. E. Chimenti
(Plenum Press, NY, 1989), Vol. 8.

EMATS FOR ROLL-BY CRACK INSPECTION OF RAILROAD WHEELS*

R. E. SCHRAMM, P. J. SHULL,
A. V. CLARK, JR., and D. V. MITRAKOVIC**
National Institute of Standards and Technology
Fracture and Deformation Division
Boulder, Colorado 80303

INTRODUCTION

Railroad safety depends on many factors. The integrity of the wheels on rolling stock is one that is subject to nondestructive evaluation. For some years, ultrasonic testing has been applied to the detection of cracks in wheel treads, with particular attention to automatic, in-rail, roll-by methods. We have begun constructing a system aimed at using relatively low frequency Rayleigh waves generated by electromagnetic-acoustic transducers (EMATs). The current design uses a permanent magnet to maintain a compact structure and minimize the size of the pocket machined into the rail. Measurements thus far indicate a responsiveness, even to small flaws. With the development of a signal processing and analysis system, field tests should soon be possible.

Cracks in railroad wheels may result from high stresses due to dynamic or static loads and residual stresses generated by such events as heating during braking. These flaws generally originate in the tread surface or flange and can lead to catastrophic wheel failure resulting in considerable equipment damage and possible derailment. This threat to personnel safety and the potential costs in time and money are inducements to search for an effective, automated method for nondestructive examination that will identify damaged wheels needing replacement.

The current method of examination is visual observation. In the early 1970's, an ultrasonic method was introduced [1-4]. This involves an in-rail system of piezoelectric transducers that generate Rayleigh waves, electronics for signal generation and processing, and a method for tagging suspect wheels. The goal is to examine each wheel of a train as it rolls by a checkpoint in a railyard. Two of these systems

* Contribution of the National Institute of Standards and Technology (formerly National Bureau of Standards), not subject to copyright.

** Guest scientist on leave from the University of Belgrade, Belgrade, Yugoslavia.

are currently in operation in this country. A companion portable handheld system subsequently verifies any flaw indications. The Fraunhofer Institute (IzfP) in Saarbrucken, Federal Republic of Germany, has been developing another ultrasonic system along this line [5], but using electromagnetic-acoustic transducers (EMATs). IzfP has placed a prototype into operation.

Our current research in this area [6-8] is the development of an ultrasonic system using EMATs designed to work on American-style wheels and rails. The objective is to check every wheel on a train, also in a roll-by mode. Like the earlier systems, ours uses Rayleigh waves that travel around the wheel tread. We are using EMATs for two main reasons: 1. No ultrasonic path in the transducer itself and low sensitivity to mode-converted signals mean a simplified, low-noise signal that is relatively easy to interpret with high reliability, even in an automated system; 2. Their noncontact nature eliminates the need for ultrasonic couplants, i.e., no water sprays or liquid-filled boots. Two extensive reviews of EMAT designs and applications have recently been published [9, 10].

EQUIPMENT

In the electronic system, a function generator provides the rf signal for a gated MOSFET power amplifier which drives the transmitter. The toneburst consists of 5-10 cycles at 500 kHz with a pulse repetition frequency (PRF) of 60 Hz. The receiver preamplifier is a very low noise design. Electronic impedance matching is very important for both transmitter and receiver to ensure maximum efficiency.

Our EMAT device (Fig. 1a) is meant for insertion into a recess cut out of the rail. Therefore, one goal in the transducer design is to keep the configuration as compact as possible to minimize both the

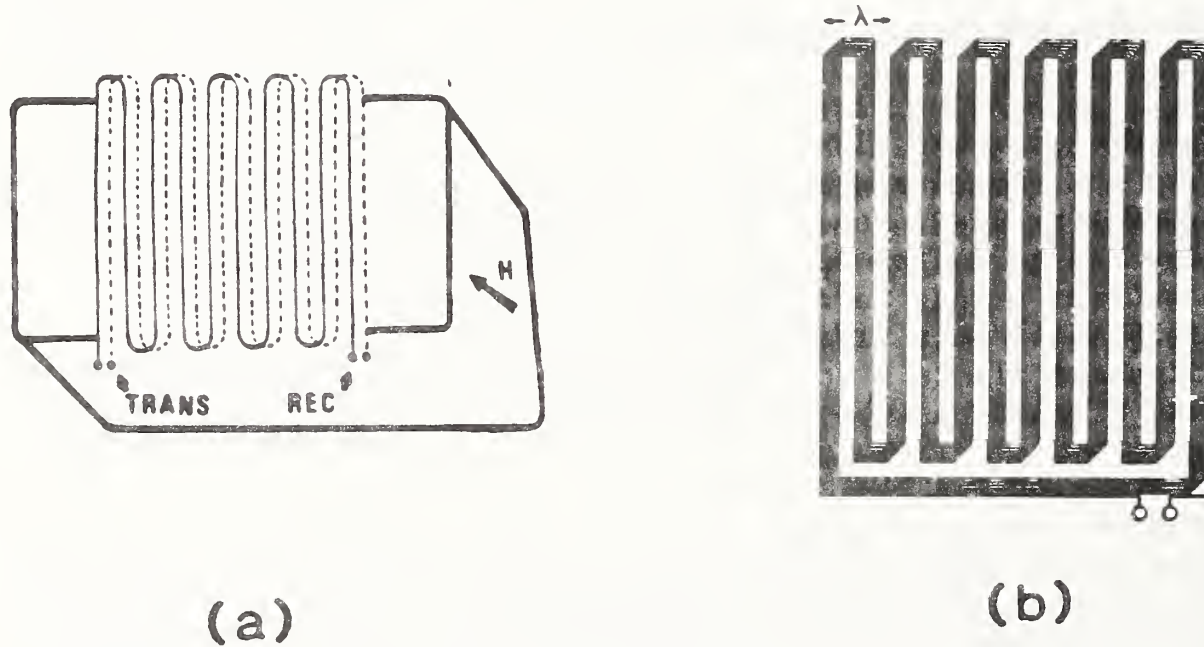


Fig. 1. Rayleigh-wave EMAT construction.

(a) Two meanderline coils, shifted to prevent shielding, placed atop a magnet with field H. A foil eddy current shield lays over the magnet and a thin, compliant foam sheet is under the coils.

(b) Details of the wirewound meanderline.

amount of required machining in the rail and the loss of weight-bearing surface. Toward this end, we use a single permanent magnet (Nd-Fe-B for maximum field strength) 32 mm X 26 mm X 52 mm with the magnetization direction along the 32 mm direction and oriented normal to the tread. For pitch-catch operation, there are separate transmitter and receiver coils. These are meanderlines with a periodicity of 6 mm to generate a Rayleigh wave with this wavelength at 500 kHz (velocity = 3 km/s). This design generates and receives bidirectional Rayleigh waves traveling normal to the coil legs.

Rather than stacking the transmitter and receiver coils directly atop one another, we shifted them by a quarter period so they do not shield each other. To prevent signal complications from ultrasound production in the magnet, we cover it with a thin foil of copper or aluminum to minimize eddy current generation in the Nd-Fe-B. Between this shield and the coils are a few millimeters of compliant material (currently, polymer foam); this layer compresses under the wheel's weight and their flexible substrate allows the meanderlines to conform to the curvature and taper of the wheel tread. This minimizes liftoff for maximum efficiency and signal/noise.

The present coil design contains eight cycles or loops in the meanderline. The receiver coil is AWG 36 enamel-coated wire that has been wound through the pattern six times on acetate-based adhesive tape (Fig. 1b). This multiplicity adds to the sensitivity since the repetitions are series-connected. The flexible tape allows the coil to conform to the wheel's curvature.

We've constructed the transmitter coil in two forms. The first is a printed circuit on polymer film. The conductor is about 1 mm wide and 0.025 mm thick. In this form, the impedance is very low (about 1.3 Ω including a current limiting resistor). Our power amplifier can deliver about 140 A of rf current into this coil. The second form is identical to the wire-wound receiver, and the much higher impedance limits the drive current to about 30 A.

The greater the current flow through the transmitter, the greater is the eddy current induced in the specimen. While the printed circuit coil permits the maximum current, the wirewound coil passes the current through the EMAT aperture multiple times and the current density (A/mm^2) induced in the specimen is roughly the same, i.e., the size of our ultrasonic signal is nearly identical with either form of transmitter. Using the lower current coil will increase the longevity of the power amplifier, and will allow an increase in the pulse repetition frequency (PRF) to as much as 250 Hz, should this prove desirable later. At present, the limit on the PRF is due to two factors in the power amplifier: ohmic heating of the MOSFET output drivers and the time required to recharge the power supply filtering capacitors.

EXPERIMENTAL RESULTS

We have recently constructed a short (4 m) section of track in which we mounted the transducer (Fig. 2). Rolling an actual wheel set (two wheels mounted on an axle) over the device much more closely simulates field conditions than our initial static measurements [7]. The goal is to debug several parts of the system: mechanical mounting, compliant coil backings, geometric variations in the size and position

of magnet and coils, triggering (if necessary), and signal collection and storage. Since the wheels have a few centimeters of side-to-side play in normal operation, this rolling test will also show us the importance of the wheel's transverse position with respect to the transducer.

For these initial measurements, we had two wheel sets, well used but nominally uncracked. The wheels were rolled onto the transducer and held stationary or rolled over the EMAT site at a few kilometers per hour. In both wheels of one set, this arrangement produces a signal which was still detectable after 16 round trips or about 42 m of travel. In both wheels of the other set, the signal traveled around the tread only six times before being attenuated into the noise level. Metallurgical variables due to such factors as manufacture, wear, etc., have a very large influence on the wheel's acoustic response. Any signal analysis will have to account for this effect.

The critical flaw depth is about 6 mm, so our interest is in distinguishing between cracks of greater depth (no longer safe) and those more shallow (safe for continued use). Initially, however, we saw-cut a very shallow circular flaw into the center of the tread along a wheel radius. This flaw depth into the wheel was almost 2 mm at the maximum; the length was oriented along the tread width and 12 mm long at the surface.

To determine how far a wheel can move across the transducers and still return a useful signal, we rolled the wheel in small steps across the EMATs and measured the signal strength as the initial contact point moved across the coils. This indicated that the effective EMAT aperture within which the wheel must be located to both transmit and receive our test signal is about 5-8 cm long. This aperture is actually slightly longer than the coils because the wheel radius is relatively so much larger, and the flexible coils conform to the tread curvature. While it would be desirable to introduce multiple pulses into the wheel in order to improve statistics for a higher signal-to-noise ratio, this may not be feasible since the Rayleigh wave travels several times around the circumference. To avoid processing confusion, it will be necessary to delay any new pulse until the prior one has sufficiently decayed. Since each round trip takes nearly one full millisecond, this means a delay interval of about 10-16 ms. To get even two test pulses into the wheel (one at the beginning and end of a 5 cm window) means the train cannot travel faster than 5 cm/10 ms or about 18 km/h. This would likely be unacceptably slow for a field system, so we shall probably have to settle for a single transmitter pulse. A likely scenario is to use a trigger device to start the pulse as the wheel enters the window. Recording just the data arriving before the return of second round trip signal (see below) takes nearly 2 ms, so the maximum train speed could be about 5 cm/2 ms, or 90 km/h. There are other factors (signal processing time, timing accuracy of pulse trigger, etc.) that will likely limit the allowable speed to somewhere under this value.

There are possibilities for triggering mechanisms to signal the proper moment during a wheel's transit to pulse the EMAT. For these initial tests, we placed a simple membrane switch between the coils and the magnet. The compliant foam transmitted the wheel pressure and switch closure triggered both the high current pulser and a digital oscilloscope to capture the transient ultrasonic signal from the single pulse. At the low speeds possible on our short test track, this system has been both reliable and consistent with our current spatial window.

The transducers are bidirectional and generate Rayleigh waves traveling clockwise and counterclockwise around the railroad wheel tread. Figure 3 indicates schematically the signal paths to a flaw and the resulting scope trace. Signals A and C are echos that have traveled about 22% and 78% of the way around the wheel circumference to the 2 mm deep flaw and then back. Signals B and D are first and second round trip signals. Signal A' is the short path echo after the initial pulse has already traveled once around the entire circumference. Frequently some splitting occurs in these signals and this likely has at least two sources. Each round trip signal is a combination of counter-rotating signals. The path length is quite long (about 2.6 m) and some phase incoherence between these two becomes likely over this distance before they again combine on arriving back at the transducer. Also, the Rayleigh wave has some tendency to spread out to the wheel flange where it has a somewhat longer path than along the tread. The amount of ultrasonic energy in a wheel depends on the closeness of EMAT coupling and the wheel condition, e.g., grain size and residual stress state. Consequently, we are presently using the amplitude of the first round trip signal as a normalizing factor; the amplitude ratios A/B and C/B are our current flaw depth indicators.

The arrival time of signal B remains constant, of course, while A and C move closer to B as the EMAT-flaw distance increases until they all coincide when the flaw is exactly opposite the transducer. Thus, there are two zones on the circumference where meaningful measurements are not possible. Both of these are about 24 cm long; one is centered at the transducer and the other is exactly opposite. The first is due to recovery of the receiver amplifier following the transmitter pulse; the second is due to the merging of the round-trip and flaw signals when their acoustic path lengths become identical. As a result, approximately 80% of the tread can be inspected with each pass. A second pair of EMATs located 0.5-1 m down track would assure 100% inspection.

FUTURE WORK

The electronics for this system fall in two basic categories: 1. transducer (high current pulser for the transmitter and amplifier for the receiver) and 2. signal processing (digitizing and logic). The designs for the first category are working very well, and we are packaging them in a form suitable for routine use. Work on the second instrumentation system has now begun.

While our present EMAT design is producing excellent signals, there are several possible improvements we will be investigating. Among these are the use of a physically smaller magnet to reduce the size of the pocket machined into the rail, alternate materials for the compliant layer under the coils, and variations in the design and physical structure of the coils. Other wheel-detection mechanisms to trigger the current pulse are possible.

Further investigation into the size discrimination capabilities of this system is also necessary. This will entail a series of measurements on artificial flaws, initially, and then actual cracks.

Our goal is to deliver a working system to the Transportation Test Center in Pueblo, Colorado, and conduct full-scale field tests.



Fig. 2. Current test configuration.

- (a) Standard wheel set rolled along a short length of track.
- (b) EMATs mounted in rail. A protective film covers the coils and they are represented schematically in this photo.

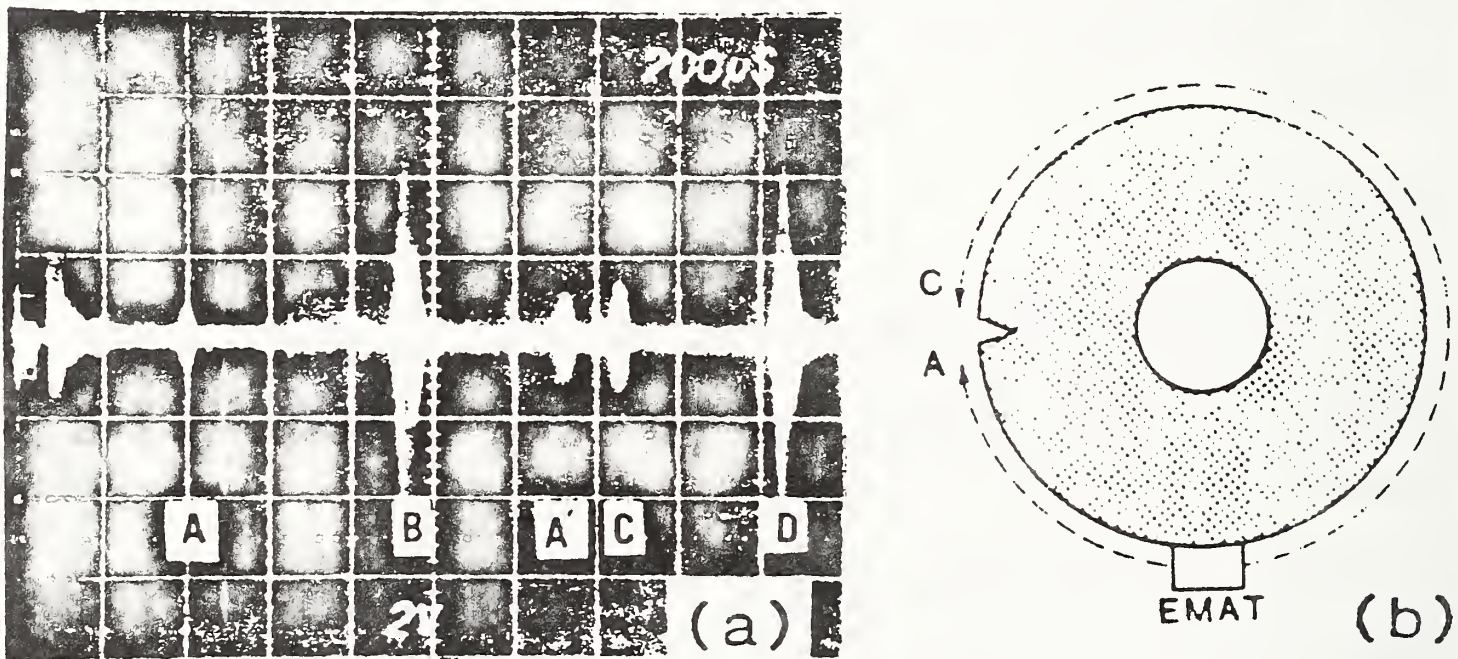


Fig. 3. Flaw echoes.

- (a) Typical oscilloscope signal for 2 mm deep cut. A and C are short and long path flaw echoes. B and D are first and second round trip signals. A' is the short path echo after a complete round trip (A + B).
- (b) Schematic of bidirectional Rayleigh-wave travel to a flaw. A is the short path and C is the long path.

ACKNOWLEDGMENTS

We are grateful for discussions with H. J. Salzburger of IzfP as well as John Cowan and Richard Conway of The Fax Corporation. This work was sponsored by the U.S. Department of Transportation, Federal Railroad Administration, Washington, D.C. We also thank the Transportation Test Center, American Association of Railroads, Pueblo Colorado, and, in particular, Britto Rajkumar and Dominic DiBrito for providing test wheels.

REFERENCES

1. Inspect Wheels "In Motion," Progressive Railroading, Jan., 1974.
2. Spotting the Defects in Railroad Wheels, Business Week, p. 44, Sept. 28, 1974.
3. Cracked-Wheel Detector "Could Save Millions," Railway Systems Control, May, 1975.
4. U.S. Patent 3,978,712: Sept. 7, 1976, John Vincent Cowan, Gerald De G. Cowan, and John Gerald Cowan.
5. H. J. Salzburger and W. Repplinger, in Ultrasonics International 83, conference organizers Z. Novak and S. L. Bailey (Butterworth & Co. Ltd., Kent, Great Britain, 1983), pp. 8-12.
6. A. V. Clark, R. E. Schramm, H. Fukuoka, and D. V. Mitrakovic, Ultrasonic Characterization of Residual Stress and Flaws in Cast Steel Railroad Wheels, in Proceedings, IEEE 1987 Ultrasonics Symposium, Vol. 2, edited by B. R. McAvoy (Institute of Electrical and Electronic Engineers, New York, 1987), pp. 1079-1082.
7. R. E. Schramm, A. V. Clark, Jr., D. V. Mitrakovic, and P. J. Shull, Flaw Detection in Railroad Wheels Using Rayleigh-Wave EMATs, in Review of Progress in Quantitative Nondestructive Evaluation, edited by D. O. Thompson and D. E. Chimenti (Plenum Press, New York, 1988), Vol. 7B, pp. 1661-1668.
8. R. E. Schramm, P. J. Shull, A. V. Clark, Jr., and D. V. Mitrakovic, EMAT Examination for Cracks in Railroad Wheel Treads, submitted to Proceedings: Nondestructive Testing and Evaluation for Manufacturing and Construction, Urbana, Ill., Aug. 9-12, 1988 (Hemisphere Publishing Corp., Washington, D. C.).
9. B. W. Maxfield, A. Kuramoto, and J. K. Hulbert, Evaluating EMAT Designs for Selected Applications, Materials Evaluation, vol. 45, no. 10, pp. 1166-1183 (1987).
10. G. A. Alers, and L. R. Burns, EMAT Designs for Special Applications, Materials Evaluation, vol. 45, no. 10, pp. 1184-1194 (1987).

Ultrasonic Characterization of Residual Stress and Texture
in a Heat-Treated Steel Railroad Wheel*

A. V. Clark, H. Fukuoka**, D. V. Mitrakovic*** and J. C. Moulder

National Bureau of Standards
Fracture and Deformation Division
Boulder, Colorado 80303

Submitted to Materials Evaluation

Some minor revisions have been made in this manuscript in
accordance with a reviewer's remarks.

** NBS Guest Worker; on leave from Osaka University, Osaka University,
Japan.

*** NBS Guest Worker; on leave from University of Belgrade, Belgrade,
Yugoslavia.

*Contribution of the National Bureau of Standards; not subject to copyright.

ABSTRACT

The state of residual stress in the rim of a heat-treated steel railroad wheel has been characterized using the acoustoelastic effect. Shear-horizontal (SH) waves were propagated through the rim thickness by transducers operating in pulse-echo mode. The difference in arrival times of orthogonally polarized SH-waves (acoustic birefringence) was measured with a precision of ± 1 ns or better. This difference is related to the state of stress and texture in the rim.

Measurements were made using two transducers; a piezoelectric device made of PZT, and an electromagnetic-acoustic transducer (EMAT). The PZT device had been used to measure residual stresses in rolled steel wheels [1] and was used as a reference against which EMAT measurements were compared.

Measurements made as a function of radial position on the rim indicated a gradient of stress (assuming constant texture). The stress gradient measured by the EMAT was in good agreement with that measured by the PZT transducer.

Measurements made around the circumference of the rim indicated an axisymmetric state of stress and texture for regions closest to the tread, with increasing departure from axial symmetry as the inner edge of the rim is approached. The EMAT and PZT measurements both indicated this trend.

The effect of surface preparation on EMAT measurements was characterized. The difference in birefringence as measured on rough surfaces was usually less than 2×10^{-4} , which gives an (approximate) difference in stress of 25 MPa.

The good agreement between EMAT and PZT values of birefringence, plus the relative insensitivity of the EMAT to surface preparation, indicate that EMATs are quite suitable for field measurements of residual stress.

INTRODUCTION

The fact that stress induces a (small) change in phase velocity in metals has been known for decades. Recently, there have been numerous experiments which use this acoustoelastic effect to map out states of applied stress; many of these results are summarized in a review article [2].

Researchers have also attempted to use the acoustoelastic effect to measure residual stress states. This problem is generally more difficult than the applied stress problem, since the effect of texture must be accounted for. (Presumably, the effect of texture can be eliminated in applied stress problems by making velocity measurements before and after application of stress. Then the change in velocity is related solely to stress.)

Measurements of residual stress due to welding have been conducted by several researchers [3,4,5,6] with good agreement with other techniques. Likewise, measurement of the residual stress state in a shrink-fit specimen have been performed [7,8,9,10] with good agreement with the theoretical values.

The acoustoelastic effect was also used to measure the state of residual stress induced by drag braking in the rim of rolled steel railroad wheels of Japanese manufacture [1]. The values of stress so determined were compared with two destructive residual stress measurement techniques; the stresses measured using acoustoelasticity agreed within 40 MPa with the destructively measured stresses.

In Ref.1, a novel piezoelectric transducer was used to make the acousto-elastic measurements. In order to protect the transducer from excessive wear, the (rough) surface of the rim was machined to a smooth state. Clearly, this machining is admissible in a laboratory setting, but is a potential limitation on the use of acoustoelasticity in the field.

In a previous paper we demonstrated the feasibility of using electromagnetic-acoustic transducers (EMATs) for characterization of the residual stress state in the rim of a cast steel railroad wheel [11]. In that work, we propagated shear-horizontal (SH) waves at normal incidence through the thickness of the rim, using both an EMAT and a piezoelectric transducer. The transducers were placed on the back face of the rim and SH-waves were reflected from the front face. (The crosssection of a typical rim is shown in Fig. 1.) Measurements of arrival times were made in pulse-echo mode, so the wave had propagated through about 290 mm of cast steel when it reached the transducer(s).

The cast steel wheel (obtained from the Department of Transportation Test Center, Pueblo, Colorado) had a sawcut. We assumed the hoop stress (induced by braking the wheel, and also by the casting process) to be relieved near the sawcuts and assumed that radial stress was negligible. We found that the acoustic axes (polarization direction for maximum and minimum arrival times of SH-waves) were oriented along the radial and circumferential directions. This was true both in the stress-relieved state (adjacent to sawcut) and in the stressed state.

Consequently, we assumed that the residual stress could be obtained from the birefringence equation [12]:

$$B = B_0 + C_A(\sigma_\theta - \sigma_r) \quad (1)$$

where σ_θ and σ_r are hoop and radial stresses, respectively, and C_A is the stress-acoustic constant.¹ The acoustic birefringence, B , is defined as the

¹It has been shown that the stresses vary with depth in the rim [13,14]. Consequently, the birefringence method will measure stresses averaged through the rim thickness. When referring to stresses, we mean thickness-averaged values unless stated otherwise.

difference of velocities of orthogonally polarized SH-waves, propagating through the same material thickness:

$$B \equiv \frac{V_\theta - V_r}{V_o} = \frac{T_r - T_\theta}{T_o} \quad (2)$$

Here V_θ is the velocity of an SH-wave polarized in the θ (hoop) direction, and T_θ is the corresponding time of flight. B_o is the birefringence in the unstressed state; V_o is the average of V_θ and V_r .

We measured B_o on both sides of the sawcut, and took the average of these two measurements. This value was subtracted from the birefringence measured at stressed locations and equation (1) was used to obtain σ_θ . The values of hoop stress thus obtained with EMAT and piezoelectric transducer were compared; we found that the peak values of hoop stress agreed within 10 MPa [11].

The present work concerns birefringence measurements made with both an EMAT and piezoelectric transducer on a cast steel wheel which has been heat treated and air quenched. This process results in a grain structure which is finer than in cast wheels. (In fact, we found that we were able to detect up to five echoes, using the EMAT, for the heat-treated wheel; for the cast wheel, we obtained only two echoes at most.) Consequently, we expect a different microstructure for the heat-treated wheel.

In Ref. 11, we measured B at the center of the back face of the rim. We wished to determine if there was a gradient of stress in the radial direction, and, if so, whether we could measure the gradient with an EMAT. Consequently, in the present study we measured B at 5 radii with our EMAT and also with a piezoelectric transducer. In general, the values of B were in good agreement.

In addition, we wished to determine whether the state of stress is axisymmetric. Obviously, it is desirable that this be the case, since axial symmetry greatly reduces the number of measurements necessary to determine the stresses in the rim of the wheel.

Furthermore, we wished to make our measurements with the transducers situated on the front face of the rim. This is the side that is accessible in the field; to reach the back face necessitates reaching around the wheel, which is considered a hazardous practice in a rail yard. Since the front face is narrower than the back face, we anticipated that problems due to acoustic beam spreading, sidewall reflections, etc. might arise. There is also a potential problem with fringing of the eddy current field induced in the rim by the EMATs; more will be said about this later.

EXPERIMENT

Method of Birefringence Measurement with EMAT

We measured arrival times (for both the EMAT and piezoelectric transducer) with a simple time-interval averaging system. The block diagram for operation with the EMAT is shown in Fig. 2.

For the EMAT measurements, we simply oriented the transducer to generate SH-waves polarized in the radial (or hoop) direction. The EMAT, which has an aperture 1 cm x 1 cm, was excited with a tone burst having center frequency of 2.4 MHz. The START time-interval probe (see Fig. 2) sends a square-wave pulse to the counter when the voltage in the exciting pulse reaches a predetermined level. The counter runs at a 100 MHz rate until it receives a STOP signal.

The echoes are received by the EMAT, which is followed by a preamplifier-tuned amplifier combination. The final stage of amplification is accomplished by a broadband receiver. The broadband receiver displays little change of d.c. level with gain; this dc shift is further suppressed by the high-pass filter. This is crucial, since we are using a zero crossing (voltage = 0) as an arrival-time marker; any change in dc level with gain could cause a change in apparent arrival time.

We chose a certain zero crossing (phase = $2n\pi$) in the first echo as a marker to determine arrival time. When this zero crossing occurs, the digital delayed gate (DDG) sends a TTL pulse to the counter.

Note that the STOP time-interval probe generates a pulse every time a zero crossing occurs. Because the signal/noise ratio using an EMAT is so low, there will be many such zero crossings unrelated to arrival of the first echo. The purpose of the DDG is to (a) effectively gate out unwanted pulses and (b) use logic circuitry to avoid distortion of the waveform (which occurs with many analog gates).

Basically, the DDG operates as follows. A one-shot device is triggered after a selected time delay. The time delay is selected to correspond (approximately) to the arrival of the selected zero crossing in the first echo. The output of the "one-shot" device (a TTL signal at logical level "1") is input to one port of a logical AND gate. The AND gate generates a TTL signal when the other port is at logical level "1". This occurs when the next square wave pulse is generated by the STOP time-interval probe. (We used a preamplifier-level shifter circuit to change the output of the probe to TTL level. The operation of the DDG is described in more detail in Ref. 11.)

With the EMAT in place, the precision of the arrival time measurement was better than ± 1 ns, for an arrival time of about 90 μ s. Consequently, the electronic precision is of the order of 10 p.p.m. To obtain this precision, we set the counter to average 10^3 arrival times per reading. This averaging allowed us to obtain good precision while operating in a noisy rf environment (proximity to a welding lab and a fatigue testing lab).

After an arrival time was measured in a given orientation, we rotated the EMAT 90° and made another arrival time measurement, taking care to use the same zero crossing as our marker.

We then rotated the EMAT to its original orientation, and repeated the arrival time measurement. Typically, we found that this (new) arrival time could be as much as ± 5 ns different from the first measurement. We attributed this to variations in the electromagnetic coupling between the EMAT and the wheel.

We measured B by making at least three measurements of T_r and T_θ at each location. This tended to reduce the uncertainty of arrival times; typically, the standard deviation of the three (or more) arrival times was about ± 3 ns. For a typical arrival time of about 90 μ s, this gives an uncertainty of about 3×10^{-5} . The birefringence was obtained from

$$B = \frac{\langle T_r \rangle - \langle T_\theta \rangle}{\langle T_0 \rangle} \quad (3)$$

where $\langle \rangle$ denotes an average.

Birefringence Measurements with Piezoelectric Transducer

The velocity (arrival time) measurement system was slightly modified when using the piezoelectric transducer; the block diagram is shown in

Fig. 3. A thin layer of couplant was used to acoustically couple the transducer and the wheel.

The transducer actually consists of two stacked PZT SH-wave transducers which have an aperture of 7 mm x 7 mm. The transducers are orthogonally polarized and bonded together so that each will propagate an SH-wave through the same couplant thickness. This is an advantage for ultrasonic stress measurement, where small changes in couplant thickness can cause errors in arrival time measurements.

The lower transducer is, of course, acoustically coupled to the wheel through the couplant. The upper transducer is coupled to the lower, so the waveforms generated by the transducers will be different. To minimize this difference, we used a shock excitation of the PZT transducers (as opposed to a toneburst for the EMAT). We also adjusted the gain on the receiver so the peak received signal is the same for both the upper and lower transducers. (More details can be found in Ref. 11.) With shock excitation the waveform is essentially the ring-down of the transducer (plus backing, etc.). We used the second zero crossing as a marker for arrival time measurements; i.e., we set the DDG to stop the counter when the second zero crossing occurred.

The stacked PZT transducer was mounted in a housing which allowed it to be pressed down on the couplant with a constant force (supplied by a spring). The housing in turn was connected to the wheel by a stand with a magnetic base:

To avoid damage to the plating on the lower transducer, we had the surface of the front face of the rim milled (in a machine shop), and then we lightly hand polished the surface with abrasive paper (up to 320 grit). A small amount of couplant was applied to the surface, the transducer was locked in place with the magnetic stand, and the spring force applied.

We measured the arrival time by exciting the lower transducer when it was polarized in, e.g., the radial direction. We then threw a switch (which allowed the pulser to shock excite the upper transducer) and measured the arrival time of the SH-wave polarized in the hoop direction. The stacked transducer was then rotated 90° (so that the lower transducer was polarized in the hoop direction) and the arrival times for both transducers measured.

To compensate for the additional acoustic path length for the upper transducer, we calculated the birefringence from

$$B = [(T_r^{(u)} + T_r^{(l)}) - (T_\theta^{(u)} + T_\theta^{(l)})]/2T_0 \quad (4)$$

where the superscripts (u) and (l) refer to the upper and lower transducers, respectively and T_0 is the average arrival time. The additional path length cancels out in the formula above.

For both transducers (EMAT and PZT) we measured B several times at the same location (usually on separate days) to check repeatability. We took the average of these measurements to give the final values of B.

RESULTS

Effect of Surface Preparation on EMAT Measurements

In our previous work (on the back face of the rim) we found that the EMAT measurements were relatively insensitive to the degree of surface preparation [11]. To see if a similar result could be obtained on the front face of the (heat-treated) wheel rim, we first measured the birefringence around the rim circumference after only hand polishing with 60 grit abrasive paper.

Measurements were made at the center of the front face of the rim. The results are shown as open circles in Fig. 4, where the angle θ is measured counterclockwise around the rim from an arbitrarily chosen location. Each

circle represents one birefringence measurement, done as described above.

We measured B every 45° (8 locations) around the rim twice.

Next, we cleaned the front face surface more thoroughly (at the 8 locations) with a hand grinder (using 60 grit paper) and followed this with hand sanding. We remeasured B, with results that are shown as solid circles in Fig. 4. The difference in B between the two surface treatments is usually less than 2×10^{-4} . Assuming a value of $-7.6 \times 10^{-6} \text{ MPa}^{-1}$ for the stress-acoustic constant, C_A , this difference of 2×10^{-4} is equivalent to a stress difference of about 25 MPa (less than 4 ksi).²

The front face was then milled in a machine shop to obtain a smooth surface. The EMAT measurements of B made on the smooth surface are shown as diamonds in Fig. 4; in general, these measurements are within 2×10^{-4} of previous measurements of B.

The fact that there is good agreement between EMAT measurements made on surfaces of varying degrees of surface preparation is quite encouraging. From a practical point of view, it is convenient to minimize the amount of time and labor necessary to prepare the surface.

The first two methods (hand polish only and hand grinding followed by hand polish) both left large pitted regions on the front face surface. Only milling removed these pits.

We initially expected that the presence of pits could be a problem for birefringence measurements with the EMAT; the pits could conceivably: (a) cause local variations in liftoff, and (b) distort the eddy current field induced in the rim. These effects might cause degradation in the acoustic

²The value of C_A was obtained in Ref. 1 for rolled steel wheels; here we assume that C_A for heat-treated wheels will be approximately the same as for rolled wheels.

signal amplitude and the purity of polarization. In addition, local variation of liftoff might cause a phase shift (in frequency space) or an equivalent time delay. However, it appears that to a first approximation that these effects average over the transducer aperature.

After the front face of the rim was milled and hand polished, measurements were made with the PZT transducer. The results are shown by the squares in Fig. 4. There is good agreement between the birefringence measured by the EMAT and by the PZT transducer; in general, the difference between these birefringence measurements is less than 2×10^{-4} .

Radial Variations of Birefringence

The data shown in Fig. 4 were taken at locations in the middle of the front face (13 mm from inner edge of rim). We were also interested in determining whether there is a radial variation of birefringence. In fact, the thickness-averaged residual stress due to braking should be largest at the outer edge of the rim [1], since it is nearest the tread (where the braking force is applied). A radial dependence of birefringence was found by Fukuoka, et al. [1] on rolled steel wheels (using the PZT transducer).

We measured the birefringence at different radii; for each radius, we measured B at 4 different circumferential positions ($\theta = 0^\circ, 90^\circ, 180^\circ, 270^\circ$). The radii were at ± 3 mm and ± 6 mm from the middle of the front face of the rim; radial position increases outward, as shown in Fig. 1. Both EMAT and PZT measurements were made after the wheel was milled.

The results of the measurements at different radii are shown in Fig. 5; the error bars represent the standard deviation of measurements of B at each of the four circumferential positions (0° , 90° , ...). The birefringence has a gradient, becoming increasingly negative as the outer edge of the rim is approached. The gradient as measured by the EMAT is almost linear.

If we assume that the texture is constant in the radial direction, then the data show that the hoop stress is becoming larger (in the positive, or tensile, sense) as the tread is approached. This is in agreement with the physics of the process whereby the residual stress in the wheel is created. The effect of braking is to cause compressive hoop stresses as the rim tries to expand during heating. These thermal stresses are, of course, largest at the tread where heat input (from braking) is applied. On cooling, a state of tensile hoop stresses results, with the largest values at the tread.

Assuming constant texture, the EMAT values show a difference of about 75 MPa between -6 and +6 mm (a gradient of about 6 MPa/mm). The PZT values indicate a difference of about 60 MPa between -6 mm and +6 mm. Note that these are differences of stresses, and not the actual stress magnitudes, since we do not as yet know the value of B_0 .

For all five radii where measurements were made, the (average) EMAT values of B are smaller than the PZT values. However, any systematic difference should not cause the EMAT value of σ_θ to differ from the PZT value since we need to subtract B_0 from B to obtain σ_θ (see equation 1). In fact, the data of Ref. 11, taken on a sawcut wheel (where we could obtain B_0), showed good agreement between σ_θ as measured by EMAT and PZT transducer.

The largest discrepancy in Fig. 5 (about 2×10^{-4}) between EMAT and PZT measurements occurs at 6 mm, the position closest to the tread. At this

radius, we found that the signal from the upper PZT crystal was different when it was polarized in the radial and hoop directions. Since this phenomenon was not noted at other radii, it may explain the difference between EMAT and PZT results at 6 mm.

Circumferential Variation of Birefringence

In the ideal case, both the texture and residual stress would be axisymmetric. If such were the case, then the standard deviations of B shown in Fig. 5 would vanish (assuming no experimental error). In fact, we see that the standard deviation is typically about 3×10^{-4} , implying that there is some asymmetry in the birefringence. (The uncertainty in arrival time measurements is about 3×10^{-5} .)

To show this asymmetry better, we have plotted the birefringence as a function of circumferential position in Fig. 6, with the radial distance (from center of the rim) as a parameter. For axial symmetry, the birefringence would be a straight line with zero slope (constant as function of circumferential position). The data in Fig. 6 (radii ± 3 mm from center of rim) show that there appears to be a departure from axial symmetry with the minimum algebraic value of B in the region 180° - 270° .

We see that the values of B as measured by the two transducers agree reasonably well for radial positions ± 3 mm from the center of the front face (to within less than about 2×10^{-4}). The agreement is not as good for the center (see Fig. 4).

The values of B (as function of circumferential position) for ± 6 mm from the center of the rim are shown in Fig. 7. Now we see a behavior which is very close to axial symmetry for $+6$ mm, for both EMAT and PZT measurements. Furthermore, there is (approximately) a constant difference between the two

sets of data at 6 mm. For -6 mm, the values of B are such as to suggest that the texture and/or the stress is rather inhomogeneous.

Effect of Edges on EMAT Measurements

As mentioned previously, the process of drag-braking the wheel usually induces the largest stresses at the largest radius in the rim. (This is because the brakes are applied on the tread.) Consequently, it is important to be able to measure the birefringence at locations as close as possible to the outer edge of the rim.

At the +6 mm position, the edge of the EMAT aperture is about 2 mm from the outer edge of the front face of the rim. We found that the signal amplitude was markedly less for $r > 6$ mm (r measured from rim center), as compared with the other radial locations. Consequently, we made no measurements for $r > 6$ mm.

We think that the drop in signal amplitude near the rim edge is due to the effect of fringing field on the EMAT.³ The EMAT generates eddy currents in the surface of the rim (within the skin depth of an electromagnetic wave). The eddy currents must form closed conduction paths. Our EMAT was designed so that the eddy currents in the surface were unidirectional, under the EMAT aperture. The effect of the edge of the conductor (rim) is not the same for different orientations of the EMAT (see Fig. 8). We conjecture that the effect of the edge is to change the effective impedance offered by the surface to the eddy currents and that this impedance change depends upon

³We note that the EMAT magnet is a single pole piece. Consequently, the magnetic induction in the rim is invariant under rotation of 90°, i.e., the magnetic induction is the same when the EMAT generates SH-waves polarized in the r - and θ - directions.

the orientation of the EMAT. These effects precluded measurement of B when the edge of our EMAT aperture was within 2 mm of the edge of the rim.

We also performed an experiment on a (cast steel) rim block whose front and back surfaces were polished so that they were plane-parallel. The edges of the flat regions are denoted as location 1 and 2 for the front face, and as 3 and 5 for the back face; see Fig. 9. Note that location 2 is directly above location 3, but locations 1 and 5 are offset.

We measured arrival times with our EMAT placed first on the front face, and then on the back face. When the center of the EMAT aperture was within 6 mm of location 1 (front face) or 3 (back face), the signal amplitude dropped and erroneous arrival times were obtained. When the EMAT was farther than 6 mm from these locations, the same value of arrival times (within ± 1 ns on the average) was obtained, regardless of which face the EMAT was on. This gave us confidence that correct arrival time could be measured when the EMAT was farther than 6 mm from an edge.

We also checked this by measuring arrival times with the EMAT on the front face, 7 mm from location 2 (7 mm from an edge). The average value was within ± 1 ns of the corresponding value obtained with the EMAT 7 mm from location 4 (27 mm from an edge). Consequently, we conclude that the effect of the edge is negligible when the EMAT is centered 7 mm or more from an edge.

These results may pertain only to this design of EMAT, operated at 2.4 MHz on steel. For other applications, frequencies, and EMATs, a similar experiment should be carried out to determine the effect of edges on EMAT operation.

DISCUSSION

We used the stacked PZT transducer (which is, of course, insensitive to the edge effect) as a check on our EMAT results. As shown in Fig. 7, the EMAT and PZT values of B agree within about 2×10^{-4} at +6 mm from the center of the rim. In contrast, we see better agreement between EMAT and PZT measurements at +3 mm (Fig. 6).

There is a possibility of a systematic difference between EMAT and PZT measurements of B , since a toneburst excitation was used for the former and shock excitation was used for the latter. In fact, a small systematic difference was noted in Ref. 11 for measurements made at the center of the back face of the rim of a cast steel wheel. However, this difference was only about 1×10^{-4} (or less). In fact, this systematic difference essentially cancelled out since the stresses are calculated from the difference $(B - B_0)$ in equation (1). In Ref. 11, we found that EMAT and PZT measurements of σ_θ were almost identical for all measurement locations on the wheel; the maximum difference was less than 10 MPa.

For the heat-treated wheel, there appears to be a systematic difference between EMAT and PZT measurements of B at radial distances of +6 and -3 mm (from center of the rim). For -6 mm, the data of Fig. 7 suggest a rather inhomogeneous texture. At the other locations, there is no clear evidence of a systematic difference; i.e., at some circumferential locations, the EMAT measurements of B are larger, while the reverse is true at other locations.

There are several issues that remain to be resolved. First, how homogeneous is the texture? This may account for the rather erratic behavior of B at -6 mm, as shown in Fig. 7. Second, is the difference in EMAT and PZT values of B at +6 mm systematic? (We found a different

waveform for the upper PZT transducers at this radius.) If so, will the difference cancel if we measure $B - B_0$?

The obvious way to resolve these issues is to cut the rim into small blocks, so that the stresses are relieved. Then one can measure B_0 with both EMAT and PZT transducers and determine whether both measurements give the same values of stress (cancellation of systematic errors).

In addition, we need to perform destructive tests on the wheel to measure the actual state of residual stress and compare within the ultrasonic results.

We hope to perform all of these tests in the near future.

CONCLUSIONS

The radial variation of $\langle B \rangle$ as measured by EMAT and PZT transducers are in good agreement for the range -6 mm to +3 mm; here $\langle B \rangle$ is the average of 4 circumferential locations. Over this range, EMAT and PZT values of $\langle B \rangle$ differ by 2×10^{-4} or less. For +6 mm the difference is less than 3×10^{-4} . Assuming no systematic differences between EMAT and PZT measurements (no cancellation of errors when taking the difference $B - B_0$), this gives a stress differences of about 27 MPa (for radii ranging from -6 mm to +3 mm from the rim center) and 40 MPa (+6 mm from rim center). If there are systematic errors which can be (removed by subtracting B_0 from B), the differences will be less.

We found that, as a function of circumferential position, EMAT and PZT values of B were in good agreement (difference less than 2×10^{-4}) for radial positions -3 mm to +3 mm. There appears to be a systematic difference (EMAT values of B less than PZT values by about 3×10^{-4} or less) at +6 mm. At

-6 mm, both sets of data are erratic, perhaps indicating inhomogeneity in texture.

It is fortunate that the birefringence displays the axisymmetric behavior at +6 mm, since this will be the radius of maximum (thickness-averaged) hoop stress [1]. The axisymmetric behavior suggests that the texture and stress may be homogeneous at this radius for the heat-treated wheel. If such is the case, then the following procedure may be used to determine value of σ_θ at +6 mm on in-service wheels.

Several heat-treated wheels would be cut into rim blocks (as in Ref. 1) to relieve the residual stress. The value of B_0 would then be measured on a statistically significant number of rim blocks. The mean value, $\langle B_0 \rangle$, would then be used when determining the value of σ_θ for an in-service wheel. To do this, the birefringence would be measured for the in-service wheel, and $\langle B_0 \rangle$ subtracted to obtain σ_θ :

$$\sigma_\theta = (B - \langle B_0 \rangle) / C_A. \quad (5)$$

This is the method used in Ref. 1 to obtain σ_θ for rolled steel wheels.

The uncertainty $\delta\sigma_\theta$ in σ_θ can be estimated from the standard deviation of B_0 measured on the population of rim blocks:

$$\delta\sigma_\theta = \delta B_0 / C_A. \quad (6)$$

We hope to perform such experiments in the future.

The EMAT measurements of B at the center of the rim are relatively insensitive to the degree of surface preparation. The degree of surface preparation was varied between the extremes of (a) handsanding to remove rust (leaving a pitted surface) and (b) milling in a machine shop, followed by handpolishing with fine abrasive paper (leaving a very smooth surface). The

EMAT measurements of B for these surface treatments were usually within 2×10^{-4} of each other. For practical applications, this indicates that a minimal amount of surface preparation may be necessary for EMAT measurements in the field.

ACKNOWLEDGMENTS

This work was supported by the Federal Railroad Administration, Department of Transportation, under the supervision of Mr. Claire Orth, Research Manager. We were greatly assisted by the generous cooperation of Britto Rajkumar of the American Association of Railroads, Pueblo, CO, who provided both the wheel and encouragement.

REFERENCES

1. Fukuoka, H., Toda, H., Hirakawa, K., Sakamoto, H., and Toya, Y., "Acoustoelastic Measurements of Residual Stresses in the Rim of Railroad Wheels," *Wave Propagation in Inhomogeneous Media and Ultrasonic Non-destructive Evaluation*, G. C. Johnson, ed., AMD-Vol. 6 (published by ASME, 1984).
2. Pao, Y. H., Sachse, W., and Fukuoka, H., "Acoustoelasticity and Ultrasonic Measurements of Residual Stress," *Physical Acoustics*, Vol. XVII, Academic Press, New York, 1984, pp. 61-143.
3. Fukuoka, H., Toda, H., and Yamane, T., "Acoustoelastic Stress Analysis of Residual Stress in a Patch-Welded Disc," *Exp. Mech.*, 18, 1978, pp. 277-280.
4. Schneider, E., "Determination of Residual Stresses by Time of Flight Measurements with Linearly-Polarized Shear Waves" *Proc. IEEE Symp. on Sonics and Ultrasonics*, 1981, pp. 956.
5. Toda, H., Fukuoka, H., and Aoki, Y., "R-value Acoustoelastic Analysis of Residual Stress in a Seam Welded Plate," *Proc. 4th Symp. on Ultrasonic Electronics*, Tokyo, 1983. *Jap. Jour. Appl. Phys.*, 23, 1984, pp. 86-88.
6. Clark, A. V., Moulder, J. C., Trevisan, R. E., Siewert, T. A., and Mignogna, R. B., "Ultrasonic Techniques for Residual Stress Measurement in Thin Welded Aluminum Alloy Plates," to be published in *Rev. Prog. in Quant. NDE*, D. O. Thompson and D. E. Chimenti, eds., 1985.
7. King, R. B., and Fortunko, C. M., "Determination of In-Plane Residual Stress States in Plates Using Horizontally Polarized Shear Waves," *J. Appl. Phys.*, 54, 1983, pp. 3027-3035.
8. Blessing, G. V., Hsu, N. N., and Proctor, T. M., "Ultrasonic-Shear-Wave Measurement of Known Residual Stress in Aluminum," *Exp. Mech.*, 24, 1984, pp. 218-222.
9. Clark, A. V., and Moulder, J. C., "Measurement of Residual Stresses in Slightly Anisotropic Aluminum Alloy Specimens by the Method of Acoustic Birefringence," *Ultrasonics*, 23, 1985, pp. 253-259.
10. Jackson, C. W., "Characterization of Stressed Metals Using Acoustic Shear Waves"; Ph.D. Thesis, Dept. of Mechanical Eng., Stanford Univ., 1984.
11. Clark, A. V., Fukuoka, H., Mitraković, D. V., and Moulder, J. C., "Characterization of Residual Stress and Texture in Cast Steel Railroad Wheels," to be published in *Ultrasonics*.
12. Iwashimizu, Y., and Kubomuro, K., "Stress-Induced Rotation of Elastic Waves in Slightly Anisotropic Materials," *Int. J. Solids Structures*, 9, 1973, pp. 99-114.

13. Nishimura, S., and Tokimasa, K., "Study on the Residual Stresses in Railroad Solid Wheels and Their Effect on Wheel Fracture," Bulletin of JSME, 19, 1976, pp. 459-468.
14. Johnson, M. D., Robinson, R. R., Opinski, A. J., and Stone, D. H., "Railroad Wheel Back Rim Face Failures III. Residual Stress Calculations on 33" D One-Wear Freight Car Wheels," Am. Assoc. of Railroads Rep. No. R-560, AAR Tech. Center, Chicago, IL, 1983.

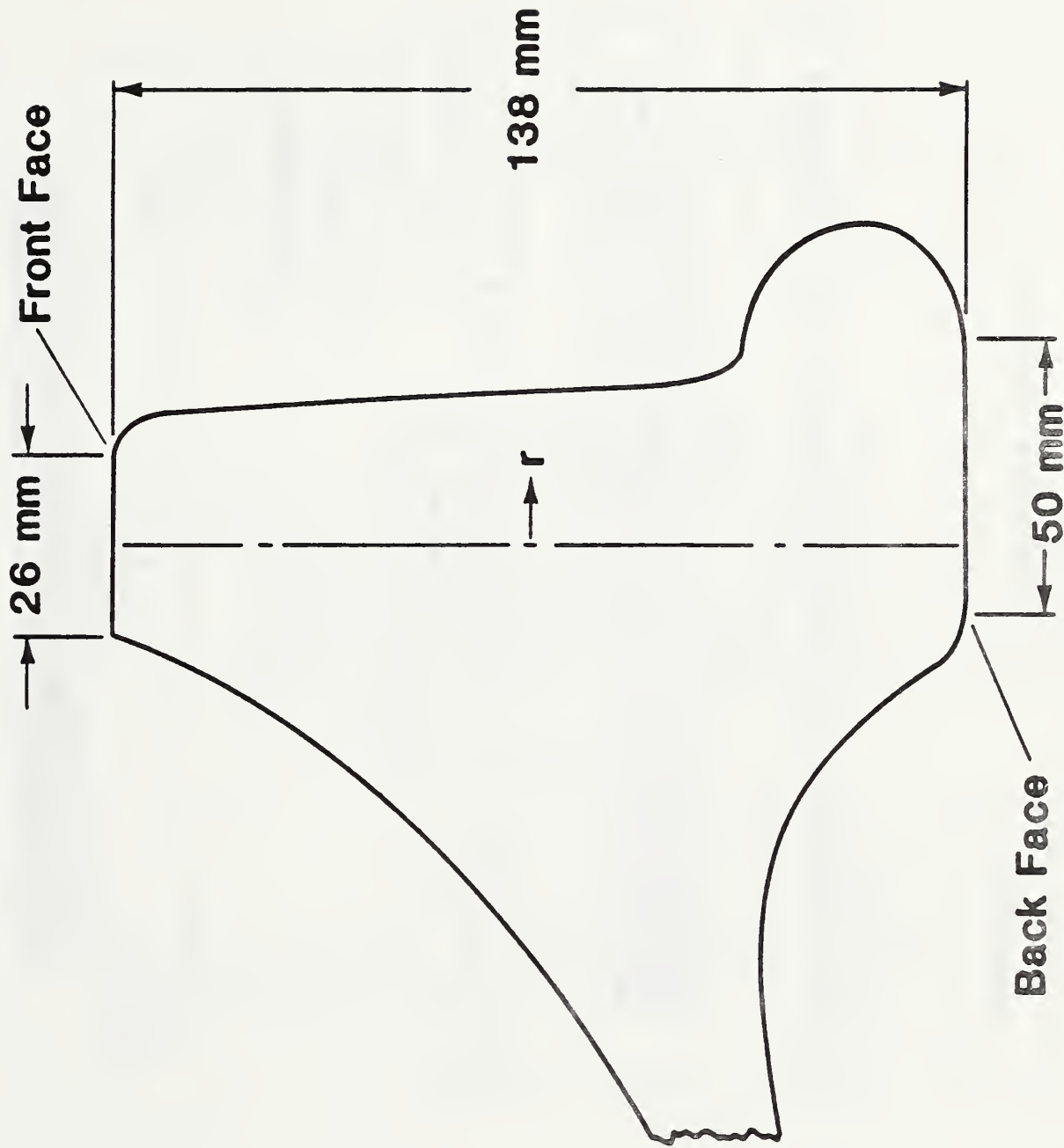


Fig. 1. Cross-section of railroad wheel tested in present work. In Ref. 11, transducers were placed on back face. In present work, transducers were placed on front face.

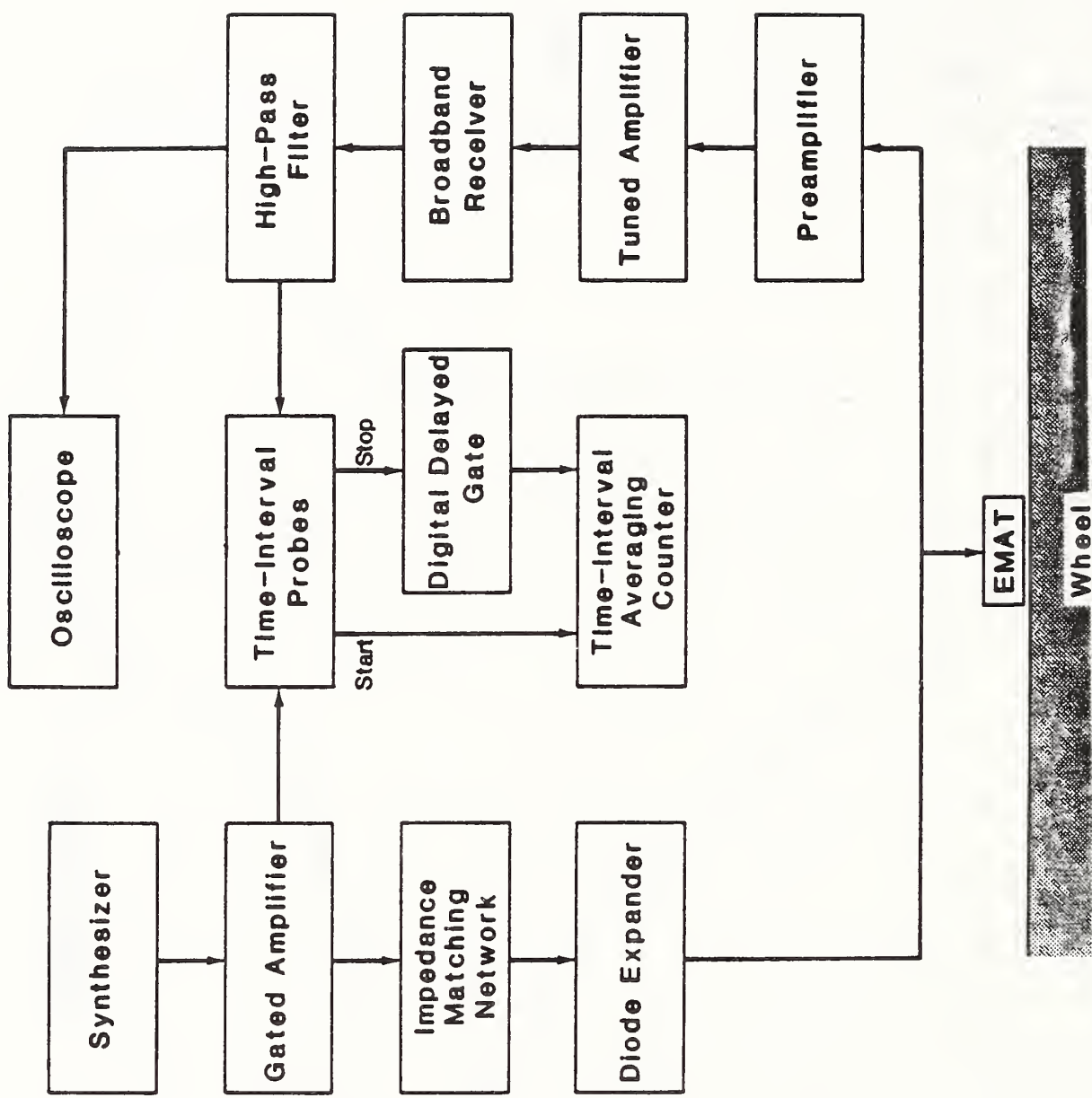


Fig. 2. Block diagram of system used to measure birefringence with EMAT.

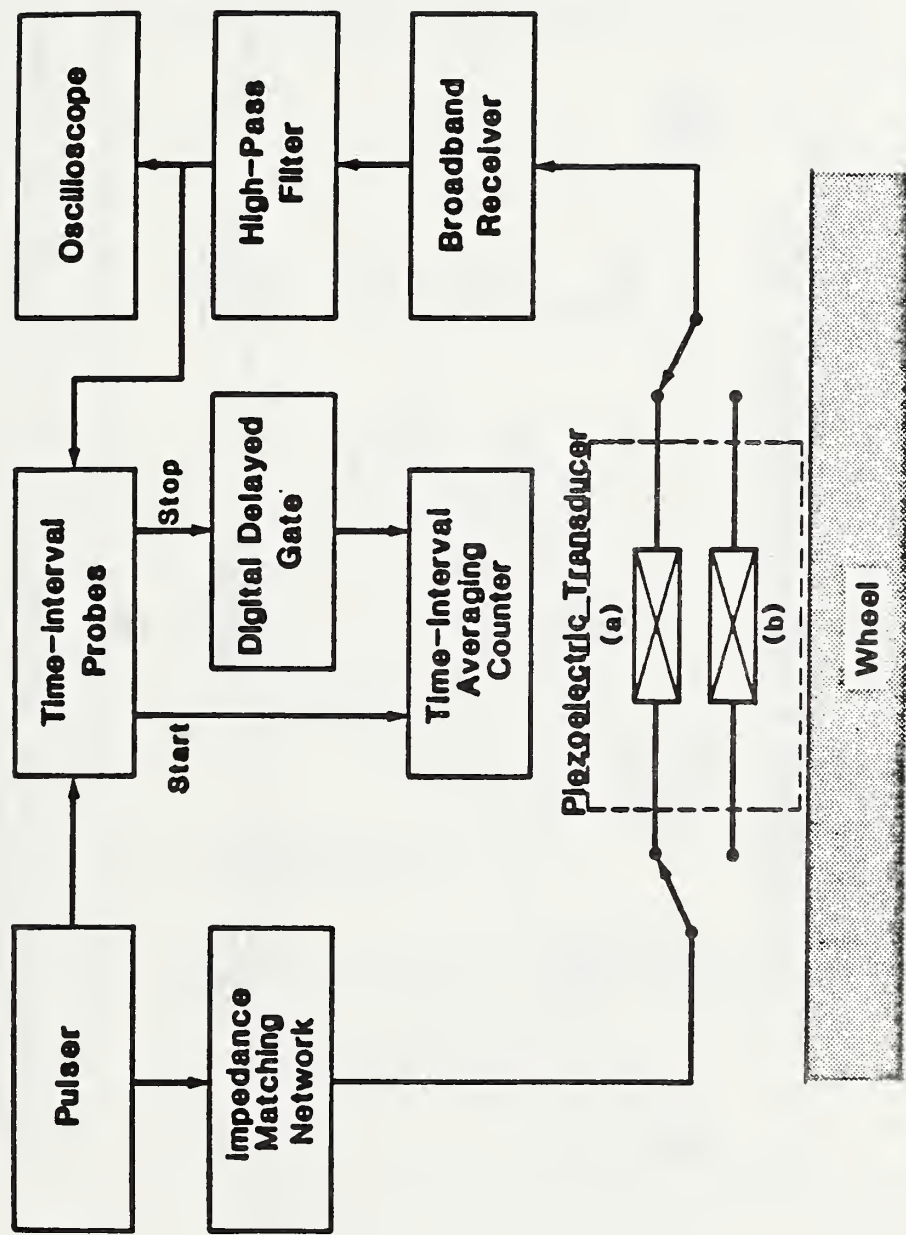


Fig. 3. Block diagram of system used to measure birefringence with PZT transducer.

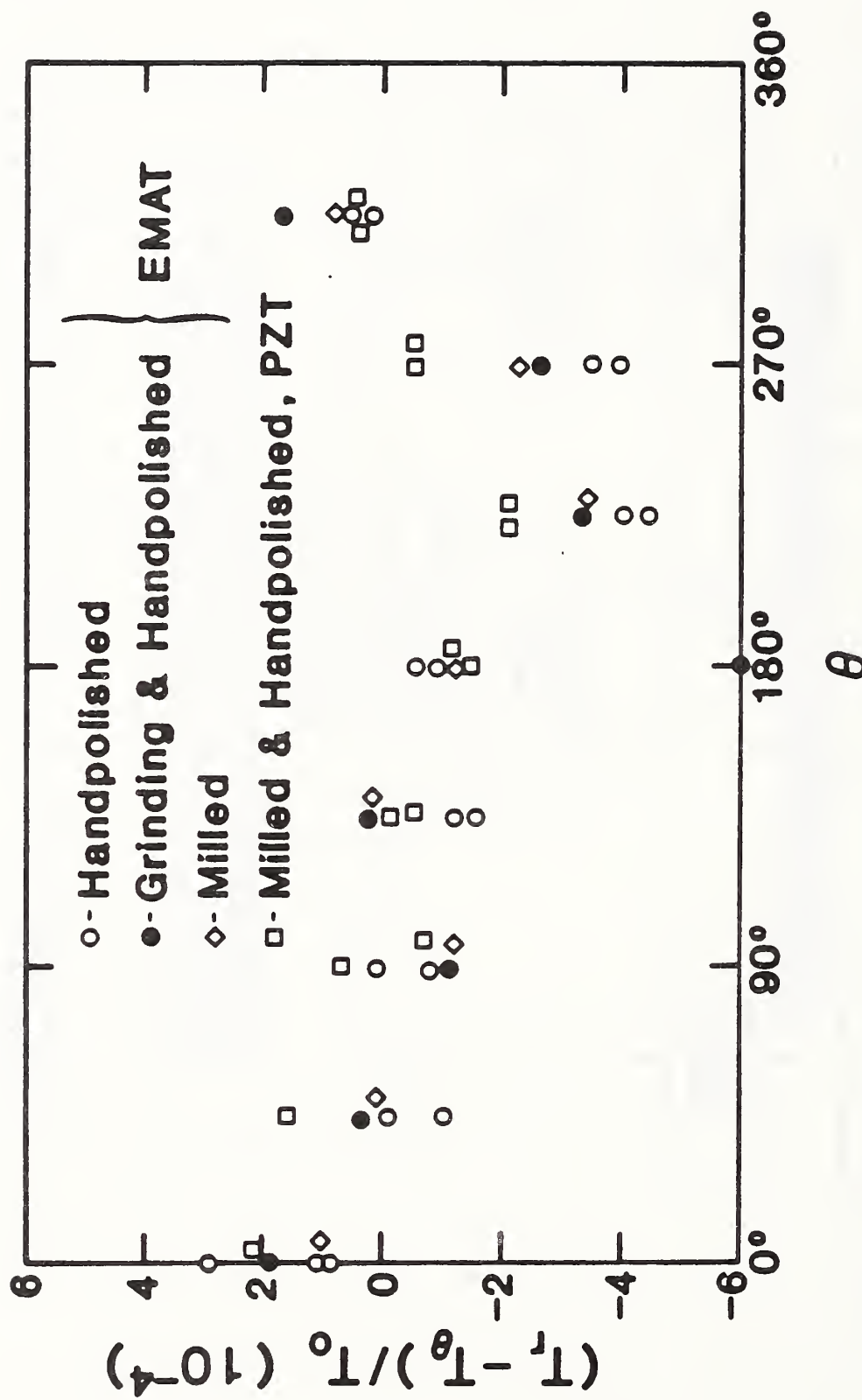


Fig. 4. Birefringence measured at center of rim, for various degrees of surface preparation.

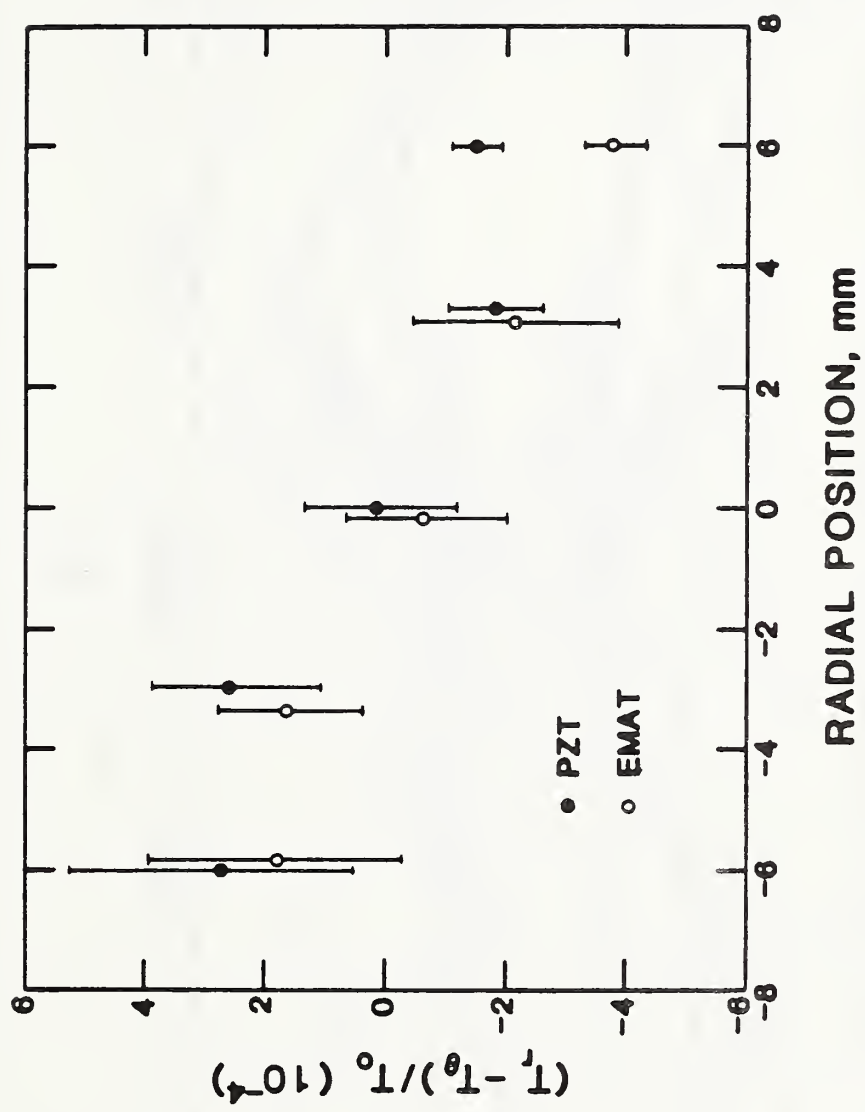


Fig. 5. Radial variation of birefringence, as measured with EMAT and PZT transducer. Radial position measured outward from center of rim.

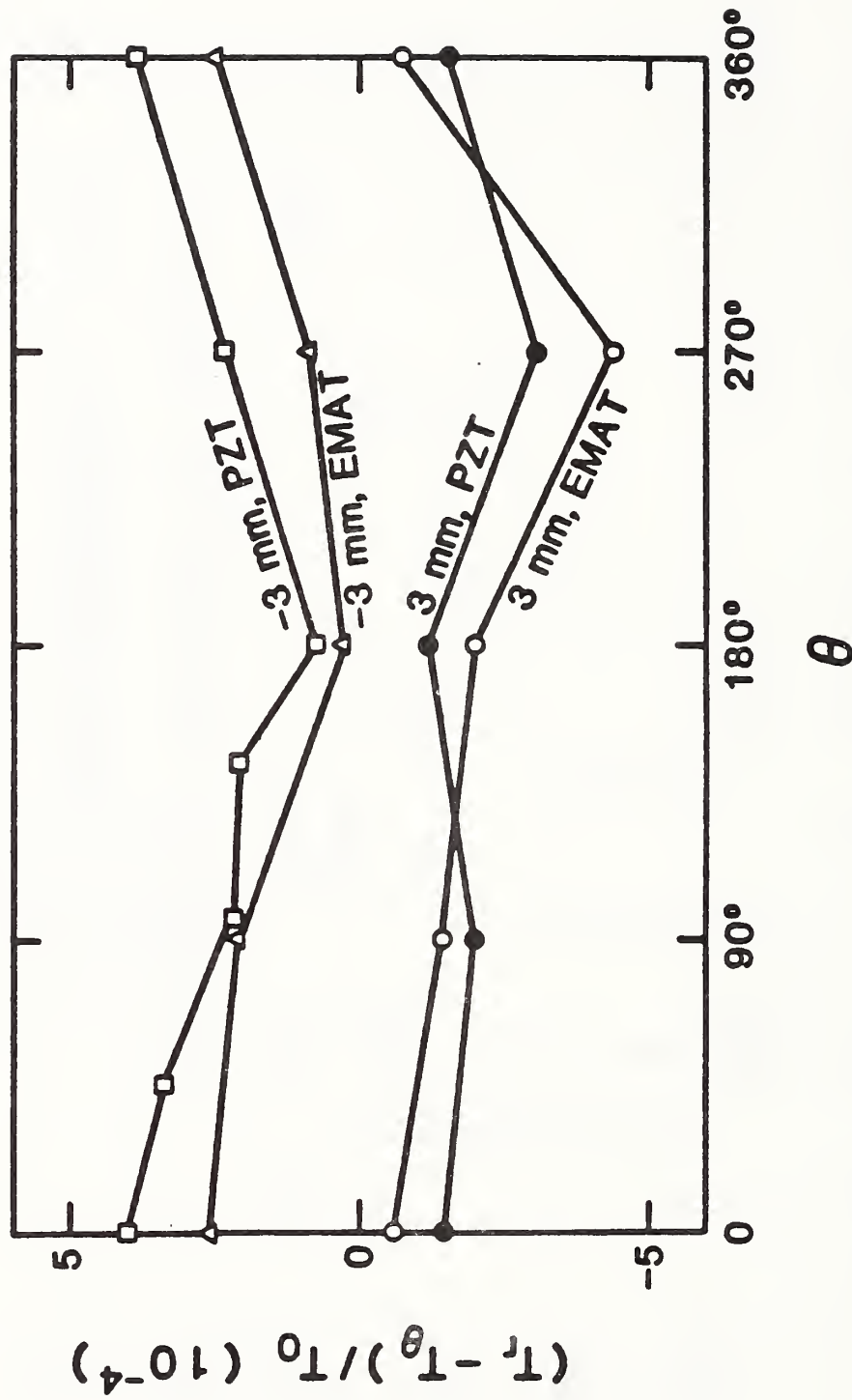


Fig. 6. Circumferential (θ) variation of birefringence, as measured with EMAT and PZT transducer. Birefringence measured at ± 3 mm from rim center.

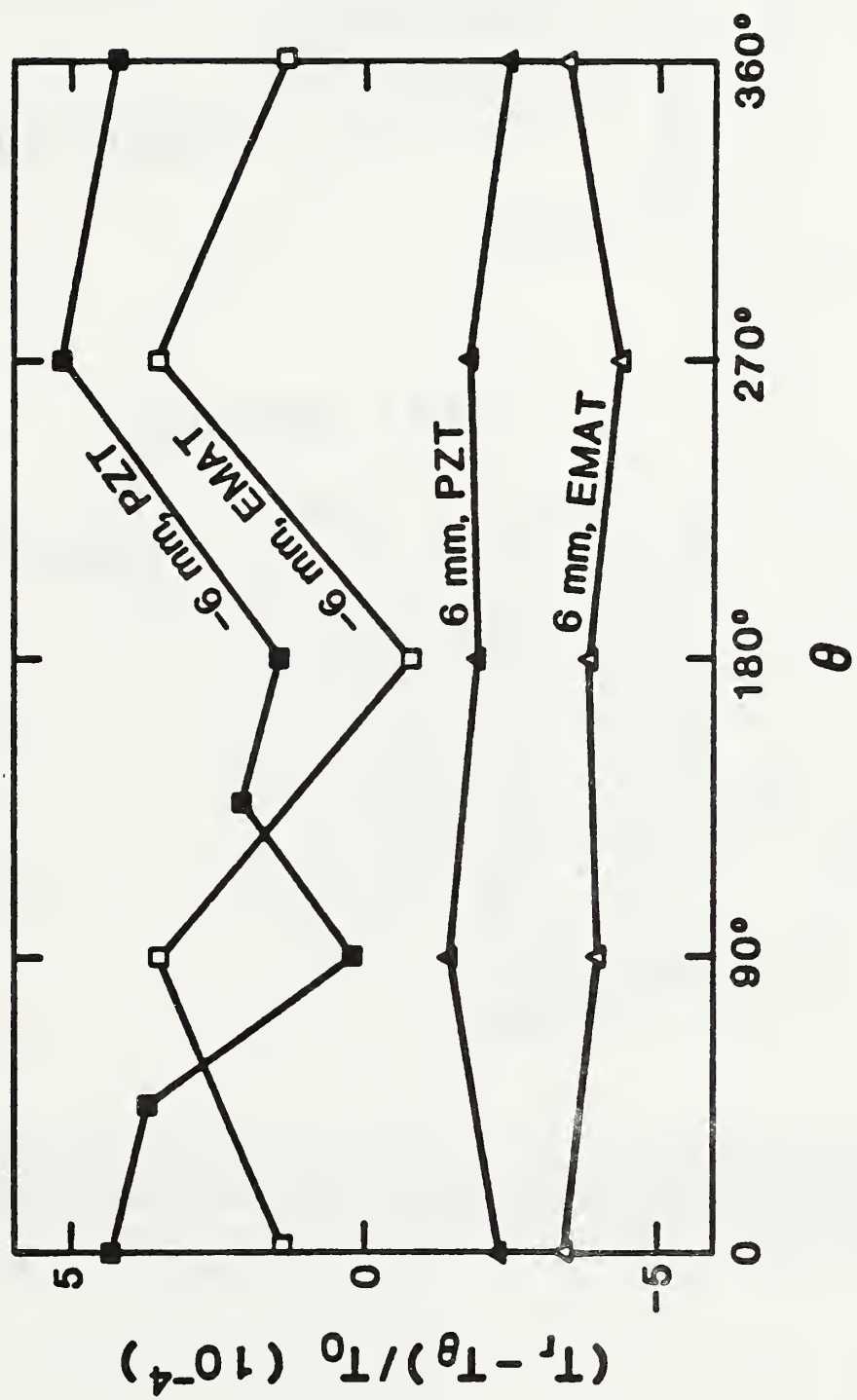


Fig. 7. Circumferential variation of birefringence at ± 6 mm from center of rim.

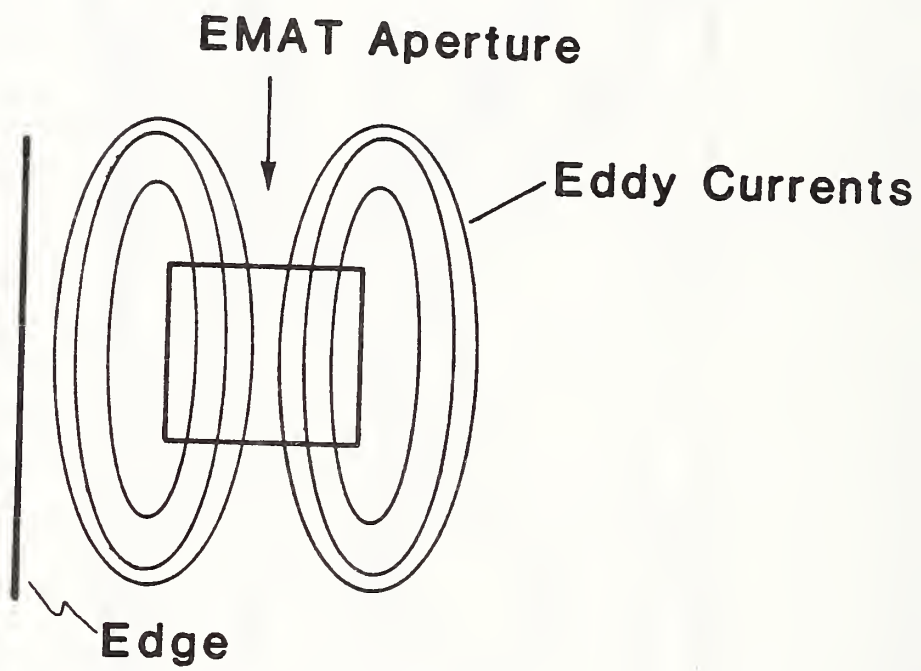
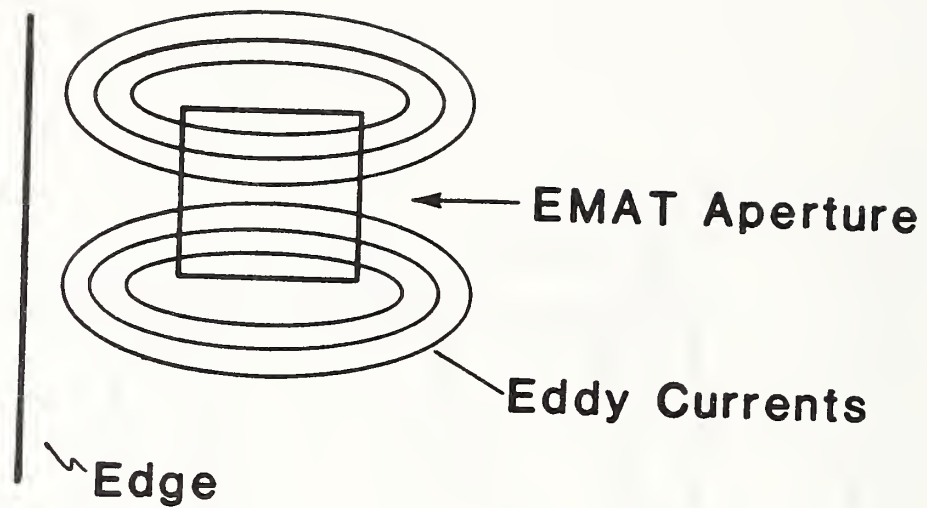


Fig. 8. Interaction of eddy current field with rim edge. EMAT oriented to generate SH-wave polarized in circumferential direction (top figure), and in radial direction (bottom figure).

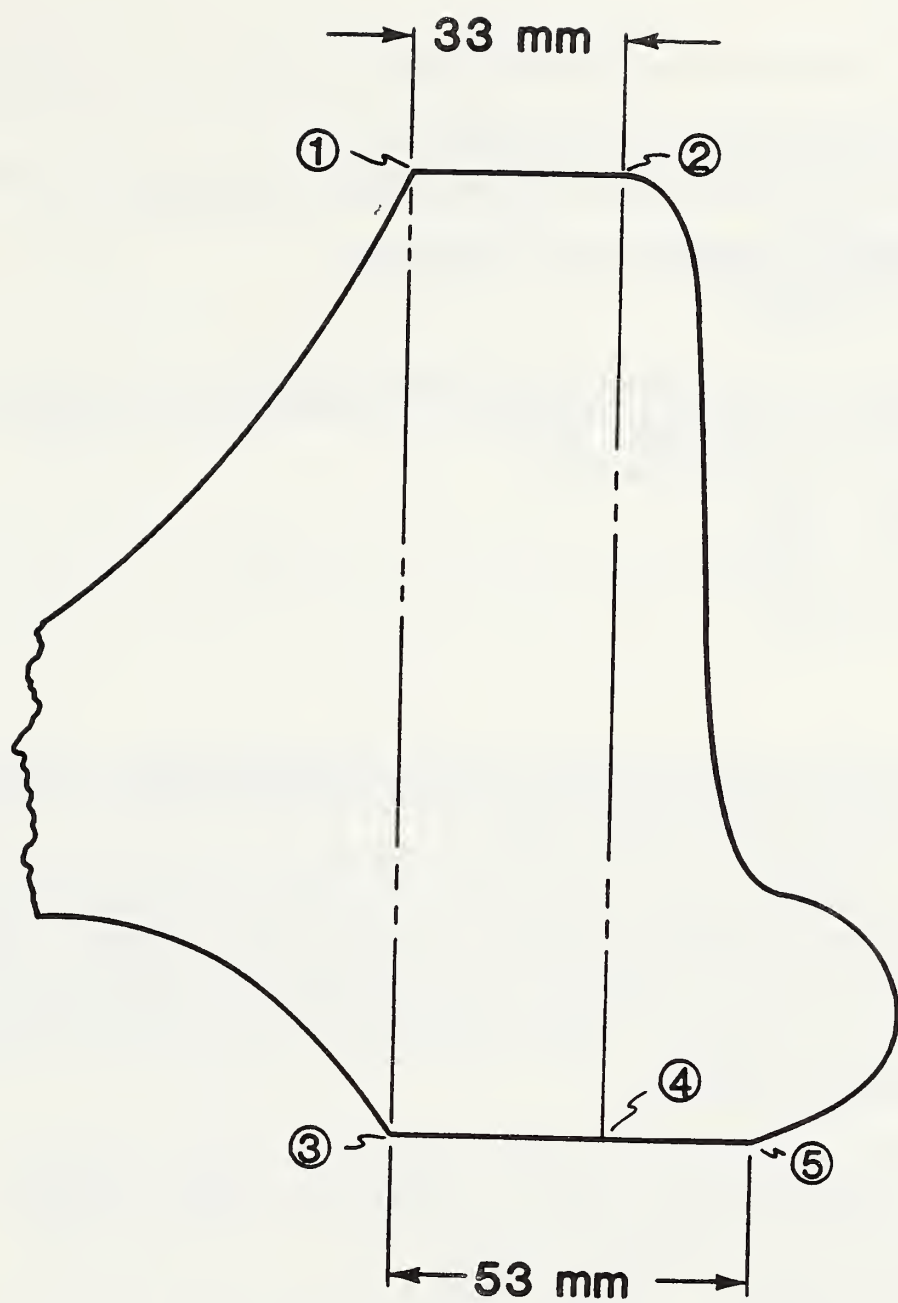


Fig. 9. Cross-section of rim block use to test effect of edges on arrival time measurements made with EMAT. Locations 1 and 3, 2 and 4 are directly opposite each other. Location 5 is where flat portion of back rim face ends.

U.S. DEPT. OF COMM. BIBLIOGRAPHIC DATA SHEET (See instructions)		1. PUBLICATION OR REPORT NO. NISTIR 88-3906	2. Performing Organ. Report No.	3. Publication Date December 1988
4. TITLE AND SUBTITLE Ultrasonic Railroad Wheel Inspection Using EMATs Report No. 18				
5. AUTHOR(S) Raymond E. Schramm and A. Van Clark, Jr.				
6. PERFORMING ORGANIZATION (If joint or other than NBS, see instructions) Institute NATIONAL BUREAU OF STANDARDS and Technology DEPARTMENT OF COMMERCE WASHINGTON, D.C. 20234			7. Contract/Grant No.	8. Type of Report & Period Covered
9. SPONSORING ORGANIZATION NAME AND COMPLETE ADDRESS (Street, City, State, ZIP) U.S. Department of Transportation Federal Railroad Administration 400 7th Street, S.W. Washington, DC 20590				
10. SUPPLEMENTARY NOTES				
<input type="checkbox"/> Document describes a computer program; SF-185, FIPS Software Summary, is attached.				
11. ABSTRACT (A 200-word or less factual summary of most significant information. If document includes a significant bibliography or literature survey, mention it here) This is report number 18 in a series covering the research performed by the National Institute of Standards and Technology (formerly National Bureau of Standards) for the Federal Railroad Administration. This issue collects seven reprints and preprints of papers written by the Fracture and Deformation Division over the last two years on the ultrasonic nondestructive evaluation of railroad wheels for the presence of residual stress and cracks. All this work concentrated on the use of electromagnetic-acoustic transducers (EMATs).				
Tensile residual stresses and tread cracks are major factors in wheel failure. Catastrophic breakdowns may lead to injuries, repair costs, and lost time. Current inspection methods are largely visual, and thus inefficient. Two ultrasonic techniques are applicable to these wear defects:				
1) Birefringence. A stress field effects the velocity of a shear horizontal wave depending on its polarization. Precise velocity measurements in a wheel rim may allow calculation of the amount and direction of stresses.				
2) Pulse-echo. A Rayleigh (surface) wave transducer mounted inside the rail can introduce a signal to interrogate the circumference of a wheel as it rolls by. An echo indicates a flaw's presence and size.				
For both systems, we hope to produce instruments for testing at a field site.				
12. KEY WORDS (Six to twelve entries; alphabetical order; capitalize only proper names; and separate key words by semicolons) EMAT; nondestructive evaluation; railroad wheel; residual stress; roll-by inspection; ultrasonic.				
13. AVAILABILITY <ul style="list-style-type: none"> <input checked="" type="checkbox"/> Unlimited <input type="checkbox"/> For Official Distribution. Do Not Release to NTIS <input type="checkbox"/> Order From Superintendent of Documents, U.S. Government Printing Office, Washington, D.C. 20402. <input checked="" type="checkbox"/> Order From National Technical Information Service (NTIS), Springfield, VA. 22161 			14. NO. OF PRINTED PAGES 88 15. Price	

